FACULTEIT WETENSCHAPPEN
Opleiding Master of Science in de geologie

Evaluation and modelling of the response of gas hydrate reservoirs to changing environmental conditions across a high-latitude continental margin

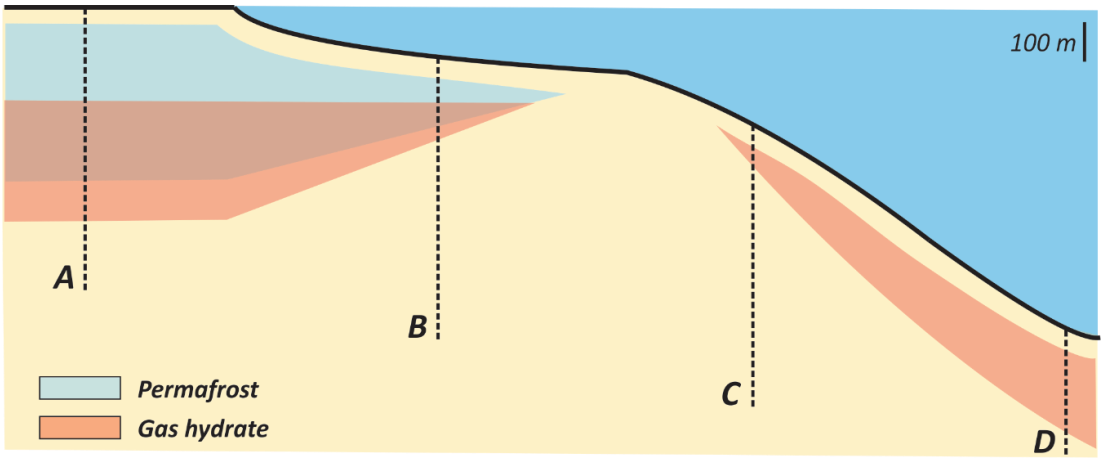

Thomas Mestdagh

Academiejaar 2014–2015

Scriptie voorgelegd tot het behalen van de graad
Van Master of Science in de geologie

Promotor: Prof. Dr. Marc De Batist
Leescommissie: Prof. Dr. Luc Lebbe, Dr. Jeffrey Poort

Cover image. *Schematic profile across a hypothetic high-latitude continental margin, with one-dimensional gas hydrate- and/or permafrost-bearing sediment columns in four distinct geographic settings: A. thick onshore permafrost; B. subsea permafrost below shallow shelves; C. feathering upper edge of the hydrate stability zone on the upper continental slope; D. deepwater setting on the lower continental slope or rise.*

ACKNOWLEDGEMENTS

I would like to make use of this first page of my master's dissertation to express my thanks to a number of people, who in one way or another all have helped to make the past months of elaborate research result in the document I happily present here.

In the first place I would like to thank my promotor, professor Marc De Batist, for giving me the chance to work on this truly fascinating topic. His input, in the form of constructive discussions, suggestions and reviews, constituted a tremendous help to me and definitely guided me in the right direction.

I also would like to dedicate some words to my classmates and friends, who have accompanied me along the way, either in Ghent or in Tromsø. Without their friendship and the countless memorable moments we passed through, the past five years would not have been the great pleasure it has been now. They made my time as a geology student simply unforgettable.

At last, I would like to thank my family, my parents and my girlfriend, for their endless support and love.

ABSTRACT IN DUTCH

Gashydraten zijn kristallijne vaste stoffen die opgebouwd zijn uit een rooster van watermoleculen waarin een gasmolecule (CO_2, CH_4 of een molecule van een zwaarder gas) gevangen zit. Ze komen voor in de natuur in de poriënruimte van sedimenten bij voldoende hoge druk en lage temperatuur (Sloan and Koh, 2007). Concreet betekent dit dat gashydraten (in de literatuur ook wel clathraten genoemd) veelal teruggevonden worden in mariene sedimenten op en aan de voet van continentale randen, bij oceaanbodemdieptes van 300 m tot 3000 m (Birchwood et al., 2010). Daarnaast komen ze voor in associatie met permafrost, die in poolnabije regio's zowel op het land als onder ondiepe zeeën kan voorkomen (Collett et al., 2011). Tenslotte zijn ook een aantal voorbeelden uit het Baikalmeer en de Zwarte Zee gekend (Khlystov et al., 2013).

Hoewel er wat onenigheid over bestaat, is de omvang van het globale gashydraatreservoir met een geschat volume van enkele honderden tot duizenden gigaton aan koolstof aanzienlijk. Deze waarde is op zijn minst in dezelfde grootteorde als de geschatte reserves aan andere conventionele koolstofbronnen zoals steenkool, aardolie of aardgas (Koh et al., 2012). Het is dan ook niet verwonderlijk dat een aanzienlijk deel van het hydraatonderzoek zich tot op de dag van vandaag toespitst op het potentieel van gashydraten als toekomstige energiebron. Deze scriptie behandelt echter een andere, maar niet minder onderzochte problematiek. Al snel groeide immers het besef dat gashydraten mogelijk een belangrijke rol kunnen spelen in de koolstofcyclus en bijgevolg in het klimaat van de Aarde (Kvenvolden, 1988). Het basisidee hierachter is dat het gas (hoofdzakelijk methaan), dat initieel gevangen zit in de clathraatstructuur, kan vrijkomen door het smelten of dissociëren van gashydraten. In de natuur kan dit bijvoorbeeld het gevolg zijn van een stijging van de temperatuur aan de zeebodem, door een opwarming van de bovenliggende watermassa's, die vervolgens in de ondergrond propageert naar dieptes waar gashydraten voorkomen, of van een zeespiegeldaling waardoor de druk in de oceaanbodemsedimenten daalt. Wanneer methaan (CH_4) en zijn oxidatieproduct koolstofdioxide (CO_2), beide broeikasgassen, door de sediment- en waterkolom migreren en uiteindelijk als vrij gas in de atmosfeer terecht komen, kunnen deze nog extra bijdragen tot de opwarming, waardoor het smelten van de gashydraten in stand gehouden of versneld wordt. Op deze manier wordt een positief feedback-mechanisme gecreëerd, dat abrupte stijgingen in atmosferische CH_4 of CO_2 concentraties en snelle klimaatschommelingen zou kunnen verklaren. Dergelijke snelle klimaatschommelingen hebben zich verschillende keren voorgedaan in de geologische geschiedenis, en werden aan het licht gebracht door metingen van koolstof- en zuurstofisotopen. Een bekend voorbeeld, waarvoor dit mechanisme voorgesteld werd, is het *Paleocene - Eocene Thermal Maximum*, afgekort PETM (Dickens et al., 1995). Andere studies opperen dat het afwisselend krimpen en aangroeien van het globale gashydraatreservoir ook een belangrijke rol kan gespeeld hebben in Laat-Pleistocene klimaatschommelingen (Loehle, 1993; Nisbet, 1990). Een bijkomende factor hierbij is dat de faseovergang van gashydraat naar vrij gas en vloeistof gepaard gaat met een volume-expansie, waardoor in weinig permeabele sedimenten de druk in de poriënruimte aanzienlijk kan stijgen. De hieraan gekoppelde daling in de sterkte van het sediment kan uiteindelijk aanleiding geven tot het barsten en afglijden van omvangrijke sedimentpakketten, waardoor grote volumes gashydraten in een korte tijdsspanne zouden kunnen smelten. Dit vormt de basis voor de *clathrate gun hypothesis*, die Kennett et al. (2003) voorstellen om Laat-Pleistocene klimaatcycliciteiten (glacialen/interglacialen en stadialen/interstadialen) te verklaren. Tenslotte veronderstelt een aantal onderzoekers ook nog dat de hedendaagse klimaatverandering, ten gevolge van menselijke activiteit zoals het massaal verbranden van fossiele brandstoffen, aanleiding kan geven tot het smelten van gashydraten in de komende eeuwen (Hunter et al., 2013; Marín-Moreno

et al., 2013), of dat dit zelfs vandaag de dag al aan de gang is op de continentale rand ten westen van Spitsbergen (Westbrook et al., 2009), wat uiteraard een bijkomstig versterkend effect zou kunnen hebben op de opwarming van de Aarde.

Deze scriptie spitst zich toe op de hierboven toegelichte potentiële, maar ook controversiële rol van gashydraten in de koolstofcyclus en het klimaat van de Aarde. De gevoeligheid van gashydraatreservoirs voor veranderende omgevingsparameters is essentiële informatie om de hierboven opgesomde theorieën te kunnen beoordelen. Dit houdt in dat vragen als waar, hoe snel en hoeveel gashydraten kunnen smelten ten gevolge van temperatuur- en/of zeespiegel-schommelingen, dienen te worden beantwoord. Deze studie probeert dit te doen voor methaanhydraatreservoirs langsheen een hypothetische continentale rand op een hoge breedtegraad, omdat klimaatveranderingen hier over het algemeen het meest uitgesproken zijn (Westbrook et al., 2009). Dit laat bovendien ook toe om vier fundamenteel verschillende omgevingen waarin hydraten kunnen voorkomen (continentale permafrost, permafrost onder ondiepe zeeën, in de zeebodem bovenaan de continentale helling, en in de zeebodem aan de voet van de continentale helling) te beoordelen en te vergelijken. Hiertoe werd een eendimensionaal numeriek model ontwikkeld in MATLAB, waarbij de evolutie van de temperatuur in de ondergrond doorheen de tijd gebaseerd is op de *finite difference method*. Realistische initiële distributies en concentraties van gashydraten in de ondergrond werden verkregen door het implementeren van bestaande vormingsmodellen (het model van Xu and Ruppel (1999) voor mariene gashydraten, en het model van Behseresht and Bryant (2012) voor hydraten geassocieerd met permafrost). Op deze manier kon ook een onderscheid gemaakt worden tussen de gashydraatstabiliteitszone (HSZ), die op basis van druk, temperatuur, en saliniteit van het poriënwater in de ondergrond kan afgebakend worden, en de zone waar gashydraten effectief voorkomen. De omvang van laatstgenoemde zone hangt nog extra af van de beschikbaarheid van methaan in de poriënruimte van de sedimenten, die groot genoeg moet zijn om ervoor te zorgen dat methaanhydraten kunnen vormen en niet oplossen (de methaanconcentratie in het poriënwater moet hiertoe groter zijn dan de oplosbaarheid van methaan in het poriënwater). In veel gevallen beslaat het volume van deze zone (en dus van de gashydraatreservoirs) slechts een fractie van de HSZ. Daarnaast dient men ook rekening te houden met de *sulphate reduction zone* in de bovenste meters van de zeebodem, waarbinnen sulfaatreducerende bacteriën methaan omzetten naar CO_2 en op deze manier de stabiliteit van methaanhydraten belemmeren. Desalniettemin nemen een aantal modelleerstudies het volume van de HSZ (verkeerdelijk) als referentie voor de omvang van gashydraatreservoirs, wat in deze studie dus vermeden werd. Voorts werd ook de consumptie van latente warmte tijdens het smelten van gashydraten in rekening gebracht.

Dit model maakt het mogelijk de respons van methaanhydraatreservoirs op temperatuurstijgingen en zeespiegelschommelingen te simuleren. In eerste instantie werd dit gedaan voor drie scenario's waarin eenzelfde verandering wordt opgelegd in elk van de vier omgevingen, met als doel te achterhalen waar methaanhydraten het meest gevoelig zijn voor wijzigingen in de omgevings-parameters. De resultaten van deze simulaties tonen aan dat methaanhydraatreservoirs in associatie met permafrost onder ondiepe zeeën en in sedimenten bovenaan de continentale helling het snelst dissociëren wanneer de temperatuur aan de zeebodem met 5 °C stijgt. Op deze locaties dissocieert het volledige hydraatreservoir respectievelijk binnen 70000 en 50000 jaar. Deze tijdsspanne wordt in beide gevallen met ongeveer 30000 jaar verlengd wanneer een simultane zeespiegelstijging van 100 m in rekening wordt gebracht, aangezien de hiermee gepaarde stijging van de hydrostatische druk in de poriënruimte een stabiliserend effect heeft op de gashydraten. Verder van belang voor deze hydraatreservoirs is de observatie dat, wanneer de nieuwe, verhoogde temperatuur aan de zeebodem de smelttemperatuur van methaanhydraat bij de druk aan de zeebodem overschrijdt,

hydraten vanaf de top van het reservoir kunnen smelten. Dit staat in contrast met diepwaterhydraten, die over het algemeen vanaf de basis smelten, zoals ook aangegeven wordt door deze studie. Wanneer de temperatuur over de continentale rand uniform toeneemt, zal bovengenoemde voorwaarde alleen vervuld zijn wanneer de waterdiepte kleiner is dan een welbepaalde kritische diepte, waarvoor een vergelijking werd afgeleid. Dit is immers belangrijke informatie, omdat methaangas dat vrijkomt aan de top van de hydraatzone op locaties waar bovendien de bovenliggende oceaan vrij ondiep is, een grotere kans heeft om uiteindelijk in de atmosfeer terecht te komen. Ook wanneer louter een zeespiegeldaling gesimuleerd wordt, neemt het effect op de stabiliteit van methaanhydraten toe naarmate de waterdiepte afneemt. Gashydraten in sedimenten aan de voet van de continentale hellingen en in associatie met dikke, continentale permafrost zijn daarentegen duidelijk minder gevoelig voor opwarming of zeespiegelschommelingen, aangezien over een periode van 100000 jaar slechts een kleine fractie of zelfs helemaal geen hydraten dissociëren. Tenslotte geeft de simulatie van de temperatuurstijging ook nog aan dat ijs in permafrost smelt op een tijdschaal van tientallen duizenden jaren. Hierover bestaat echter een grotere mate van onzekerheid dan over de tijdschaal die werd afgeleid voor het dissociëren van gashydraten, aangezien een aantal basisveronderstellingen over permafrostbodems (o.a. omtrent de grootte van de fractie van de poriënruimte die ijs initieel inneemt) nogal moeilijk te bepalen zijn.

In het tweede deel van deze studie werd de respons van methaanhydraatreservoirs op de klimaatveranderingen tijdens de deglaciatie volgend op het *Last Glacial Maximum* (LGM), tijdens het PETM, en tijdens de huidige opwarming van de Aarde expliciet nagebootst, om de theorieën die hieromtrent geformuleerd zijn te kunnen evalueren. Elk van deze simulaties toont aan dat de tijdschaal voor het destabiliseren van gashydraten ook in deze specifieke gevallen tientallen duizenden jaren bedraagt. Dit komt niet overeen met de responstijd van duizenden jaren, zoals vooropgesteld in de *hydrate dissociation hypothesis* voor het PETM (Dickens et al., 1995), en de *clathrate gun hypothesis* voor Laat-Pleistocene klimaatschommelingen (Kennett et al., 2003). Dit contrast is zelfs nog groter met de voorgestelde tijdsintervallen van enkele eeuwen (Hunter et al., 2013), of zelfs decennia (Westbrook et al., 2009), voor het dissociëren van gashydraten als een gevolg van de hedendaagse klimaatverandering. Deze studie toont aan dat deze snelle tijdschalen enkel van toepassing kunnen zijn op methaanhydraten die zich heel ondiep (i.e. enkele meters tot tientallen meters) in de ondergrond bevinden. Echter, gashydraten op dergelijke kleine dieptes zijn waarschijnlijk eerder uitzondering dan regel. De zogenaamde 'stratigrafische' hydraatreservoirs, die lateraal continu zijn en het overgrote deel van het globaal volume aan gashydraten bevatten, bevinden zich immers doorgaans op tientallen tot honderden meters diepte. Enkel waar een zeer hoge aanvoer van methaangas ervoor zorgt dat de vorming van hydraten de anaerobe oxidatie van methaan door sulfaatreducerende bacteriën en de diffusie van methaan uit de hydraatstabiliteitszone naar de bovenliggende oceaan overschrijdt, kunnen hydraten vlak onder, of zelfs tot op de zeebodem bestaan. Aan deze voorwaarde kan over het algemeen enkel zeer lokaal voldaan worden, bijvoorbeeld ter hoogte van breuken of moddervulkanen, en zijn dus eerder uitzonderlijk (Archer et al., 2009a). Bovendien vormt de oceaan nog een extra buffer tussen de atmosfeer en de hydraatreservoirs in de geosfeer, omdat het eventuele vrijgekomen methaangas ook hier oplost in het oceaanwater en verder geoxideerd kan worden tot CO_2. De volumes volatiel CH_4 die vanuit methaanhydraatreservoirs snel naar de atmosfeer getransfereerd kunnen worden zijn dus waarschijnlijk te klein om significante schommelingen in atmosferische broeikasgasconcentraties en het klimaat teweeg te kunnen brengen.

De algemene conclusie is dat, van de vier fundamenteel verschillende settings langsheen een (Ant)Arctische continentale rand die in deze studie geëvalueerd werden, de stabiliteit van methaanhydraten in associatie met offshore permafrost en in sedimenten bovenaan de continentale helling het gevoeligst is voor veranderingen in temperatuur en druk. Niettemin geeft het model aan dat de tijdschaal voor het dissociëren van gashydraten lang is (tienduizenden jaren), en dat deze voor continentale permafrost of diepwater hydraatreservoirs zelfs nog een grootteorde groter is (honderdduizenden jaren). Het grootste deel van het globale gashydratenreservoir is dus niet gevoelig voor smelten op tijdschalen van tientallen, honderden of duizenden jaren. Hierdoor is het onwaarschijnlijk dat een positief feedback-effect ontstaat dat snel een significante toename van methaan in de atmosfeer en dus een bijkomende opwarming kan veroorzaken. Verder blijkt dat de tijdschalen waarop variaties in atmosferische broeikasgasconcentraties en klimaatschommelingen doorheen de geologische geschiedenis hebben plaatsgevonden, sneller zijn dan de tijdschaal waarop het volume van het globale gashydraatreservoir kan slinken en terug aangroeien. Dit impliceert dat gashydraatreservoirs doorgaans in een onstabiele, vergankelijke toestand moeten zijn, ook vandaag. Voortdurend smelten hydraten of worden er hydraten gevormd, maar dit gebeurt traag, en waarschijnlijk niet (zoals in talrijke studies wordt gepostuleerd) als een directe en dynamische weerspiegeling van veranderingen in het klimaat, die zich doorgaans tien tot honderd keer zo snel manifesteren.

TABLE OF CONTENTS

CHAPTER I. INTRODUCTION, OBJECTIVES & OUTLINE

1.1. Introduction

Gas hydrates or clathrates are ice-like crystalline compounds of water and gas that are stable at low temperatures and sufficiently high pressures (Sloan, 1998). Natural gas hydrates occur in the pore space of marine sediments along deep continental margins (Birchwood et al., 2010), in the sedimentary infill of deep lakes (Khlystov et al., 2013), as well as in polar regions in association with continental and sub-shelf permafrost (Collett et al., 2011). Over the last decades, gas hydrate bearing deposits have been discovered abundantly, either directly during scientific drilling programs (Paull et al., 1996), or indirectly through interpretation of well logs (Collett and Lee, 2011) or the observation of a bottom simulating reflection on seismic reflection profiles (Shipley et al., 1979). Many studies have attempted to estimate the extent of the global gas hydrate inventory, with the most recent values generally ranging from 500 to 3000 Gton of carbon (Boswell and Collett, 2011; Buffett and Archer, 2004; Milkov, 2004).

Such vast volumes of gas hydrate constitute a significant prospective energy resource, representing an amount of energy in the same order of magnitude as the energy recoverable from conventional resources like coal, oil and natural gas (Koh et al., 2012). In addition to their potential as energy resource, scientists quickly realized that gas hydrates may also play an important role in the carbon cycle and influence global climate (Loehle, 1993; Nisbet, 1990; Paull et al., 1991). The gas, of which methane constitutes the most abundant component (Kvenvolden, 1993), is stored very efficiently in the hydrate structure; a volume of gas hydrate expands between 150-fold and 180-fold when released at standard pressure and temperature (Collett et al., 2011). If only a small portion of the clathrate inventory would destabilize, for example due to increasing ocean bottom temperatures, significant volumes of methane gas could be released into the ocean and possibly into the atmosphere, where it would act as a greenhouse gas and contribute to global warming (Archer et al., 2009a; Mienert, 2012). This positive feedback mechanism constitutes the base for a number of scientific hypotheses that claim that past, but also present (geologically) rapid climate change and fluctuations in atmospheric greenhouse gas levels, can be closely linked to variations in the size of the global gas hydrate reservoir. Widely debated examples are the *gas hydrate dissociation hypothesis* for the Palaeocene-Eocene thermal maximum (PETM), originally formulated by Dickens et al. (1995), the *clathrate gun hypothesis* for Late Quaternary glacial/interglacial and stadial/inter-stadial climatic oscillations (Kennett et al., 2003), and the hypothesis that contemporary anthropogenic climate warming will induce melting of hydrates during the upcoming centuries (Hunter et al., 2013; Marín-Moreno et al., 2013), or is already doing so on the continental slope west of Svalbard (Westbrook et al., 2009). An additional mechanism to be regarded is the build-up of excess pore pressure in continental slope sediments during hydrate dissociation, as a result of the volume expansion that accompanies the phase transition from gas hydrate to free gas and water. This can initiate submarine sediment failure and sliding, a process that could rapidly destabilize large volumes of gas hydrates (Sultan et al., 2004).

1.2. Objectives

This study aims to address the sensitivity of gas hydrate reservoirs to changing environmental parameters, which is a fundamental issue to assess the suggestive, but controversial role of gas hydrates in the carbon cycle and global climate (Buffett and Archer, 2004). It will be focused on gas hydrates in high-latitude regions, where clathrates are especially sensitive to climatic variability as a result of the greater degree of environmental change compared to lower latitude regions (Westbrook et al., 2009) and the shallower water depth below which hydrates can exist (Hunter et al., 2013).

The complexity in this discussion is that gas hydrate systems are controlled by the interplay of geological, chemical, physical and biological processes, each working in a certain direction, at a specific rate, and according to an imposed small or large set of parameters (Kvenvolden, 2002; Xu and Ruppel, 1999). Changing one parameter can alter multiple others and trigger a variety of feedback mechanisms. Many studies have focused on one specific aspect of the gas hydrate system, hereby forgetting the dynamic nature of the system and ignoring interrelated processes potentially impacting on the presented results. Indeed, the role of gas hydrates in global change is suggestive, but should however, to be fully understood, be subjected to critical and integrated research that considers the system as a whole. This dissertation therefore, in the first three chapters, attempts to provide a comprehensive overview of the processes that govern gas hydrate systems and their potential role in the carbon cycle and global climate.

Thereafter a MATLAB model is developed, based on the physical parameters and thermodynamic principles that in the first chapters are proven to be the most decisive for the scope of this study, i.e. evaluating the long-term behavior of hydrate reservoirs in response to changing environmental conditions on a large scale. It is aimed to obtain this information for methane hydrates in four distinct geographic settings across a hypothetic high-latitude continental margin, which are expected to display varying susceptibilities to changing climate (Ruppel, 2011a): (i) thick onshore permafrost, (ii) subsea permafrost below shallow shelves, (iii) feathering upper edge of the hydrate stability zone on the upper continental slope, and (iv) deepwater setting on the lower continental slope to continental rise (figure 1). At each location a one dimensional hydrate-bearing sediment column is considered, with initial temperature, pressure and hydrate or ice saturation profiles obtained from existing clathrate formation models.

Through a first set of simulations, this study aims to examine if the gas hydrate inventory in these settings is affected by realistic shifts in temperature or pressure. If so, the main questions to be answered concern the timescales, the fashion, and the extent to which this occurs. Evaluating each geographic setting individually will allow to make a side-by-side comparison of their sensitivity to environmental changes, and to predict where gas is most likely to be transferred from the gas hydrate reservoir to the atmosphere.

In a second set of simulations, it is attempted to explicitly mimic the response of high-latitude hydrates to the environmental changes accompanying the PETM, the deglaciation following the last glacial maximum (LGM), and contemporary climate warming, in order to verify the aforementioned hypotheses on the role of gas hydrates in these rapid climate change events. It is hoped that the simulations will help to elucidate if hydrate reservoirs are likely to be as sensitive as claimed by these studies. The involved hydrate volumes and timescales that appear from this study will be analyzed,

which is essential information and will add to the discussion regarding the hypothesized close connection between changes in the size of the global gas hydrate inventory and climate.

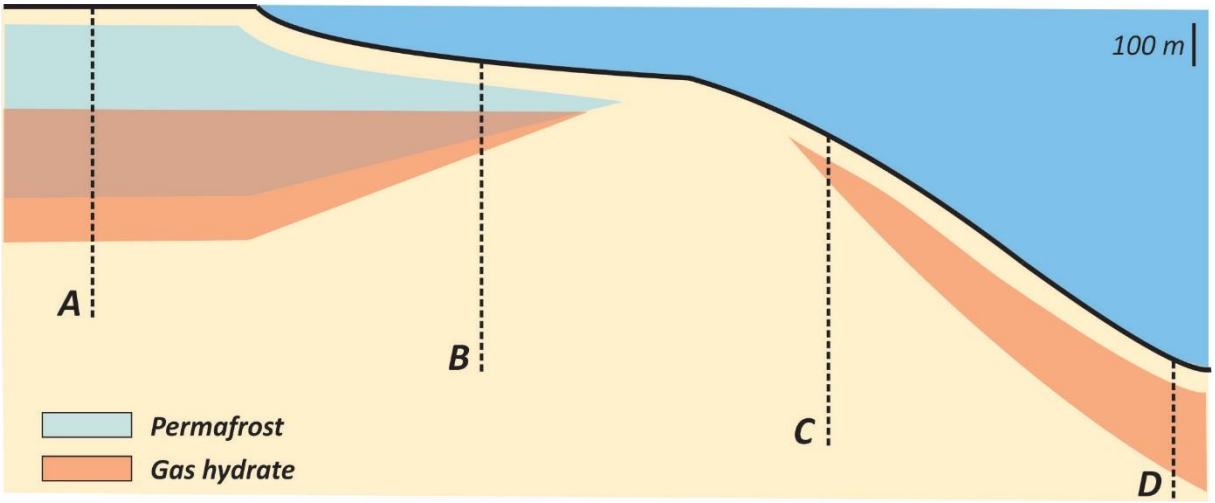

Figure 1. *Schematic profile across a hypothetic high-latitude continental margin, with one dimensional gas hydrate- and/or permafrost-bearing sediment columns in four distinct geographic settings: A. thick onshore permafrost; B. subsea permafrost below shallow shelves; C. feathering upper edge of the hydrate stability zone on the upper continental slope; D. deepwater setting on the lower continental slope or rise. In the case of Arctic continental margins the horizontal scale can range from less than 100 km to 1000 km (Ruppel, 2011a).*

1.3. Thesis outline

The first part of this dissertation (chapter 2, 3 and 4) outlines a concise summary of the wide body of literature that has originated during the past decades of gas hydrate research. Chapter 2 provides a description of the various components of the gas hydrate system, the underlying chemical and physical concepts, and the natural processes that affect gas hydrate stability. This theoretical base is utilized in chapter 3, where the formation, natural occurrence and global volumes of gas hydrates are considered. These topics have proven to be essential in studies that assess the role of the gas hydrate inventory in the Earth's carbon cycle and climate, which are addressed in chapter 4.

Chapter 5 describes the methods that are used in this study. This comes down to a discussion of how the model is built, which formulas are employed, and which assumptions are made. At the end of this chapter the different scenarios of environmental change that will be simulated are addressed. The results of these simulations are shown and shortly commented in chapter 6, while the implications of these results are discussed in chapter 7. This section also considers on which points the findings from this dissertation concur or differ with previous research, and whether the model simulations support the hypotheses that have been formulated on the role of gas hydrates in global climate. The last paragraph of this chapter comments on the strengths and the weaknesses of the model. Finally, an overview of the conclusions that can be drawn from this study is provided in chapter 8.

2.1. The gas hydrate thermodynamic-chemical system in the pore space of sediments

Gas hydrates are ice-like crystalline compounds of water and gas. The crystal structure is composed of stacks of cages formed by water molecules, in which a guest gas molecule is trapped that stabilizes the structure. Several structural types can be distinguished based on the way the cages are stacked (figure 2). The structural type generally depends on the size of the guest gas molecules. Structure I (sI) hydrate is the most common type in marine sediments, and contains small gas molecules like methane, ethane or carbon dioxide. Propane and butane mostly form structure II (sII) type hydrates, while larger hydrocarbon molecules are generally confined to structure H (sH) hydrates (Collett et al., 2009). Normally, each cage can hold at most one gas molecule, although instances of multiple occupancy of small guest molecules in the cavities of sII hydrates at very high pressure are known (Sloan and Koh, 2007). Hydrates do not form perfect crystals, i.e. not all the cages contain a guest molecule. This is quantified by the cage occupancy, which is dependent on pressure, temperature and gas composition. Cage occupancy values typically vary from 30 to 90 % when the cavity for the guest molecule in the cage is small, and can exceed 95 % for larger cavities (Sloan and Koh, 2007).

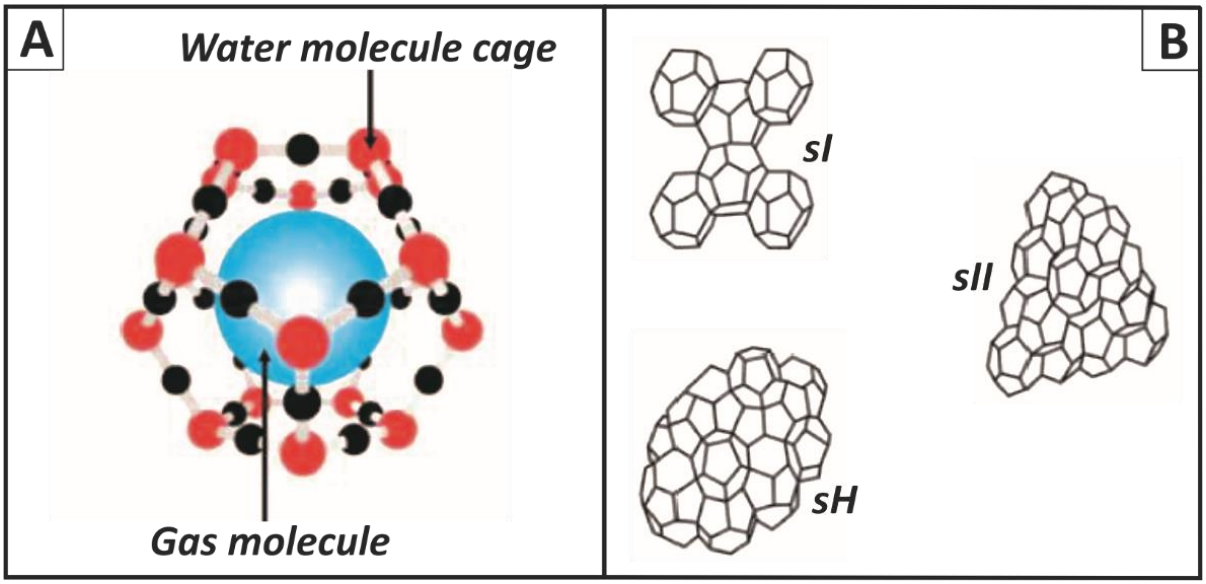

Figure 2. *The gas hydrate crystal structure, composed of cages formed by water molecules that enclose a guest gas molecule (A). These cages can be stacked in different ways, depending on the structural type (B): structure I (sI), structure II (sII) or structure H (sH) (modified after Collett et al., 2009).*

As soon as gas hydrates began to be discovered in nature, it readily appeared that they occupy the pore space of sediments if low temperature and high pressure conditions prevail, and if an adequate supply of gas is available (Davie and Buffett, 2001). To accurately describe the stability of gas hydrates in a column of sediments, the pore space of this column needs to be considered as a thermodynamic system with a number of chemical components, distributed over a number of phases. The concerned chemical components are (i) gas (predominantly methane), (ii) water, and (iii), if seawater is considered, salts and other additives. The possible phases are (i) a liquid phase (seawater with dissolved gas and salts), (ii) a free gas phase, (iii) a solid methane hydrate phase

(Zatsepina and Buffett, 1998), and (iv) an extra solid ice phase in case a permafrost-bearing column is studied. The stable phase at a specific temperature and pore pressure within the sediment column depends on the phase equilibria, that represent the state of the system with minimal free Gibbs energy (Zatsepina and Buffett, 1998).

Figure 3 shows the temperature for the three phase equilibrium T_3 between gas hydrate, free gas, and seawater as a function of depth or pore pressure P. Various experimental studies have established this relationship by fitting a curve to laboratory or field measurements, and hence multiple expressions exist, which are each valid over a certain temperature or pressure range (Dickens and Quinby-Hunt, 1994; Sloan, 1998; Tishchenko et al., 2005).

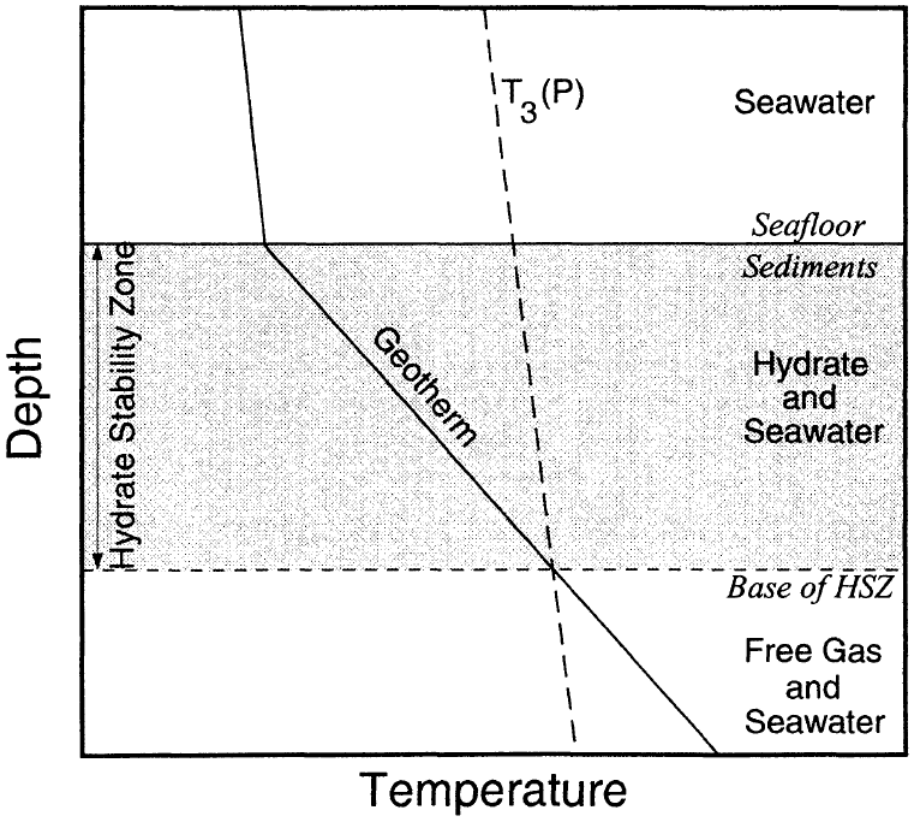

Figure 3. *Schematic profile of the hydrate stability zone in a marine sediment column. The base of the hydrate stability zone is defined by the depth where the geotherm (solid line) intersects the temperature for three phase equilibrium $T_3(P)$ (dashed line) between hydrate, aqueous solution and free gas (after Davie and Buffett, 2001).*

The depth where the geotherm exceeds $T_3(P)$ defines the base of the hydrate stability zone (HSZ): above (where $T < T_3$) hydrates are stable, while free gas is confined to the zone below. The latter is the case in the naturally most common situation where the amount of water in the pore space exceeds the amount that is stoichiometrically required to convert all the free gas to gas hydrate, so that after hydrate formation, hydrates coexist with water. In the exceptional situation where there is excess gas available in the pore space during the formation of gas hydrates, a 'dry' HSZ can be created in which hydrates coexist with free gas, because all the water is consumed to form hydrates (Behseresht and Bryant, 2012). The transition from gas hydrate to free gas constitutes a large P-wave contrast and hence commonly appears as a bottom simulating reflection (BSR) on reflection seismic profiles (Shipley et al., 1979). The extent of the HSZ is thus governed by the in situ pore pressure (dependent on water depth and pressure gradient in the sediment column), by the temperature at the seabed and the geothermal gradient in the sediments, and by $T_3(P)$, which additionally depends

on the salinity of the pore water (Dickens and Quinby-Hunt, 1994) and gas composition (Sloan, 1998). The addition of salts tends to depress $T_3(P)$, while adding other gas components than methane shifts T_3 (P) to higher values.

However, the HSZ only delineates the maximal extent of hydrate occurrence. Inside the HSZ, hydrates will solely form if the concentration of dissolved gas in the pore water equals or exceeds the solubility. If not, all the gas will remain dissolved in the pore water. The same accounts for the free gas underneath the HSZ: gas bubbles will only evolve from the liquid phase if there is excess gas in the system (Davie and Buffett, 2001). The solubility of the gas in seawater is determined by the two-phase equilibria between gas hydrate and seawater within the HSZ, and between free gas and seawater below the HSZ. These again vary with pressure, temperature, salinity and gas composition (Tishchenko et al., 2005). Figure 4 shows the solubility of methane in seawater as a function of depth below the seafloor, which increases from the seafloor to the base of the HSZ, and remains nearly constant below because of the opposing effects of increasing temperature and pressure (Zatsepina and Buffett, 1998).

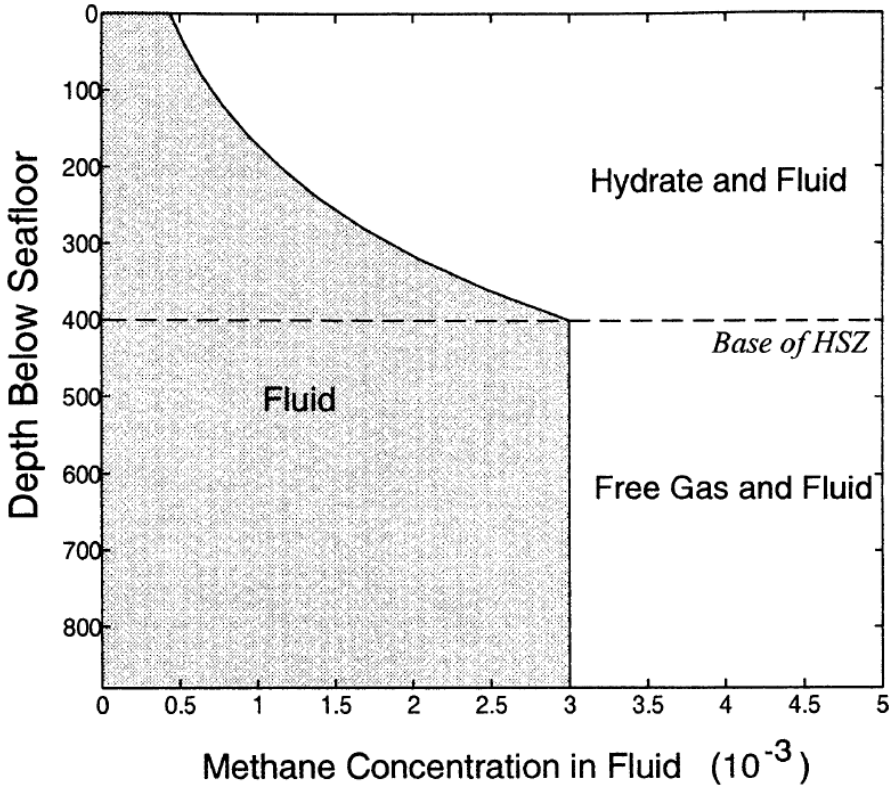

Figure 4. *Solubility of methane as a function of depth below the seafloor (in m). The solubility increases from the seafloor to the base of the HSZ, and remains fairly constant below because of the counteracting effect of pressure and temperature. If the methane concentration exceeds the solubility, methane hydrate is stable above the base of the HSZ and free gas is stable below. If not, methane remains dissolved in the pore fluid. Methane concentration in the pore fluid is expressed as a mass fraction (after Davie and Buffett, 2001).*

As an important result, illustrated in figure 5 for methane clathrate, gas hydrates not necessarily occur over the entire depth interval of the HSZ, and hence the actual zone of gas hydrate occurrence does not always coincide with the HSZ (Xu and Ruppel, 1999). It should be noted that the top of the sediment column is almost always unoccupied by gas hydrates because the mass fraction of dissolved gas in the pore water decreases rapidly towards the seafloor. This is a result of the low gas concentration in the ocean bottom water, which causes the gas to diffuse from the sediment column

to the overlying ocean (Davie and Buffett, 2001). Anaerobic oxidation of methane (AOM) by sulphate reducing bacteria further depletes the pore water in the upper meters of the seabed in methane (Knittel and Boetius, 2009). Similarly, the low gas concentrations in the ocean bottom water also explains why gas hydrates generally do not form within the water column above the seafloor, although the temperature of the bottom water usually falls below T_3, as shown in figure 3 (Archer et al., 2009a). Only at locations where a large supply of gas is sustained over a long period, hydrate formation can prevail over hydrate dissolution, so that hydrates occur closer to or even at the seafloor at those specific sites (Archer, 2007). Nevertheless, as clathrates have a lower density than seawater, buoyancy effects will detach hydrates from the seafloor and carry them initially through, and eventually out of the water column HSZ, which further impedes the presence of hydrates at the seafloor (Buffett and Archer, 2004).

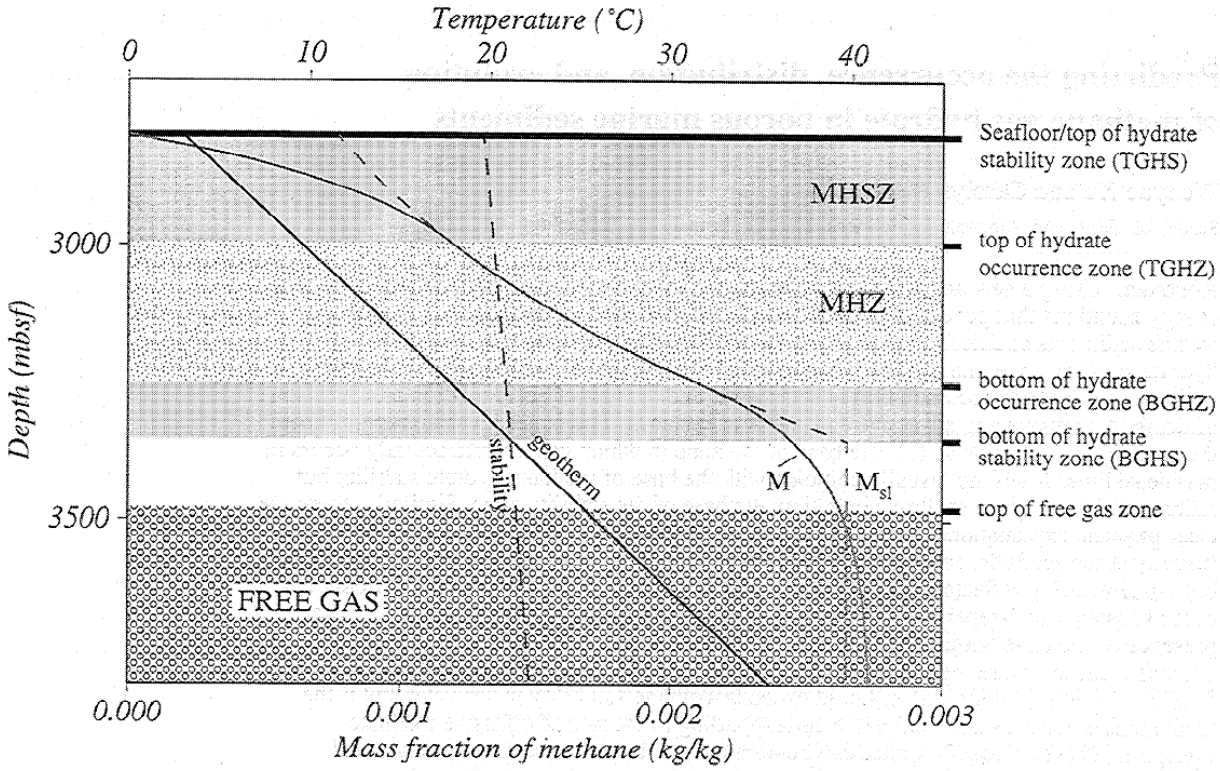

Figure 5. *The relationship between (i) the methane hydrate stability zone (MHSZ), bordered by the seafloor and the intersection of the geotherm with the T_3 (P) stability boundary, and (ii) the methane hydrate occurrence zone (MHZ), which is subjected to the additional constraint that the fraction of dissolved methane (M) should equal or exceed the methane solubility (M_{sl}). Similarly, below the HSZ free gas only exists at depths where M exceeds M_{sl} (after Xu and Ruppel, 1999).*

Figure 5 illustrates that a sustainable and adequate supply of gas is needed for gas hydrates to occur and remain stable (Xu and Ruppel, 1999). The most abundant gas component in natural clathrates is methane (Kvenvolden, 1993), which is produced within the sediment column by microbial conversion of organic matter (Buffett and Archer, 2004). The amount of organic carbon supplied to the seafloor is linked to water depth, with the highest values at shallower water depths because of enhanced primary production rates as a result of coastal upwelling, nutrient runoff from rivers and nutrient recycling from shallow sediments (Buffett and Archer, 2004). For a fixed amount of organic carbon, the sedimentation rate controls the rate of carbon supply (Davie and Buffett, 2001). However, the fraction of organic carbon that subsequently gets buried below the upper meters of sediment into the so-called methanogenesis zone, where the conversion to methane by microbial activity

eventually takes place, is small, and is most sensitive to the amount of organic carbon rain and the O_2 concentration of the overlying water (Buffett and Archer, 2004). The time that bacteria spend inside the methanogenesis zone, and hence the fraction of organic carbon that can be converted to methane, also depends on sedimentation rate: rapid sedimentation implies less time for bacteria to generate methane (Davie and Buffett, 2001). Next to in situ production, biogenic or thermogenic methane and other hydrate forming gases from a deeper source can be brought into the system by an upward flux of gas, by diffusion down the compositional gradient, as gas dissolved within migrating pore water (i.e. advection), or as a separate gas phase (Collett et al., 2011; Rempel and Buffett, 1997). The light isotopic composition of carbon retrieved from gas hydrate samples, with $\delta^{13}C$ values around -60 ‰ (Milkov, 2005), indicates that biological sources predominate in most cases (Archer and Buffett, 2005), although instances of thermogenic gas hydrates are also known (Collett et al., 2011; Sassen et al., 1999).

2.2. Sediment properties and bulk properties of the sediment column

In addition to the processes operating within the pore space of sediments, which are outlined in the previous section, the characteristics of the sediment itself and the sediment column as a whole also need to be evaluated. These can have important repercussions for the stability of gas hydrates in the natural environment, for the temperature and pressure evolution in the subsurface, for the system's response to possible temperature, pressure or salinity anomalies, and for processes like pore fluid flow.

Firstly, besides the above described importance of the organic content in the sediments, the mineralogy of the sediments can also affect hydrate stability. Some researchers have argued that the presence of some clay types, like bentonite, facilitate methane hydrate crystallization from aqueous solution, because the clays provide nucleation sites for the formation of hydrates (Cha et al., 1988; Park and Sposito, 2003; Seo et al., 2009). Contrary, other studies have predicted that the presence of clays can depress water activity by bonding water molecules to hydrophilic clay surfaces, which would inhibit hydrate formation (Clennell et al., 1999). Dewatering of clays at depth can also reduce salinity, and consequently has an indirect impact on the stability of clathrates (Davie and Buffett, 2001).

Secondly, core observations that gas hydrates preferentially form in coarse sands have raised the question how grain size controls hydrate distribution (Garg et al., 2008). A first explanation is that permeabilities are generally higher in coarse grained sediments and therefore, according to Darcy's law, allow higher fluid flux and methane supply (Burwicz et al., 2011). Furthermore, grain size distribution, together with the packing of the sediments, impact on the pore size distribution, which in turn determines to what extent capillary effects will act at the liquid-hydrate or liquid-gas interface (Liu and Flemings, 2011). Capillary effects cause an increase of the methane solubility in the pore water, and thus inhibit hydrate growth in the two phase (liquid + hydrate) zone. This effect is more pronounced if the water depth is large and the mean pore size small (Liu and Flemings, 2011). In addition, capillary effects between the pore water and both free gas and gas hydrate, allow free gas to exist above, and hydrates to exist below the base of the HSZ. A significant consequence is a widening of the three-phase equilibrium boundary marking the base of the HSZ, as described above, to a three-phase zone, where gas hydrate, free gas and liquid can coexist over a certain depth interval within the sediment column. The thickness of this interval correlates to the wideness of the

pore-size distribution (Liu and Flemings, 2011). The occurrence of such a three-phase region in marine sediments can alternatively be attributed to changes in salinity that accompany hydrate formation at the base of the HSZ. Salt is assumed to remain confined to the liquid phase during hydrate formation, and hence salinity increases as hydrates form. This adds an extra thermodynamic degree of freedom and allows gas hydrate, free gas and liquid to coexist over a particular depth range. A large and fast supply of gas into the HSZ is required to produce meaningful changes in salinity (Clennell et al., 1999; Zatsepina and Buffett, 1998).

Further significant properties of the sediment column when assessing gas hydrate stability are porosity and permeability. Porosity decreases exponentially with depth because of compaction, and as a result, the pore fluid is pressurized (Burwicz et al., 2011; Davie and Buffett, 2001). As already mentioned above, the permeability of the sediments (along with the viscosity of the fluid) will control if this will result in pore fluid flow: in high permeable sediments the pressurized pore fluid is squeezed out easily, and hence the excess pressure that results from compaction is released by upward fluid flow. In contrast, impermeable sediments do not allow fluid flow and excess pore pressure accumulates in the pores (Burwicz et al., 2011). It is noted that the presence of gas hydrates in the pores can prevent normal sediment compaction and reduce the porosity decrease with depth (Sultan et al., 2004).

To complete this section, some final parameters have to be considered. Firstly, the thermal conductivities and heat capacities of the sediment and the individual phases in the pore space can be combined to the bulk thermal conductivity and bulk heat capacity of the sediment column, based on the densities and volume saturations of the different phases in the pore space (Rempel and Buffett, 1997; Xu and Ruppel, 1999). The bulk thermal conductivity determines how easily heat is conducted through the sediment column, although heat can also be transported by advection through the fluid (Rempel and Buffett, 1997). The pressure regime, volume saturations and densities of the phases in the pore space will also determine the mechanical properties of the sediment column. The sediment strength determines how easily the sediments will deform and if failure is likely to occur (Sultan et al., 2004; Xu and Germanovich, 2006). The significance of such processes is discussed below.

CHAPTER III. FORMATION AND NATURAL OCCURRENCE OF GAS HYDRATES

The location and distribution of gas hydrates in the subsurface can be determined directly by scientific or industrial drilling (e.g. Paull et al., 1996), or can be inferred through interpretation of geophysical borehole data (Collett and Lee, 2011) or a bottom simulating reflector (BSR) on seismic profiles (Shipley et al., 1979). The thus discovered gas hydrates are shown in figure 6.

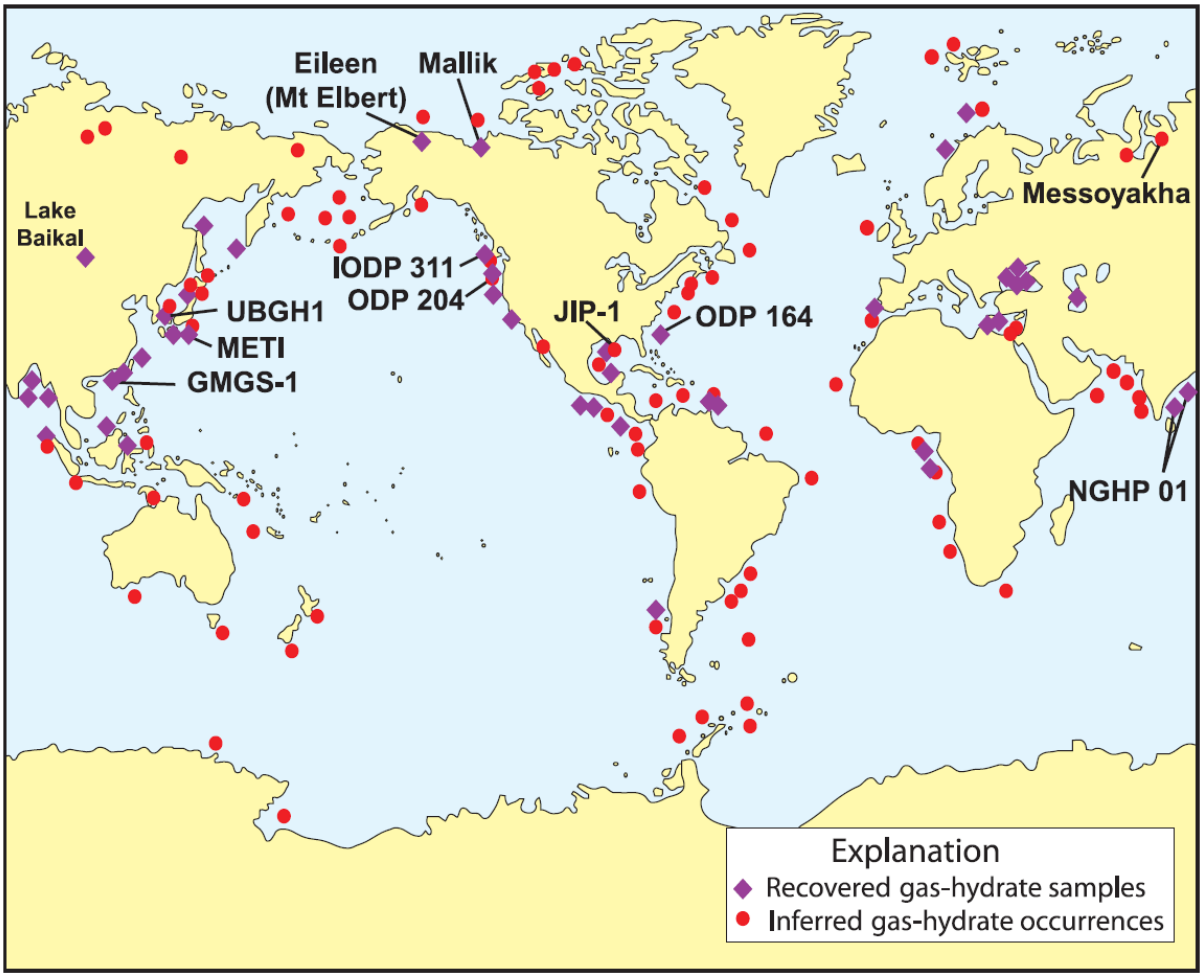

Figure 6. *Location of recovered and inferred gas hydrates. Most of the recovered gas hydrate samples have been retrieved during drilling or coring programs (IODP = Integrated Ocean Drilling Program; UBGH1 = Ulleung Basin Gas Hydrate Expedition 1; ODP = Ocean Drilling Program; JIP = Joint Industry Project; METI = Ministry of Economy, Trade, and Industry; GMGS = Guangzhou Marine Geological Survey; NGHP = India National Gas Hydrate Program). Most of the inferred gas hydrate occurrences result from observations of a BSR on reflection seismic profiles (after Collett et al., 2009).*

3.1. Formation models

To expand this fragmented record of natural gas hydrate occurrences and to assess the extent of the global gas hydrate inventory, formation models have been developed. With these models it is aimed to elucidate where clathrates occur in nature, how they are distributed in the subsurface, and how fast they accumulate. All models employ the above described theoretical framework, but each model

has a specific approach, attaches importance to different aspects, and relies on varying basic assumptions.

A first set of models considers a porous sediment column, in which hydrates start to accumulate as fluxes of heat, methane, and pore fluid pass through the sediments (Rempel and Buffett, 1997; Xu and Ruppel, 1999). Rempel and Buffett (1997) derive an analytical solution for hydrate growth in a porous, uniform half-space when it is cooled at its boundary, by solving mass and energy balance equations for a two phase system (water + gas hydrate). This essentially comes down to solving a moving phase-boundary problem, also called Stefan problem (Caldwell and Kwan, 2004). The release of latent heat during hydration formation is a crucial process which needs to be accounted for in the energy equation. Conversely, during hydrate dissociation, latent heat constitutes an important heat sink in the energy equation (Sultan et al., 2004). Rempel and Buffett (1997) further account for the kinetic barriers to the growth of hydrate crystals, which could lead to hydrates existing in thermodynamic disequilibrium with the surrounding fluid. However, they conclude that these nonequilibrium effects are negligible in natural environments, since the growth time associated with nonequilibrium effects is much shorter than the thermal and chemical diffusion times. Their results indicate an increase in hydrate volume of 1% of the pore space per 10^5 yr, in response to an instantaneous cooling of 5°C, with the hydrate saturation decreasing from the base of the hydrate layer to the top. Xu and Ruppel (1999) extended the work of Rempel and Buffett (1997) by considering a three phase system, thus additionally accounting for gas bubbles (free gas phase) in the system, and by allowing diffusion of gas through the pore fluid in addition to advection. Importantly their analytical model explains the existence of a three phase zone of finite thickness, and validates possible disparities between the hydrate stability zone from pressure-temperature conditions and the real hydrate occurrence zone, and between the position of the top of the free gas zone and the base of the hydrate stability zone (figure 5). They denote that gas hydrates accumulate at a slower rate, over thinner intervals, and in a more uniform fashion in diffusion-dominated systems than in advection-dominated systems, and conclude that most natural gas hydrate systems must be advective-dominated, with active continental margins representing a high flux advective end-member, and passive margins representing a low flux advective end-member (rather than a diffusion-dominated end-member). Another early study (Clennell et al., 1999) complements above models by also accounting for the properties of the host sediments, which can interfere with hydrate growth kinetics and stability, for example through capillary effects, as already outlined above. They conclude that gas hydrates can be distributed very heterogeneously, as a result of variations in the sediment's mineralogy and texture throughout the sediment column.

In this first set of models, gas hydrates can actually accumulate until almost the entire pore space is filled as long as the gas supply is maintained (Davie and Buffett, 2001). However, measurements of gas hydrate volumes in nature rarely exceed 10 to 20 % of the pore volume, an observation which demands a thorough evaluation of how the gas supply is regulated (Davie and Buffett, 2001). The numerical model of Davie and Buffett (2001) meets this demand, and quantifies the supply of carbon to the sediments through sedimentation, and the subsequent microbial conversion to methane. Thus assuming that in situ production of methane is the only source of gas, their model reaches a steady state after a 5 to 10 Ma period of sedimentation, meaning that the depth profiles of dissolved methane concentration, hydrate saturation and free gas saturation do not longer change through time. They find that in the absence of upward fluid migration, the hydrate saturation at steady state

is limited to 7 % of the pore space at the base of the hydrate zone when a reasonable organic content in the sediments at the seafloor of 1.5 % is assumed. Like in previous models this value decreases towards the top of the hydrate bearing column. Importantly, the existence of a steady state implies that hydrate saturation cannot be used to estimate accumulation time when solely in situ production of methane is considered. Higher hydrate saturation values can be attained, but this requires an upward fluid flow or gas diffusion through the pore water to supply additional gas to the HSZ (Davie and Buffett, 2001).

The above models, and later models that largely rely and build further on them (Davie and Buffett, 2003; Garg et al., 2008; Xu, 2004) all focus on the marine environment. The formation of gas hydrates associated with permafrost is less elaborated. Clathrates can be linked to both onshore and subsea permafrost, where the latter is generally accepted to represent relic onshore permafrost, formed during periods of sea level lowstand, and later flooded during subsequent sea level rise (Rachold et al., 2007). The sub-permafrost gas hydrate deposits observed in the Mount Elbert Stratigraphic Test Well, North Slope Alaska, are interpreted as converted free gas accumulations (Boswell et al., 2011). This mechanism, in which an original free gas accumulation is later converted to a gas hydrate accumulation after the imposition of gas hydrate stability conditions, is also accepted for other Arctic hydrate reservoirs, like in the Prudhoe Bay and Kuparuk River areas on the North Slope of Alaska (Collett, 1993). The base of the HSZ actually moves down to and through an existing petroleum system when Arctic conditions start to prevail, which happened around 1.8 Ma ago on the Alaska North Slope (Collett, 1993; Dai et al., 2011).

As the base of the HSZ moves down, gas hydrate is formed and the accompanying volume reduction is compensated by the influx of a volume of free gas ΔV_g and/or a volume of water ΔV_w, which causes the gas-water contact (GWC) at the base of the gas column to rise. The resulting gas saturation profile is shown in figure 7. Modelling of this process shows that the volume change accompanying hydrate formation and the sediment properties (which influence capillary entry pressures) are key factors in predicting hydrate saturations in such ‘converted free gas’ hydrate reservoirs (Behseresht and Bryant, 2012). After the conversion of free gas to gas hydrate, conditions favoring the formation of permafrost are installed. Hence, a certain fraction of the pore water will freeze, so that over a certain depth interval gas hydrates can coexist with ice. Permafrost is defined as sediment or rock that has remained at a temperature at or below 0 °C for at least two years (Rachold et al., 2007). Hence permafrost can be ice-bonded (also called ‘frozen’) when the pore space is entirely cemented by ice, but ice-bearing or ice-free (‘unfrozen’) permafrost also exist, especially when the freezing point of the pore water is depressed by the presence of salts (Rachold et al., 2007).

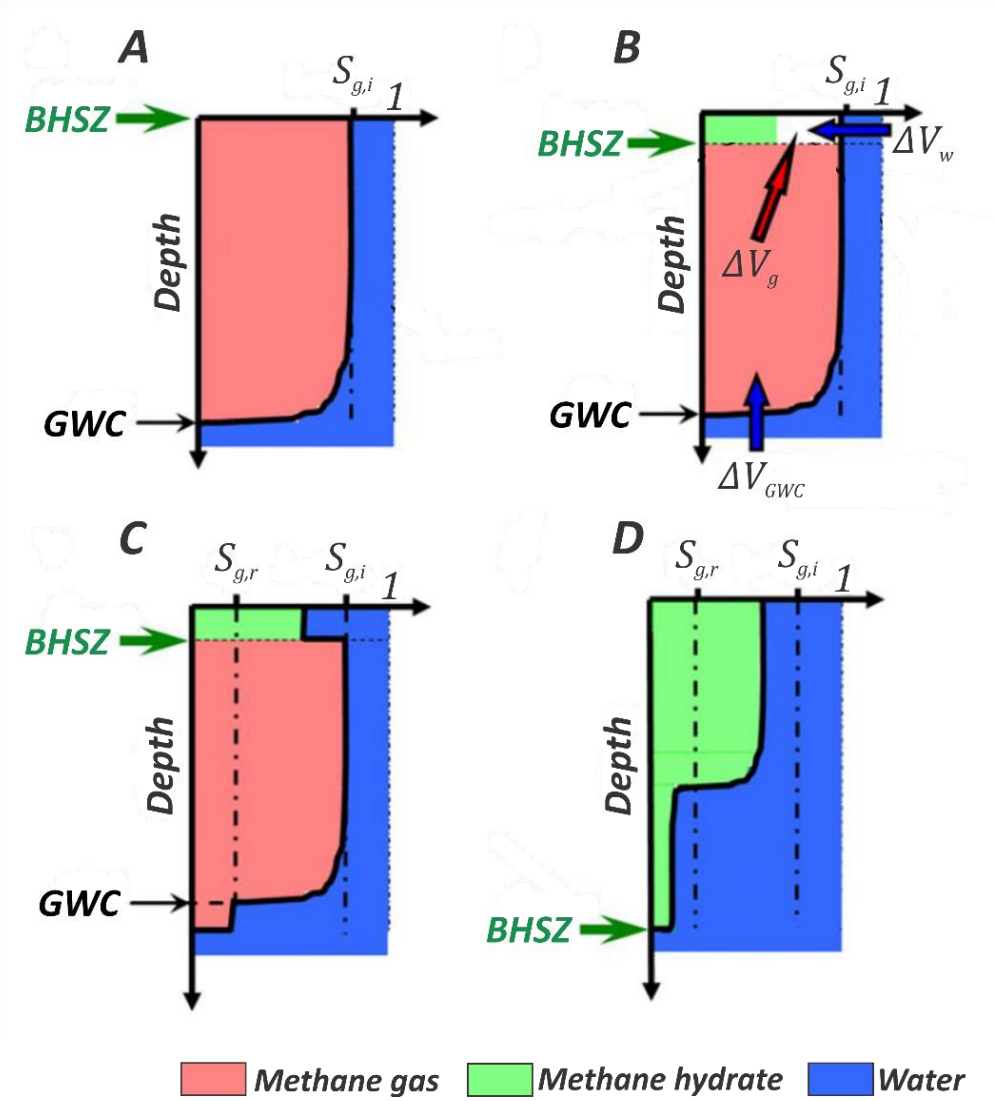

Figure 7. *Formation model for 'converted free gas' hydrate accumulations. The base of the HSZ (BSHZ) moves down an isolated free methane accumulation with an initial gas saturation profile $S_{g,i}$ (A). As a result methane hydrates form, and the accompanying volume reduction is compensated by the influx of a volume of gas ΔV_g and a volume of water ΔV_w, which causes the gas-water contact (GWC) to rise as a volume of water ΔV_{GWC} imbibes from below (B-C). The initial free gas saturation in the imbibed volume at the base decreases to the residual gas saturation $S_{g,r}$. The resulting hydrate saturation profile is shown in (D) (modified after Behseresht and Bryant, 2012).*

3.2. Gas hydrate occurrences in nature and size estimates of the global gas hydrate inventory

Suitable pressure-temperature conditions and sufficient gas supply for gas hydrates to be stable exist in nature in continental margin sediments below water depths ranging from 1000 to 3000 m (Kvenvolden, 1993), and in deposits below shallower water depths in higher latitude and permafrost regions (Collett et al., 2009). Examples of gas hydrates in the sedimentary infill of lake Baikal (Khlystov et al., 2013) and the Black Sea (Zillmer et al., 2005) are also known. Formation models and field measurements have pointed out that gas hydrate saturations depend on local factors like gas supply and oxygen level in the water. Active continental margins differ from passive margins because of the more pervasive fluid migration which scavenges gas from a broader region. This will result in

higher hydrate saturations on active margins compared to passive margins (Buffett and Archer, 2004). In addition, localized faults constitute preferential conduits for pore fluid and gas, from which confined high saturation (up to 30 to 50 %) hydrate accumulations can originate (Buffett and Archer, 2004). Furthermore, lower oxygen levels in the Pacific Ocean imply an enhanced preservation of organic carbon compared to the Atlantic Ocean, so the largest portion of the global hydrate inventory is expected to occur in the Pacific (Archer et al., 2009a).

The size of this global gas hydrate inventory is an important point in gas hydrate research. Many studies have addressed this question, and hence a wide range of estimates is available. These estimates rely on observational studies, in which field measurements are extrapolated, or on numerical modelling, which often employ above described formation models as a guide (Burwicz et al., 2011). As reviewed by Milkov (2004), estimates before 2001 generally converged towards a 'consensus' value of 10,000 Gton of methane carbon (Kvenvolden, 1993). This estimate relied on the assumptions that gas hydrates occur over large portions of continental margins and at relatively high hydrate saturations (around 10 %). However, results from drilling campaigns showed that both the assumed area occupied by hydrate-bearing sediments and the hydrate saturations were too high (Milkov, 2004). Subsequent studies (Archer et al., 2009a; Boswell and Collett, 2011; Buffett and Archer, 2004; Burwicz et al., 2011; Milkov, 2004; Piñero et al., 2013) generally report lower values of maximum 3000 Gton carbon, although higher and exceptionally high estimates of over 60,000 Gton methane carbon (Klauda and Sandler, 2005) have been suggested.

Ruppel (2011a) recognizes five distinct geographic sectors over which the total gas hydrate inventory is distributed, and roughly estimates which percentage of the inventory is present in each setting. Clathrates related to onshore and shallow offshore subsea permafrost, like on the Alaska North Slope (Boswell et al., 2011; Collett, 1993) or the East Siberian Arctic shelf (Romanovskii et al., 2005), both account for less than 1% of the global hydrate volume, while very located hydrate deposits that occur in association with gas seeps like in lake Baikal or the Black Sea (Khlystov et al., 2013; Zillmer et al., 2005) constitute only a trace component. Consequently, most gas hydrates can be found in the deep water realm, either in sediments on the lower continental slope and continental rise (± 95.5% of the global inventory), or in upper continental slope sediments at the so-called feather edge of the HSZ (± 3.5% of the total hydrate volume on Earth).

Nevertheless, a clear consensus value on the global extent of the gas hydrate reservoir has not emerged during the past years of research, which poses a major problem in evaluating the potential role of gas hydrates in the Earth's climate (Piñero et al., 2013). Furthermore, the above estimates in most cases solely apply to gas hydrate volumes, while the amount of gas dissolved in the pore water or free gas trapped below gas hydrates is not considered. However, significant estimates of 2000 Gton carbon in the form of methane bubbles below the HSZ have been made (Buffett and Archer, 2004), which implies that these reservoirs cannot be overlooked, and need to be taken into account when assessing the role of clathrate-bound gas in the global carbon cycle and climate (Dickens, 2011).

CHAPTER IV. ROLE OF CLIMATE-SENSITIVE GAS HYDRATE RESERVOIRS IN GLOBAL CLIMATE

4.1. Gas hydrates in the global carbon cycle and climate

The above outlined amounts of gas, either sequestered in gas hydrates or occurring as dissolved or free gas, soon motivated the belief that a dynamic gas hydrate system could play a major role in the global carbon cycle, and consequently in global climate, especially because of the relatively shallow depth of this gas reservoir in the Earth's geosphere (Kvenvolden, 1988; MacDonald, 1990). Disturbances at the surface or seafloor, like a rise in temperature or a decrease in pressure (e.g. as a result of falling sea level) inhibit the stability of the hydrate reservoir, which is believed to be one of the most significant carbon pools in the global carbon cycle (Buffett and Archer, 2004; Kvenvolden, 2002). If this actually results in dissociating hydrates, large amounts of gas, most notably the potent greenhouse gases methane and its oxidation product CO_2, can be released into the near-surface environment and eventually into the atmosphere, which certainly would contribute to climate warming (Archer, 2007). Conversely, the gas hydrate reservoir also works as a sink for methane, when hydrate stability conditions are favored when pressure increases (for example through rising sea level) or climate cools (Kvenvolden, 2002). Importantly, the timescales for hydrate formation and dissociation are different: the clathrate reservoir is believed to have accumulated over millions of years in response to gradual cooling ocean temperatures over geologic time (Davie and Buffett, 2001; Xu and Ruppel, 1999), while melting of hydrates could take place over time spans in the order of thousands of years (Archer et al., 2009a).

Several cases of past changes in atmospheric methane concentration, inferred from terrestrial and oceanic isotopic records, have been interpreted as abrupt (regarding geological timescales) methane escape from melting methane hydrates. A first and famous example is the onset of the Palaeocene-Eocene thermal maximum (PETM), where a large amount of isotopic light carbon was added to the atmosphere as indicated by a negative excursion in carbon isotope values ($\delta^{13}C$) of 2-4 ‰ in benthic and planktic foraminifera, or even exceeding 5 ‰ in terrestrial carbonates and organic matter, within a time period of maximum 60 kyr (Dickens, 2011; McInerney and Wing, 2011). The observed carbon isotope excursion (CIE) across the PETM requires a release of ± 2000-3500 Gton of methane carbon with $\delta^{13}C$ = -60 ‰ from hydrates (Archer, 2007). A simultaneous shift in $\delta^{18}O$ values indicates that this global event was accompanied by a temperature increase of 4-6 °C, and lasted for less than 200 kyr after the initiation period of max. 60 kyr (McInerney and Wing, 2011). Further research has indicated that this event is not a unique case, and, though being the most pronounced, fits within a series of 'hyperthermal' events occurring during a period of long-term warming in the early Paleogene (Zachos et al., 2010). Quaternary climatic oscillations constitute a second example of how changes in the size of the global methane clathrate inventory may influence atmospheric methane concentrations and climate. The *carbon pump hypothesis*, which states that methane is rapidly released from melting hydrates in high-latitude regions after a small triggering event (e.g. release of methane from shallow gas pools), has been invoked as an explanation for the observed rise in atmospheric CH_4 and CO_2 levels at the end of the last and penultimate glaciation (Loehle, 1993; Nisbet, 1990). Other studies argue that clathrates already start to destabilize as the glaciation progresses, because of falling sea level and subsequent decreasing pressures. The resulting gradual

buildup of atmospheric methane and warming limits the extent of the glaciation (Paull et al., 1991). The *clathrate gun hypothesis* (Kennett et al., 2003) adopts similar ideas as formulated in the *carbon pump hypothesis*, but applies them to additionally explain higher frequency millennial-scale atmospheric methane oscillations. The authors of the theory also attribute abrupt warming events and negative carbon isotope excursions in the Late Quaternary record to an enhanced methane flux from the marine hydrate reservoir to the atmosphere, which is believed to be a response to changing ocean circulation patterns that bring warmer bottom waters over continental margins at intermediate water depths. Kennett et al. (2003) note that the elevated atmospheric methane levels seem to coincide with episodes of sediment slumping and sliding along continental margins. As such, large volumes of clathrate could destabilize on a very short timescale, followed by a massive and rapid input of methane in the atmosphere during Quaternary interstadials.

Above investigations were the first to involve gas hydrates in the debate concerning the labile Quaternary climate. However, the *clathrate gun hypothesis*, as well as the *gas hydrate dissociation hypothesis* for the PETM, are not unequivocally accepted within the research community. The amount of methane carbon released and the rate at which this happened are contested. Furthermore, at the time the *clathrate gun hypothesis* was formulated, no compelling evidence existed that methane from melting hydrates effectively reaches the seafloor or the sea surface (Dickens, 2003). However, this issue was instigated after the discovery of presently active gas seeps on the West Svalbard continental margin (Westbrook et al., 2009). Acoustic images show that plumes of gas bubbles emanate from the seafloor between 150 m and 400 m water depth, and rise at some locations to 50 m below the sea level. Westbrook et al. (2009) argue that this phenomenon is at least partly connected to a downslope retreat of the feather edge of the HSZ, because of the melting of hydrates in response to a 1 °C warming of the West Spitsbergen current over the past thirty years. This hypothesis is supported by seismic studies (Sarkar et al., 2012) and numerical modelling (Reagan et al., 2011). However, the late 20th century timing for the onset of hydrate-controlled methane seepage off Svalbard is opposed by Berndt et al. (2014). Isotopic measurements on carbonate crusts, resulting from authigenic precipitation driven by microbial anaerobic oxidation of methane, provide evidence that methane seepage has been going on for at least 3 kyr. Therefore, the observed gas flares off Svalbard cannot be considered as compelling evidence for enhanced hydrate destabilization in response to increasing bottom water temperatures over the last thirty years (Berndt et al., 2014). In addition, other research on the continental margin off NW-Svalbard has indicated that the position of gas seeps is mainly controlled by lithological variations in the continental slope sequences, which dictate the migration pathways of deeper thermogenic gas (Rajan et al., 2012). The impermeable glacigenic debris flow deposits prevent vertical migration towards the seabed, and instead force the gas to migrate upslope along permeable hemipelagic strata at their base. Acoustic flares, detected by the echo sounder system, prove that the gas is consequently expelled on the shelf where the permeable strata outcrop at the seabed. This shows that the positions of the gas flares not necessarily need to be linked to dissociating gas hydrates. Furthermore, circular depressions on the seafloor without associated gas flares, interpreted as pockmarks, also indicate past methane release activity (Rajan et al., 2012).

4.2. Susceptibility of the clathrate inventory to changing environmental parameters

Apart from the debate whether present-day active gas seeps are already a manifestation of contemporary climate change or not, if due to anthropogenic greenhouse gas emissions ocean

temperatures keep rising, as foreseen in various climate reports (IPCC, 2013), a significant part of the global gas hydrate reservoir is likely to melt. Similar to the situation at the PETM and last glaciation, this could induce rising atmospheric methane concentrations and add to further climate warming (Archer et al., 2009a). Assessing the role of this feedback loop in past and future climate change scenarios requires a thorough evaluation off how the hydrate reservoir reacts when the parameters that govern it are altered.

Evidently a temperature increase at the top of a gas hydrate bearing sediment column will progressively disturb the temperature profile in the subsurface. After some time, depending on the thermal properties of the sediments and phases in the pore space of the column, the temperature pulse will reach the hydrate-bearing zone. If gas hydrates are no longer stable at the newly imposed temperature, they can disappear either through dissociation or dissolution. Dissociation of hydrates commonly occurs at the base of the HSZ, at depths where the temperature exceeds the temperature for three phase equilibrium T_3. This results in the generation of free gas and water. Dissolution of gas hydrates takes place within the HSZ, when the dissolved gas concentration at a certain depth falls below the solubility of the gas in seawater, the latter raised by the temperature increase. Dissolution generally does not result in generation of free gas in natural environments. It is important to differentiate between dissociation and dissolution of gas hydrates, as the generation of free gas can result in excess pore pressure due to the increase in volume associated with the dissociation process, provided that the permeability of the sediments is too low for the excess volumes to be rapidly expelled from the pore space through increased fluid flow (Xu and Germanovich, 2006). Excess pore pressure reduces the sediment strength, and can create or reactivate faults, fluid flow channels or even slope failure. Such mechanisms constitute very efficient pathways for the migration of free gas from melting hydrates, and would cause a catastrophic release of gas to the ocean (Sultan et al., 2004). However, increasing pressure also tends to stabilize clathrates, and the buildup of excess pore pressure will thus impede further dissociation (Holtzman and Juanes, 2011). This inhibition mechanism for gas hydrate dissociation is further supported by the accompanying decrease in salinity, as pure water incorporated in the clathrate structure is progressively added to the pore water. This raises T_3 and thus has a stabilizing effect (Xu and Germanovich, 2006). An even more pronounced effect arises when hydrates dissociate at temperatures below 273 K. In this case a layer of ice forms around the dissociating hydrate crystal, which coats and seals the interior hydrate and thus prevents further dissociation (Takeya et al., 2005). This effect was called self-preservation (Yakushev and Istomin, 1992), and causes hydrates below 273 K to remain stable at anomalously low pressures (Sloan, 1998). Another factor to take into account is the consumption of heat during gas hydrate dissociation, in the form of latent heat associated with the phase transition. This delays the propagation of the temperature pulse through the subsurface. Therefore, the time required for the sediment column to obtain a new equilibrium temperature profile is largely dependent on the thickness of the hydrate occurrence zone (Archer, 2007). Finally, it should also be noted that increasing bottom water temperatures are likely to be associated with a rising sea level. This causes an increase in hydrostatic pressure in the pore space, and will thus counteract hydrate dissociation upon warming. Reversely, hydrate destabilization in response to a sea level fall-induced decrease in pressure, will be counteracted by the accompanying climate cooling (Buffett and Archer, 2004).

The above discussion demonstrates that evaluating the susceptibility of gas hydrates to changing environmental conditions is not straightforward. There are a variety of processes and subsequent

feedback mechanism, each influencing hydrate stability to a certain extent. It is important to know at which timescales these mechanisms operate, which are the most decisive, and what part of the clathrate inventory is susceptible to change. To assess these issues, field campaigns and laboratory measurements have been complemented by modelling studies, which in contrast to the above described steady state formation models, address the time-dependent behavior of the clathrate inventory upon climatic and anthropogenic forcing (Archer and Buffett, 2005). One of the first dynamic models was presented by Xu (2004), which lead to the conclusion that gas hydrate systems respond relatively fast (< 10^5 yr) to theoretical environmental changes like a pressure drop or temperature increase at the seafloor. Later models have employed a similar approach to integrate scenarios of future climate and sea level change with a dynamically behaving clathrate reservoir. Archer et al. (2009) estimate a potential escape of 35-940 Gton of carbon worldwide in response to 3 °C bottom water temperature warming, which would cause a 0.4 – 0.5 °C rise in temperature over timescales of millennia and longer. Under the worst-case future climate change scenario, global methane fluxes through the seabed from destabilizing hydrates of 30-50 Mton methane per year are foreseen by 2100 (Hunter et al., 2013). The models predict that shallow Arctic and Subarctic gas hydrate reservoirs will be most susceptible to contemporary global warming (Biastoch et al., 2011). It is suggested that for the Arctic Ocean west of Svalbard alone, approximately 5000 to 30000 ton of methane per year may be released from melting hydrates during the upcoming centuries as a result of ocean warming (Marín-Moreno et al., 2013). Warming North Atlantic water over the past 5 kyr, caused by changes in the Gulf Stream, is also inferred to be currently destabilizing 2.5 Gton of methane hydrate on the western North Atlantic margin (Phrampus and Hornbach, 2012).

4.3. Does methane reach the atmosphere?

After all, one key issue remains to be discussed: does methane (or other gas components) from melting hydrates reach the atmosphere? If this is the case, the increase in the atmospheric concentrations of methane and its oxidation product CO_2, which are both greenhouse gases, is expected to add to already warming climate (Archer, 2007). This positive feedback loop is of major concern in contemporary climate research, but is however poorly constrained.

In a first step, the liberated gas from melting clathrates has to migrate through the sediments towards the seafloor. Along this trajectory, several factors can impede the gas to reach the ocean. Firstly, if the free gas saturation is low, gas bubbles will stay immobile by the effects of surface tension and remain trapped where they originated, or they will dissolve in the pore water (Davie and Buffett, 2001; Ruppel, 2011a). If free gas bubbles do rise through the sediments, they first have to pass the hydrate stability zone in the overlying cooler sediments, where the gas will be recycled to form hydrates. Above this ‘physical cap’, the sulphate reduction zone constitutes an additional ‘chemical cap’ in the near-seafloor sediments (Archer et al., 2009a). In this zone, sulphate reducing bacteria will further deplete the pore fluids in methane (Knittel and Boetius, 2009). Nevertheless, the occurrence of features like pockmarks on the seafloor, as well as ‘wipe-out’ zones on seismic profiles, prove that it is possible for the gas to pass these barriers within the sediment column (Archer et al., 2009a). Critical factors to achieve this are the thickness of the sediment column through which the gas has to migrate, the bubble volume (i.e. the fraction of free gas in the pore fluid), and the rate at which the bubbles rise (Archer et al., 2009a; Kvenvolden, 2002; Ruppel, 2011a). Gas from shallow hydrate reservoirs is more likely to reach the seabed, as well do rapidly rising gas bubbles at high saturations. The presence of structural features like faults also provide conduits for rapid migration

of gas (Buffett and Archer, 2004). Lastly, build-up of excess pore pressure during hydrate melting and potential subsequent slope failure is one more scenario that has often been put forward to provide rapidly large quantities of gas to the ocean (Archer, 2007).

Except for continental permafrost-related settings, the gas released from the sediments still has to ascend through the water column before entering the atmosphere. However, gas bubbles easily dissolve in the ocean water, and may thereafter also be oxidized by aerobic microbes (Archer, 2007; Ruppel, 2011a). For example, the plumes of gas observed along the western continental margin of Svalbard all originate at sites shallower than 400 m water depth, but none of them extends up to the sea surface (Westbrook et al., 2009). Furthermore, studies of gas bubble plumes in the Black Sea have shown that, even when these plumes reach the sea surface, it is unlikely that they still contain methane, because methane is dissolved into the seawater and replaced by other gases like oxygen and nitrogen during the ascent to the sea surface (Greinert et al., 2006; McGinnis et al., 2006). It is concluded that gas may only reach the atmosphere at sites where the ocean is sufficiently shallow (only a few tens of meters deep), as is for example the case on the East Siberian shelf, where methane from melting clathrates is at present thought to be released to the atmosphere (Archer, 2007; Shakhova et al., 2010). Nevertheless, it should be remarked that, although the direct climate impact of methane liberated at the seafloor is buffered by the water column, an indirect impact may still appear, since oxidation of methane to CO_2 depletes the water column in O_2 and acidifies the ocean. Consequent equilibration between CO_2 levels in the atmosphere and the ocean may cause a transfer of CO_2 to the atmosphere, and hence increases atmospheric greenhouse gas concentrations (Ruppel, 2011b).

5.1. Constraining the study area

Multiple studies have addressed the sensitivity of gas hydrates to changing environmental conditions in mid- to high-latitude marine settings (Archer and Buffett, 2005; Archer et al., 2009a; Biastoch et al., 2011; Hunter et al., 2013). This study focuses on a high-latitude continental margin, where hydrates additionally occur in association with continental and relic subshelf permafrost. Considering a cross-section through such a margin hence allows to evaluate four adjacent but distinct geographic settings: (i) thick onshore permafrost, (ii) shallow marine subshelf permafrost, (iii) feathering upper edge of the HSZ on the upper continental margin, and (iv) deeper water setting on the lower continental slope (figure 1). The profile shown in figure 1 is hypothetic, but could for example be a schematic representation of the present-day situation on the Alaska North slope or the East Siberian Arctic shelf (figure 8). Polar regions are of specific interest in climate research, because of the greater degree of temperature change compared to lower latitude regions (Westbrook et al., 2009). Furthermore, gas hydrates are expected to be most sensitive to climatic variability at high latitudes because clathrates are prevalent below shallower water depths (Hunter et al., 2013).

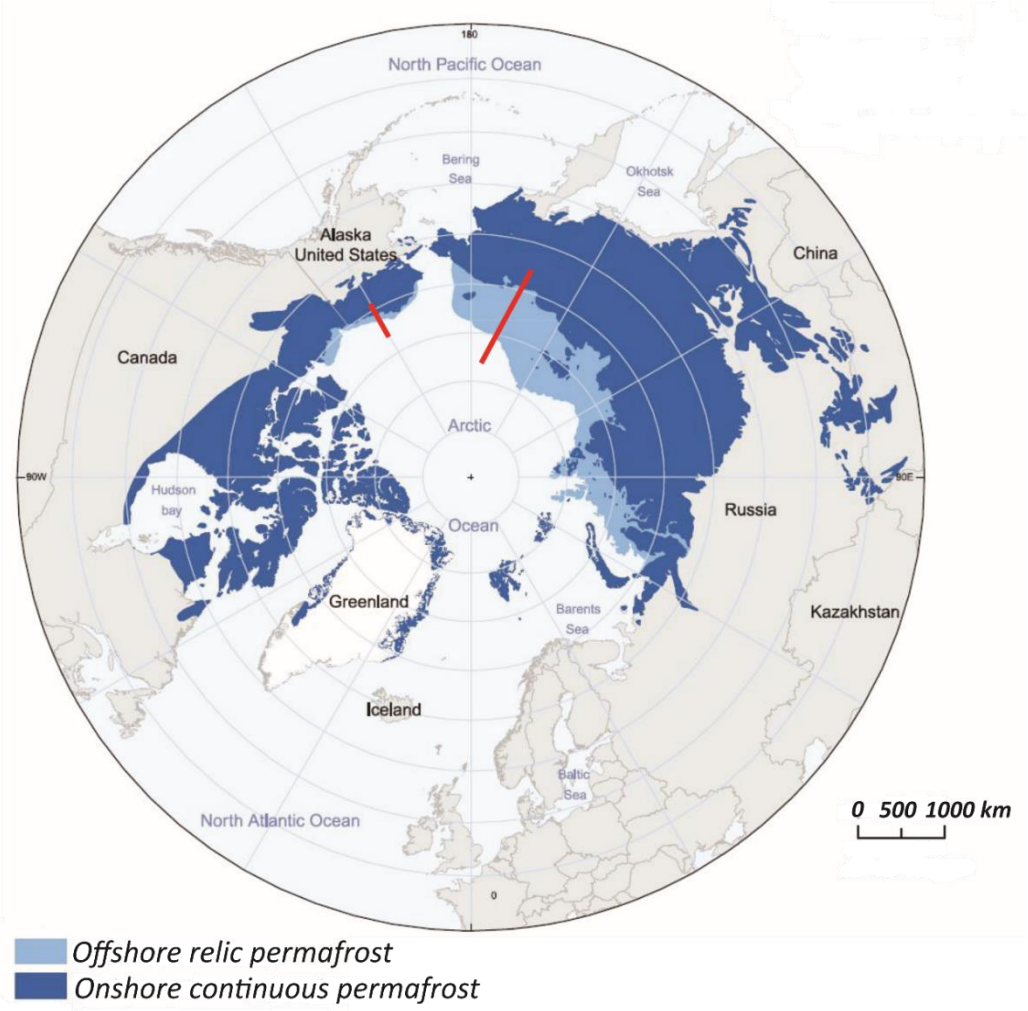

Figure 8. *Distribution of onshore and relic offshore permafrost in the Northern Hemisphere, anno 2009. The red lines indicate potential locations on the Alaska North slope or East Siberian shelf for the continental margin cross-section presented in figure 1 (after Collett et al., 2009).*

5.2. Model description

A MATLAB model is developed to evaluate the response of the gas hydrate inventory to a set of climate change scenarios. At each of the four geographic settings a one dimensional sediment column is considered. This section explains how the model is elaborated. It is opted for a 1D model for reasons of simplicity, and because most hydrates occur in stratigraphically constrained reservoirs, which lack significant lateral variations (Archer et al., 2009a). The MATLAB code can be found in the appendix, or can be requested for by e-mailing to Thomas.Mestdagh@UGent.be.

5.2.1. Modelling the initial configurations

It is aimed to constrain realistic starting conditions. For that reason, existing formation models are implemented in MATLAB to establish initial temperature, pressure and gas hydrate saturation profiles.

The model of Xu and Ruppel (1999) is adopted to design the initial conditions for the permafrost-free marine sediment columns on the upper and lower continental slope. This analytical model provides equations to calculate the positions of the top and base of the hydrate stability and occurrence zones, and derives an expression for the rate of hydrate accumulation as a function of depth, by solving momentum, mass and energy balance equations. The considered gas is methane, which is supplied through advection or diffusion. In situ biogenic methane production through ongoing sedimentation is not considered (sedimentation rate = 0 m/s). The constant fluxes of total mass and energy, q_f and q_e respectively, are given by:

$$q_f = \frac{-k\rho_l}{\mu_l}\left(\frac{dP}{dz} + \rho_l g\right) \qquad [1]$$

$$q_e = q_f\, C_{pl} T - \lambda \frac{dT}{dz} \qquad [2]$$

where z is the spatial coordinate that is 0 at the seafloor and points upward, k is permeability, μ_l and ρ_l represent the viscosity and density of the aqueous phase, g is the gravitational acceleration, C_{pl} denotes the isobaric specific heat capacity of the liquid, and λ stands for effective thermal conductivity. Integration of [1] and [2] yields expressions for pressure P (in Pa) and temperature T (in °C) as a function of z, q_f and q_e:

$$P - P_0 = -\left(\frac{q_f \mu_l}{k\rho_l} + \rho_l g\right) z \qquad [3]$$

$$z = \begin{cases} -\dfrac{\lambda}{q_f C_{pl}} \ln\left(\dfrac{q_e - q_f C_{pl} T_0}{q_e - q_f C_{pl} T}\right) & q_f \neq 0 \\ -\dfrac{\lambda}{q_e}(T - T_0) & q_f = 0 \end{cases} \qquad [4]$$

with T_0 and P_0 the temperature and pressure at the seafloor. Substituting equation [4] into [3] gives an expression that relates the temperature at depth z directly to the pressure at this depth.

The above equations can now be coupled with empirical methane hydrate stability curves to determine the top and base of the hydrate stability zone (HSZ), respectively denoted with the

symbols z_{st} and z_{sb}. By fitting a trendline to $P - T_{diss}$ datapoints obtained from the CSMHYD software by Sloan (1998), an equation is acquired that provides the temperature for hydrate dissociation T_{diss} (in K), which is equivalent to the temperature for three phase equilibrium T_3, at a given pressure (in kPa) between 0 and 20000 kPa and a salinity of 35 ‰:

$$T_{diss} = \begin{cases} 9.6349 \cdot \ln(P) + 197.65 & P \geq 2576.74\ kPa \\ 0.0158 \cdot P + 232.7 & P < 2576.74\ kPa \end{cases} \quad [5]$$

To obtain the best fit through the empirical datapoints, two separate equations are regarded. For pressures above 2576.74 kPa (equivalent to $T_{diss} \approx 273.15\ K$), $T_{diss}(P)$ can be described by a logarithmic expression with an R^2 value of 0.9985. Below 2576.4 kPa, $T_{diss}(P)$ behaves linearly (R^2 = 0.9984). The depths at which the temperature exceeds T_{diss} define the top and the base of the HSZ. However, for marine settings the top of the HSZ generally falls within the ocean and not within the sediment column, hence the seafloor constitutes the uppermost limit of hydrate stability if only the sub-seabed domain is considered.

Equations [6] and [7] allow to determine the depth of the top of the hydrate occurrence zone (z_{ot}), i.e. the depth below which hydrates are actually present:

$$z_{ot} = \begin{cases} -\dfrac{\emptyset \mathrm{K}_m}{q_f} \ln\left(\dfrac{q_{mt} - q_f M_0}{q_{mt} - q_f M_{sl}(z_{ot})}\right) & qf \neq 0 \\ -\dfrac{\emptyset \mathrm{K}_m}{q_{mt}} \left(M_{sl}(z_{ot}) - M_0\right) & qf = 0 \end{cases} \quad [6]$$

where

$$q_{mt} = q_f M_{sl}(z_{ot}) - \emptyset K_m \left(\frac{dM_{sl}}{dz}\right)_{z=z_{ot}} \quad [7]$$

The base of the hydrate occurrence zone (z_{ob}) can be determined iteratively using following equation:

$$q_m = q_f M_{sl}(z_{ob}) - \emptyset K_m \left(\frac{dM_{sl}}{dz}\right)_{z=z_{ob}} \quad [8]$$

The variable q_m represents the depth-dependent methane flux, with q_{mt} denoting the value at the top of the hydrate occurrence zone, while ∅ is the porosity and K_m equals the product of the fluid density and the dispersion-diffusion coefficient D_m. M_0 denotes the mass fraction of methane dissolved in the bottom water, which is in most cases negligible and hence assumed to be 0 kg/kg. To solve equations [6] - [8], the solubility of methane in the liquid phase as a function of depth, $M_{sl}(z)$, has to be known. This is obtained from Davie et al. (2004), who present a practical method to calculate methane solubility within the HSZ as a function of temperature for fresh and saline water:

$$M_{sl}(T) = M_{sl,3}(T_3, P, S) \cdot exp\left(\frac{T - T_3}{\alpha}\right) \quad [9]$$

In this equation M_{sl} is expressed in mM, α is an empirical constant equal to 14.4 °C, and $M_{sl,3}(T_3, P, S)$ is the methane solubility for the conditions at the base of the HSZ, i.e. for water with salinity S at three phase equilibrium temperature T_3 and pressure P, given by:

$$M_{sl,3}(T_3, P, S) = (1 - \beta S) \times \left\{ M_{sl,3}(T_{ref}, P_{ref}) + \frac{\partial M_{sl,3}}{\partial T}(T_3 - T_{ref}) + \frac{\partial M_{sl,3}}{\partial P}(P - P_{ref} \right\} \quad [10]$$

with $M_{sl,3}(T_{ref}, P_{ref})$ a reference solubility equal to 156.36 mM at T_{ref} = 292 K and P_{ref} = 20 MPa, and empirical values β, $(\partial M_{sl,3})/\partial T$ and $(\partial M_{sl,3})/\partial P$ equal to 0.1 mol^{-1}, 6.34 mM/°K and 1.11 mM/MPa respectively. Writing equation [4] explicitly to T and substituting this expression for T in [9], yields M_{sl} as a function of depth below seafloor z, expressed in mM. After conversion to mass fraction (kg/kg) values, $M_{sl}(z)$ can be adopted in equations [6] – [8] to calculate z_{ot} and z_{ob}. Similar to the approach of Davie et al. (2004), M_{sl} is assumed to be constant and equal to $M_{sl}(z_{sb})$ below the base of the HSZ (cfr. figure 4).

Finally Xu and Ruppel (1999) provide equations to determine the hydrate saturation throughout the hydrate occurrence zone. The time required for methane hydrate to fill the pore space to a hydrate saturation S_h is approximated by:

$$\tau' \approx S_h \left(\frac{\partial S_h}{\partial t} \right)^{-1} \quad [11]$$

where the methane hydrate accumulation rate $\partial S_h/\partial t$ at depth z is calculated by evaluating following equation at that depth:

$$\frac{\partial S_h}{\partial t} = \frac{1}{\emptyset(\rho_h M_h - \rho_l M_{sl})} \left(\emptyset K_m \frac{d^2 M_{sl}}{dz^2} - q_f \frac{dM_{sl}}{dz} \right) \quad [12]$$

with ρ_h and M_h being the methane hydrate density and the mass fraction of methane in the hydrate phase. Equations [11] and [12] allow to calculate the hydrate saturation profile throughout the hydrate occurrence zone after any period of accumulation τ' when methane is supplied through diffusion and advection.

The above approach for marine sediments cannot be applied to the onshore and subshelf permafrost bearing sediment columns, since these settings require consideration of an extra solid ice phase. On the Alaska North Slope, this type of hydrate deposits has been interpreted to result from conversion of free gas accumulations after conditions conducive to hydrate formation are imposed (Boswell et al., 2011). In this study, the clathrates in the permafrost related settings will also be considered as such converted free gas accumulations, and the model of Behseresht and Bryant (2012) is applied to set the initial hydrate saturation profiles. This model assumes that the base of the HSZ migrates down the sediment column in response to cooling at the surface, instead of presuming a fluid flux into the HSZ like in the marine model described above. A box model is developed to assess the resulting hydrate saturation profile, for a homogenous sediment column with a converted methane gas accumulation that is sealed at the top and isolated from the gas source. This column is considered as a stack of open boxes of 1 m^3, with an initial gas saturation $S_{g,i}$. As a result of the downward movement of the base of the HSZ, free methane gas is gradually converted to methane hydrate, which is associated with a decrease in volume. The volume reduction is compensated by the influx of a volume of free gas ΔV_g and/or volume of water ΔV_w, which causes the gas-water contact (GWC) at the base of the gas column to rise. The parameter R_v is defined as the ratio of the volume of gas that entered the box, to the total volume of gas and water that entered the box:

$$R_v = \frac{\Delta V_g}{\Delta V_g + \Delta V_w} \quad [13]$$

The abundance of water in the marine environment and the high permeability of the sediments considered in this study assure that excess water is provided to the boxes to convert all the gas into gas hydrate, so that after conversion the box is occupied by hydrate and water (cfr. figure 7). The resulting hydrate saturation is given by:

$$S_h = \frac{\bar{V}_h}{R_v\left(\bar{V}_h - \bar{V}_g - N\bar{V}_w\right) + \bar{V}_g} S_{g,i} \quad [14]$$

with $\bar{V}_h$, $\bar{V}_g$ and $\bar{V}_w$ representing the molar volumes of hydrate, gas and water, which can be calculated by dividing the molecular weight by the density of these components. N denotes the hydration number in the hydrate lattice, $CH_4.N(H_2O)$, which is assumed to be constant and equal to 6. Per converted box of 1 m^3 at the top of the gas accumulation, the gas water contact rises over a distance equal to:

$$\Delta GWC = \frac{\Delta V_{GWC}}{\left(1 - S_{g,r}\right) \times \emptyset} \quad [15]$$

where $S_{g,r}$ stands for the residual gas saturation after water imbibes the boxes at the base of the gas accumulation from below. ΔV_{GWC} can be calculated as follows:

$$\Delta V_{GWC} = \left\{\frac{N\bar{V}_w + \bar{V}_g}{\bar{V}_h} - 1\right\} \times S_h \emptyset R_v \quad [16]$$

Once the base of the HSZ descends below the position of the GWC, the hydrate saturation can be calculated using $R_v = 0$ and $S_{g,r}$ instead of $S_{g,i}$ in equation [14]. This way a hydrate saturation profile similar to that shown in figure 8 is obtained. The timescale for the formation of this column is not considered. Subsurface temperatures are defined by assuming a value at the seafloor or surface and a geothermal gradient, which is smaller in permafrost (G_{pf}) than in ice-free sediments (G). The subsurface pressure regime is presumed to be hydrostatic. It is assured that the initial free gas accumulation spans a depth interval that falls within the limits for hydrate stability for the newly imposed cooler conditions. The deepest occurrence of permafrost is denoted by the intersection of the geothermal gradient and the freezing temperature of water, which varies with pressure and salinity according to the formula of Millero and Leung (1976):

$$T_{freeze} = -0.0575 \cdot S + 1.710523 \cdot 10^{-3} \cdot S^{\frac{3}{2}} - 2.154996 \cdot 10^{-4} \cdot S^2 - 7.53 \cdot 10^{-4} \cdot P \quad [17]$$

where T_{freeze} is expressed in °C, P in dbar and S in ‰. The initial free gas accumulations considered in this study are located at subsurface depths where, upon cooling, the base of the HSZ migrates first down the column and subsequently the water-ice phase transition, so that in the end hydrates can coexist with ice. The ice is assumed to occupy a fraction $(1 - S_h)$ of the pore space.

The units of the parameters used in the above equations might differ, since they are assembled from a variety of publications. As for the continuation of the model, all parameters are converted to SI units, with the spatial coordinate z originating at the seafloor and pointing downwards, which is opposite as was done when implementing the formation model of Xu and Ruppel (1999).

5.2.2. Modelling heat flow and hydrate dissociation

In the next step the response of the above established sediment columns to imposed changes in the environmental conditions are modelled. A change in bottom water temperature or temperature at the Earth's surface will disrupt the entire subsurface temperature profile, which is assumed to originally be in equilibrium with the geothermal heat flow at the specific location of the column. The evolution of the temperature profile through space (z) and time (t) towards a new equilibrium situation is described by the heat conduction equation, which for a one dimensional column appears as:

$$\frac{\partial T(z,t)}{\partial t} = \kappa \frac{\partial^2 T}{\partial z^2} + s(z,t) \qquad [18]$$

where $s(z,t)$ is a term added to account for possible heat sources or sinks, and κ is the effective thermal diffusivity (in m^2/s) equal to:

$$\kappa = \frac{\lambda}{\rho_l C_{pl}} \qquad [19]$$

λ represents the bulk thermal conductivity of the sediment column, and hence λ and also κ (through equation [19]) depend on the relative amounts of sediment and different phases present in the pore space at depth z and time t. However, these parameters are assumed to be constant in this study. The small variability of ρ_l with P and T is also ignored. Equation [18] is initially numerically solved using the finite difference method, without accounting for term $s(z,t)$:

$$T_{nk} = T_{(n-1)k} + \frac{\kappa \Delta t}{\Delta z^2}\left(T_{(n-1)(k-1)} - 2T_{(n-1)k} + T_{(n-1)(k+1)}\right) \qquad [20]$$

The temperature at time n and depth k is calculated based on the temperature at the previous time step n-1 at depths k, k-1 and k+1. Δt and Δz represent the time step and depth step respectively, and are bound to the condition for the numerical solution to be stable:

$$\Delta t \leq \frac{\Delta z^2}{2\kappa} \qquad [21]$$

A set of boundary conditions needs to be defined to solve equation [20]. At $t = 0$, the temperature at each depth is defined by the formation model of Xu and Ruppel (1999) as described by equation [4], or set according to the assumptions made when implementing the formation model of Behseresht and Bryant (2012) for permafrost-bound gas hydrates. The temperature evolution through time at the top boundary, i.e. the seafloor (or Earth's surface in the case of the onshore permafrost setting), is prescribed by the considered climate change scenario. A constant heat flux is assumed at the bottom of the column.

It is acknowledged that $s(z,t)$ constitutes an important term in equation [18] when a hydrate- and/or ice-bearing column is considered. The dissociation of gas hydrates and melting of ice involves a phase transition and consumes heat. During the phase transition heat is added while temperature remains constant at T_{diss} (for dissociating hydrates) or T_{freeze} (for melting ice), as shown in figure 9. In order to melt all clathrates or ice, the added heat needs to exceed the latent heat of gas hydrate or ice, L_h and L_I respectively. The temperature can only resume to rise again after all hydrates or ice are melted. This constitutes a sink of heat and delays the propagation of a temperature pulse through the column. To account for this process in the model, an approach similar to that of Roose et

al. (2006) is adopted. At each time step, the temperature profile through the column is first calculated using equation [20]. At depths within the hydrate occurrence zone this temperature is then corrected to T_{diss} if the initially calculated temperature exceeds T_{diss} (obtained from equation [5]). Similarly, the temperature is corrected to T_{freeze} (from equation [17]) at depths where ice is present but thermodynamically unstable. If both ice and gas hydrates are present and supposed to be melting, the temperature is readjusted to the minimum of T_{freeze} and T_{diss}. Per time step and at each depth where a phase transition is taking place, an amount of heat dQ, equal to:

$$dQ = C_p \cdot dT \qquad [22]$$

is then added to the heat that has accumulated (Q_{acc}) over previous time steps since the start of the phase transition. Equation [22] applies to a unit mass of hydrate or ice, with C_p denoting the isobaric heat capacity of these phases. dT is the temperature difference between the initially calculated temperature from equation [20] and the temperature after correction for the presence of melting hydrates and/or ice. The response of the hydrate and ice saturation (S_h and S_I) to the accumulation of heat upon melting is approximated as follows:

$$S_{h/I} = S_{i,h/I} \times \frac{L_{h/I} - Q_{acc,h/I}}{L_{h/I}} \qquad [23]$$

where $S_{i,h/I}$ represents the initial hydrate or ice saturation. S_h and S_I decrease as heat accumulates, and eventually turn zero once the accumulated heat equals L_h or L_I. Hereafter temperature can rise again according to equation [20]. By tracking the shallowest and deepest occurrence of gas hydrate and ice at each time step, the evolution of the top and base of the hydrate occurrence and permafrost bearing zone through time are reconstructed.

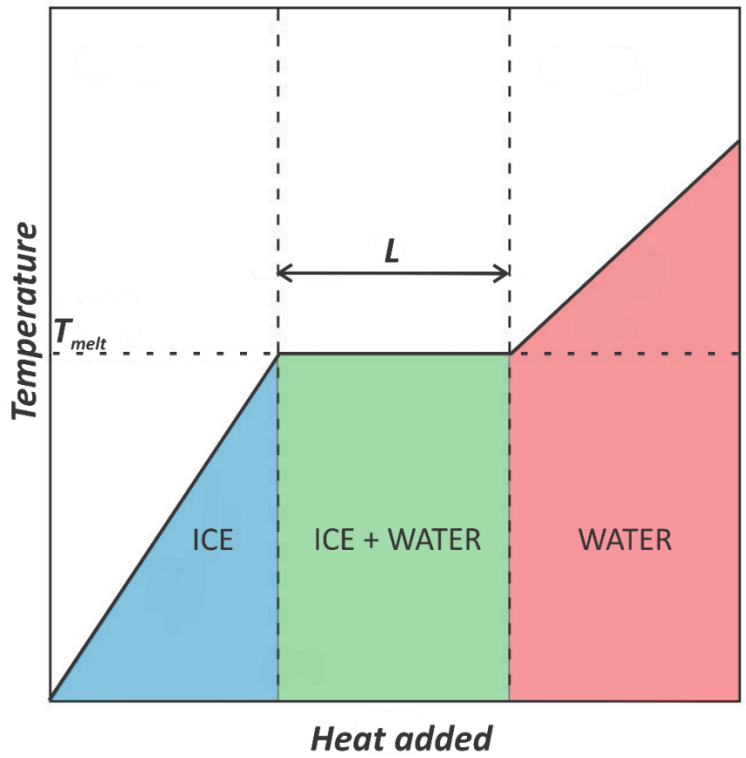

Figure 9. *Temperature evolution during the melting of ice. As heat is added, temperature initially increases until the melting temperature of ice, T_{melt}, is reached. Temperature then remains constant during the phase transition, until the heat added (since the start of melting) exceeds the latent heat for melting of ice L. Once all the ice is converted to water, temperature can rise again upon heating. The same story applies to dissociation of gas hydrates (after Giancoli, 2007).*

Parameter	*Definition*	*Value*	*Unit*
z	Depth, origin at seafloor, positive values below sea floor		m
t	Time		s
Δz	Depth interval	5	m
Δt	Time interval	3.1557×10^7	s
P	Pressure		Pa
T	Temperature		K
S	Salinity	35 [1]	‰
G	Geothermal gradient	0.05 [1]	K/m
G_{pf}	Geothermal gradient in permafrost	0.02 [2]	K/m
g	Gravitational acceleration	9.81 [1]	m/s^2
$\emptyset$	Porosity	0.5 [1]	m^3/m^3
k	Permeability	1×10^{-14} [1]	m^2
λ	Effective thermal conductivity	1.7 [3]	$W/(m \cdot K)$
κ	Thermal diffusivity (equation [19])	3.9×10^{-7} [3]	m^2/s
C_{pl}	Isobaric specific heat capacity of the liquid	4.18×10^3 [1]	$J/(kg \cdot K)$
C_{ph}	Isobaric specific heat capacity of hydrate	2.16×10^3 [7]	$J/(kg \cdot K)$
C_{pI}	Isobaric specific heat capacity of ice	2.03×10^3 [8]	$J/(kg \cdot K)$
L_h	Latent heat of melting gas hydrate	4.30×10^5 [6]	J/kg
L_I	Latent heat of melting ice	3.34×10^5 [8]	J/kg
Q, Q_{acc}	Heat, heat accumulated during phase transition		J
μ_l	Dynamic viscosity of liquid phase	8.87×10^{-4} [1]	$kg/(m \cdot s)$
ρ_l	Density of liquid phase	1024 [1]	kg/m^3
ρ_h	Density of methane hydrate	930 [4]	kg/m^3
ρ_m	Density of methane gas	55 [5]	kg/m^3
S_h, S_g, S_I	Saturation, i.e. volume percent of pore space occupied by gas hydrate, free gas, ice		m^3/m^3
D_m	Dispersion-diffusion coefficient	1.3×10^{-9} [1]	$kg/(m \cdot s)$
K_m	$D_m \times \rho_l$		$kg^2/(m^4 \cdot s)$
z_{st}, z_{sb}	Depth of top HSZ, depth of base HSZ		m
z_{ot}, z_{ob}	Depth of top of hydrate occurrence zone, depth of base of hydrate occurrence zone		m
z_{pft}, z_{pfb}	Depth of top of permafrost bearing zone, depth of base of permafrost bearing zone		m
q_f	Flux of total mass	4×10^{-8} [1]	$kg/(m \cdot s)$
q_e	Flux of energy	0.05 [1]	W/m^2
q_m	Flux of methane	6×10^{-11} [1]	$kg/(m \cdot s)$
M_l	Mass fraction of methane in the liquid		kg/kg
M_h	Mass fraction of methane in methane hydrate	0.134 [4]	kg/kg
M_{sl}	Solubility of methane in the liquid phase		kg/kg
τ'	Period of hydrate accumulation	5.93×10^{13} [2]	s
$\Delta V_w, \Delta V_g$	Transported volume of water, transported volume of gas		m^3
R_v	Gas phase volume ratio of transported phases (equation [13])	0.55 [5]	$dimensionless$
$\bar{V}_w$	Molar volume of water	1.3×10^{-4} [5]	$m^3/mole$
$\bar{V}_h$	Molar volume of methane hydrate	2.9×10^{-4} [5]	$m^3/mole$
$\bar{V}_g$	Molar volume of methane	1.8×10^{-5} [5]	$m^3/mole$
N	Hydration number: $CH_4.N(H_2O)$	6 [5]	$dimensionless$

Subscripts	
i, f	Initial, final conditions
o	Seafloor conditions
r	Residual
ref	Reference value
GWC	Gas-water contact

Table 1. *Summary of parameters and units used in this study. The choice of parameter values is based on previous modelling studies: [1] Xu and Ruppel (1999) ; [2] Collett et al. (2011) ; [3] Biastoch et al. (2011) ; [4] Davie and Buffett (2001) ; [5] Behseresht and Bryant (2012) ; [6] Xu and Germanovich (2006) ; [7] Waite et al. (2007) ; [8] Giancoli (2007).*

5.2.3. Further assumptions and choice of parameter values

A summary of the parameters and units used throughout this study are listed in table 1. The values of the parameters that are presumed to be fixed are also mentioned in this table. All calculations are done assuming a homogenous sediment column, which implies constant permeability and porosity, and for pure methane hydrate. The initial temperature, pressure and hydrate saturation profiles are in equilibrium with the environmental conditions. As mentioned above, the thermal properties of the column are taken to be constant, although these essentially can vary as the relative amounts of the phases present in the pore space change upon melting. Variations in pressure at the surface are assumed to propagate instantaneously throughout the entire sediment column, and the pressure regime in the pore space is considered to be hydrostatic at any time. The latter is not evident in permafrost, but can for example be established through the presence of open taliks in fault zones, on the continental slope, or below large rivers and lakes (Romanovskii et al., 2005). The tectonic regime is supposed to be stable and isostatic effects are neglected, so that pressure variations solely result from falling or rising sea level and not from tectonic movements or glacial rebound. The generation of excess pore pressure upon dissociation of hydrates is not taken into account, since this is predicted to be low in the highly permeable sediments considered in this study (Xu and Germanovich, 2006). Indeed, a modelling study by Roose et al. (2006) with similar parameters as in this research did account for the build-up of excess pore pressure, and showed that this is too small to initiate slope failure. All calculations are performed for a constant pore water salinity of 35 ‰, despite the fact that it is acknowledged that the pore water can freshen upon melting of ice or dissociation of hydrates. Changes in solubility, due to temperature or pressure shifts, and consequent hydrate dissolution are not considered, because these processes generally do not generate free gas (Xu and Germanovich, 2006), and hence have no direct impact on the potential release of methane to the seafloor and atmosphere. While running the model, restoration of previously dissociated hydrates is neglected, since hydrate formation acts at a significantly longer time-scale than the considered modelling time-frame (100 kyr). Kinetic effects during the growth and dissociation of hydrate crystals are ignored, as well as the capillary effects on hydrate stability. By neglecting capillary effects and rapid salinity changes, a three phase zone cannot form, so that gas hydrates, free gas and the liquid phase can only coexist over an infinitesimal interface at the base of the hydrate stability zone. Formation of ice around dissociating hydrate crystals below the freezing point of water (i.e. the self-preservation effect of hydrates) is not accounted for in the model.

5.3. Simulated destabilization scenarios

The above established model is now employed to simulate a set of environmental change scenarios applied to the high-latitude continental margin considered in this study. The objective of the simulations is twofold: (i) evaluating in what fashion and how fast hydrate reservoirs degrade, in

order to understand how this varies between the four distinct geographic settings across a high-latitude continental margin, and (ii) verifying a number of scientific hypotheses that have been formulated on the role of gas hydrates in global climate.

Case I, II and III serve the purpose of the first line of inquiry of this dissertation, which is making an assessment of how the climate sensitivity of methane hydrates varies between the four geographic settings presented in figure 1. These hypothetic cases of uniform changes in temperature and/or sea level across the margin are: (i) a uniform gradual temperature increase of 5 °C over 5 kyr (case I), (ii) a uniform temperature increase of 5 °C and simultaneous sea level rise of 100 m over a period of 5 kyr (case II), and (iii) a gradual sea level fall of 100 m over 5 kyr (case III). These cases, along with the initial conditions in each setting, are summarized in figure 10. The values of the initial environmental conditions are chosen so that they represent a naturally realistic situation and allow hydrates to be initially stable in each of the four environments. This especially applies to the initial surface temperatures in the permafrost settings (column A and B in figure 10), which have to be low enough for hydrates and permafrost to prevail in the subsurface. The initial surface temperature in column A is assumed to be lower than in column B because of the more continental location of this column, which may imply that the moderating effect of the ocean is less strong or absent. The possible proximity to continental ice sheets can further depress the temperature in the continental permafrost setting (Miller et al., 2010). The extent and rate of environmental change modelled in cases I to III are selected in order to illustrate a variety of possible dissociation patterns. They are not based on a specific past climate change event (as will be done for cases IV-VI; see below), but nevertheless fall within the limits of what has been inferred from the geological record.

In the second part the model is applied to verify a number of hypotheses that are currently matter of scientific debate and which concern the role of destabilizing gas hydrates in examples of past, contemporary and future climate change. First the deglaciation after the Last Glacial Maximum (LGM) is simulated to verify the significance of the *carbon pump hypothesis* and *clathrate gun hypothesis* in Late Quaternary climatic oscillations (case IV). Next it is checked if late 20th century ocean warming can contribute to melting hydrates and presently active gas seeps off Svalbard, and if the predicted climate change during the upcoming centuries will have repercussions for the size of the Arctic clathrate inventory (case V). In this case the permafrost-related settings are not considered, since realistic initial temperatures are too high for gas hydrates to occur in a stable initial state in these environments. Finally, the situation at the onset of the PETM is mimicked to see if melting hydrates could have been the culprit for the observed negative carbon isotopic excursion (case VI). Here only methane hydrates in the deep water realm are evaluated, as this is expected to be the only location where clathrates would have been initially stable because of the warm Arctic conditions during the Early Cenozoic (Miller et al., 2010). No major ice sheets existed yet, whose build-up and disintegration dictate fluctuations in sea level, and therefore sea level is assumed to be constant during the PETM. The initial conditions and the extent and rates of change adopted in cases IV-VI are outlined in table 2.

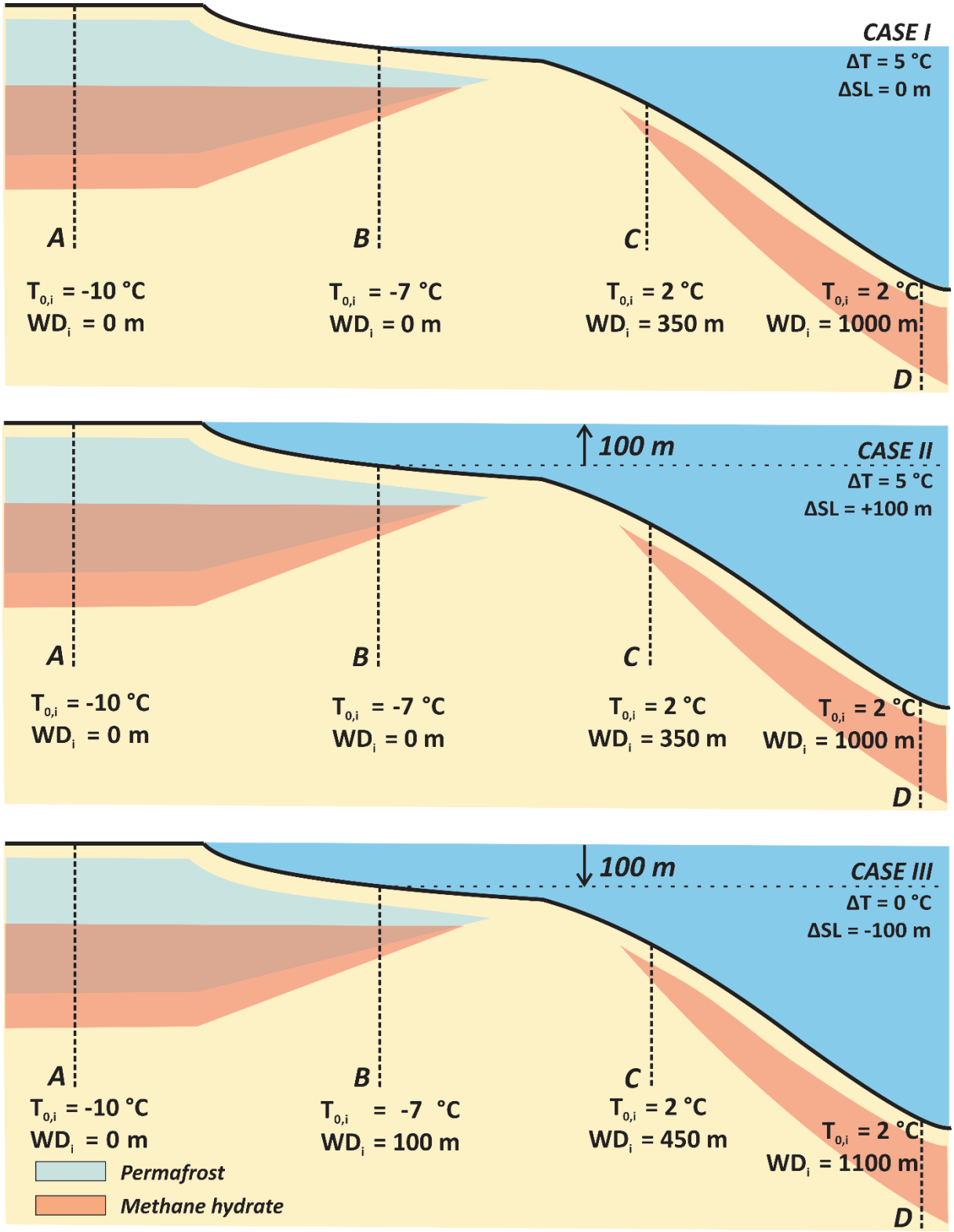

Figure 10. *Summary of cases I-III.* ***Case I:*** *uniform gradual temperature increase of 5 °C over a period of 5 kyr.* ***Case II:*** *uniform gradual temperature increase of 5 °C and simultaneous gradual sea level rise of 100m over a period of 5 kyr.* ***Case III:*** *gradual sea level fall of 100 m over a period of 5 kyr. The initial temperature at the seafloor ($T_{0,i}$) and initial water depth (WD_i) are indicated for each of the geographic settings: A. onshore permafrost; B. subsea permafrost; C. upper continental slope; D. lower continental slope or continental rise.*

	Onshore permafrost	***Offshore permafrost***	***Upper continental slope***	***Lower continental slope***
CASE IV				
$T_{0,i} \rightarrow T_{0,f}$	$-15 \rightarrow 2$ °C [1]	$-10 \rightarrow 2$ °C [1]	$-1 \rightarrow 2$ °C [2]	$-1 \rightarrow 2$ °C [2]
$WD_i \rightarrow WD_f$	$0\ m$	$0 \rightarrow 120\ m$ [3]	$300 \rightarrow 420\ m$ [3]	$1000 \rightarrow 1120\ m$ [3]
$period\ \Delta T\ \&\ \Delta WD$	$3000\ years$ [4]			
CASE V	$(*)$			
$T_{0,i} \rightarrow T_{0,f}$			$1 \rightarrow 5$ °C [5]	$0 \rightarrow 4$ °C [5]
$WD_i \rightarrow WD_f$			$400 \rightarrow 401\ m$ [6]	$1000 \rightarrow 1001\ m$ [6]
$period\ \Delta T\ \&\ \Delta WD$			$200\ years$ [6]	
CASE VI	$(*)$			
$T_{0,i} \rightarrow T_{0,f}$				$11 \rightarrow 15$ °C [7]
$WD_i = WD_f$				$1000\ m$
$period\ \Delta T$				$8000\ years$ [7]

Table 2. *Summary of cases IV-VI.* ***Case IV:*** *simulation of the deglaciation after the LGM. Initial ($T_{0,I}$) and final ($T_{0,f}$) surface or seafloor temperatures from [1] Miller et al. (2010) and [2] Waelbroeck et al. (2002). Initial (WD_i) and final (WD_f) water depths and duration of temperature and sea level change from [3] Bard et al. (1990) and [4] Landvik et al. (1998).* ***Case V:*** *simulation of contemporary and future climate change. Values from [5] Biastoch et al. (2011) and [6] IPCC (2013).* ***Case VI:*** *simulation of the PETM. Values from [7] Dickens et al. (1995). (*) Realistic initial temperatures are too high for gas hydrates to occur in a stable initial state in these environments, hence these settings are not evaluated.*

6.1. Case I: uniform gradual temperature increase of 5 °C over a period of 5 kyr

Figures 11 and 12 illustrate how a converted free gas accumulation in permafrost-rich environments responds to a gradual temperature increase of 5 °C. The initial free methane gas is considered to have accumulated between 250 and 350 m depth in the sediment column, occupying 80 % of the pore space. The resulting initial methane hydrate saturation profile after the imposition of hydrate stability conditions in association with the formation of thick onshore permafrost is illustrated in figure 11B. The hydrate saturation is constant and equal to 73.6 % of the pore space above the 'fossil' gas-water contact at 305 m depth, and 1.4 % below. Hydrates coexist with ice in the pore space of the sediment column, since the base of the permafrost locates at 630 m depth in the column. The first hydrates disappear at the base of the hydrate occurrence zone only 64 kyr after the onset of the temperature increase. The hydrate-bearing section of the column also shrinks from the top, but at a slow rate and only after 74 kyr (figure 11C). The permafrost decreases from the base, first at a fairly constant rate, which slows down after approximately 60 kyr (figure 11E). After 100 kyr, the interval over which ice occurs in the pore space has decreased by app. 55 %, while the hydrate occurrence zone has shrunk by 30 %. The temperature profile after 100 kyr is constrained by the presence of melting ice and hydrates in the subsurface, and hence has not reached an equilibrium state (figure 11A).

Hydrates do not coexist with, but occur below the permafrost in the subshelf permafrost setting. They dissociate both from the top and the base of the hydrate occurrence zone, with a slightly higher dissociation rate at the base than at the top. The model predicts the column to be completely bare of hydrates after 71 kyr (figure 12C). The ice-bearing interval only shrinks from the base of the column, at an initially slightly decreasing rate, which increases again after approximately 75 kyr (coinciding with the dissociation of the ultimately present hydrates). The propagation of the temperature pulse in the subsurface is delayed by the presence of both melting hydrates and ice. After 100 kyr, the temperature is still at the melting temperature of ice in the upper 25 m of the column where ice is melting, and hence a new equilibrium profile has not established within the considered time span (figure 12A).

The column in the upper continental slope setting initially features methane hydrates between 55 m and 175 m depth below seafloor (figure 13A). Gas hydrates occupy 7.5 % of the pore space at the base of the hydrate occurrence zone, which gradually decreases towards a value of 6 % at the top. The base of the HSZ coincides with the base of the hydrate occurrence zone. The model predicts hydrate dissociation both from the top and the base of the column, with the highest dissociation rate at the top. The uppermost 5 m of hydrates are dissociated after 4.6 kyr, while the lowermost hydrate-bearing 5 m interval is disintegrated after 11.8 kyr. All hydrates in the column dissociate within 50.5 kyr after the start of the temperature increase, with the last hydrates dissociating at around 150 m depth (figure 13C). At first the temperature rises slowly in the hydrate-bearing section of the column, but then the temperature profile steadily reaches its new equilibrium state within 30 kyr after all hydrates vanished (figure 13A).

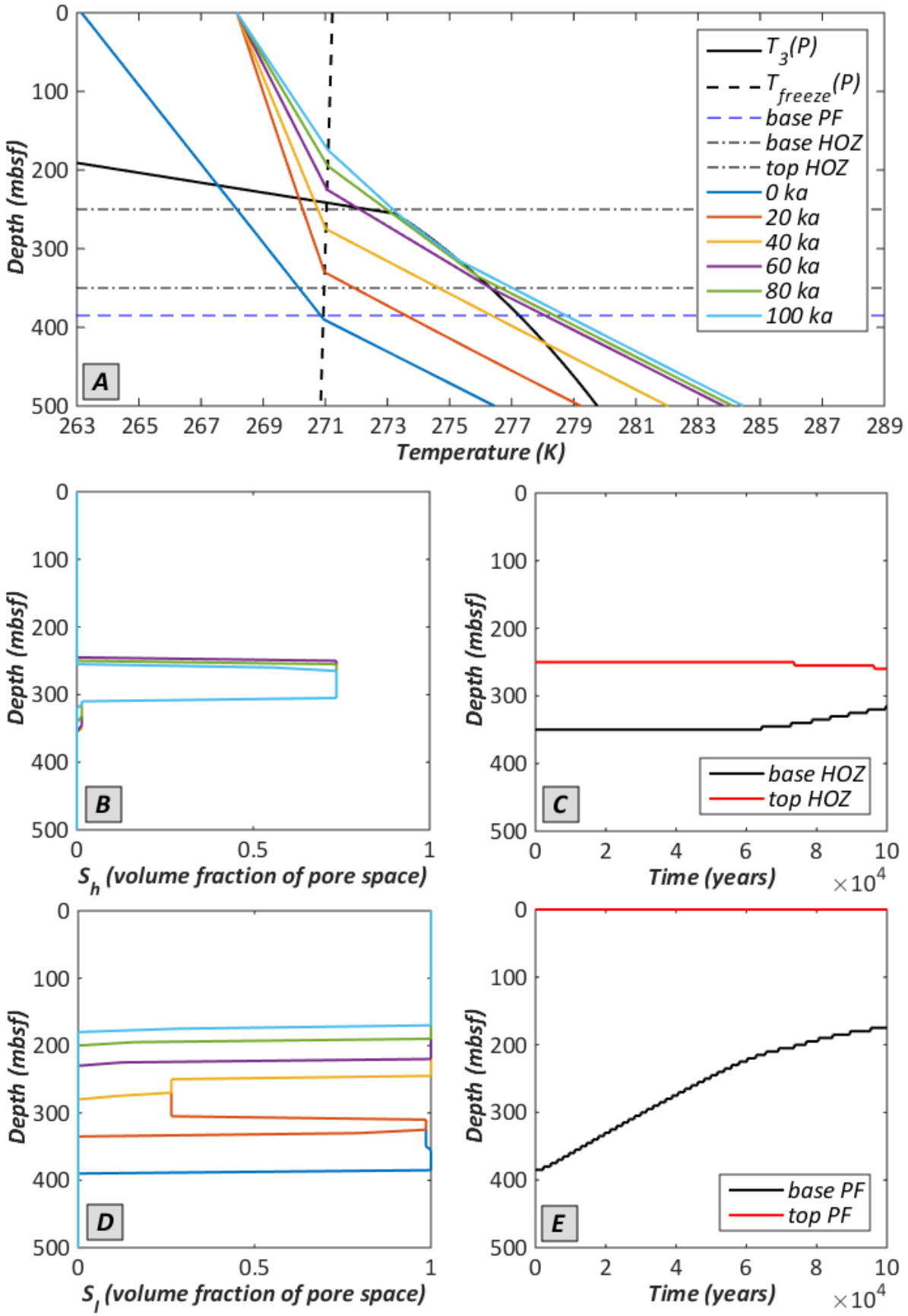

Figure 11. *Evolution of (A) the temperature profile, (B) hydrate saturation profile, (C) base and top of the hydrate occurrence zone (HOZ), (D) ice saturation profile, and (E) base and top of the permafrost (PF), in response to case I environmental changes in a sediment column in the onshore permafrost setting. The legend in (A) also applies to (B) and (D).*

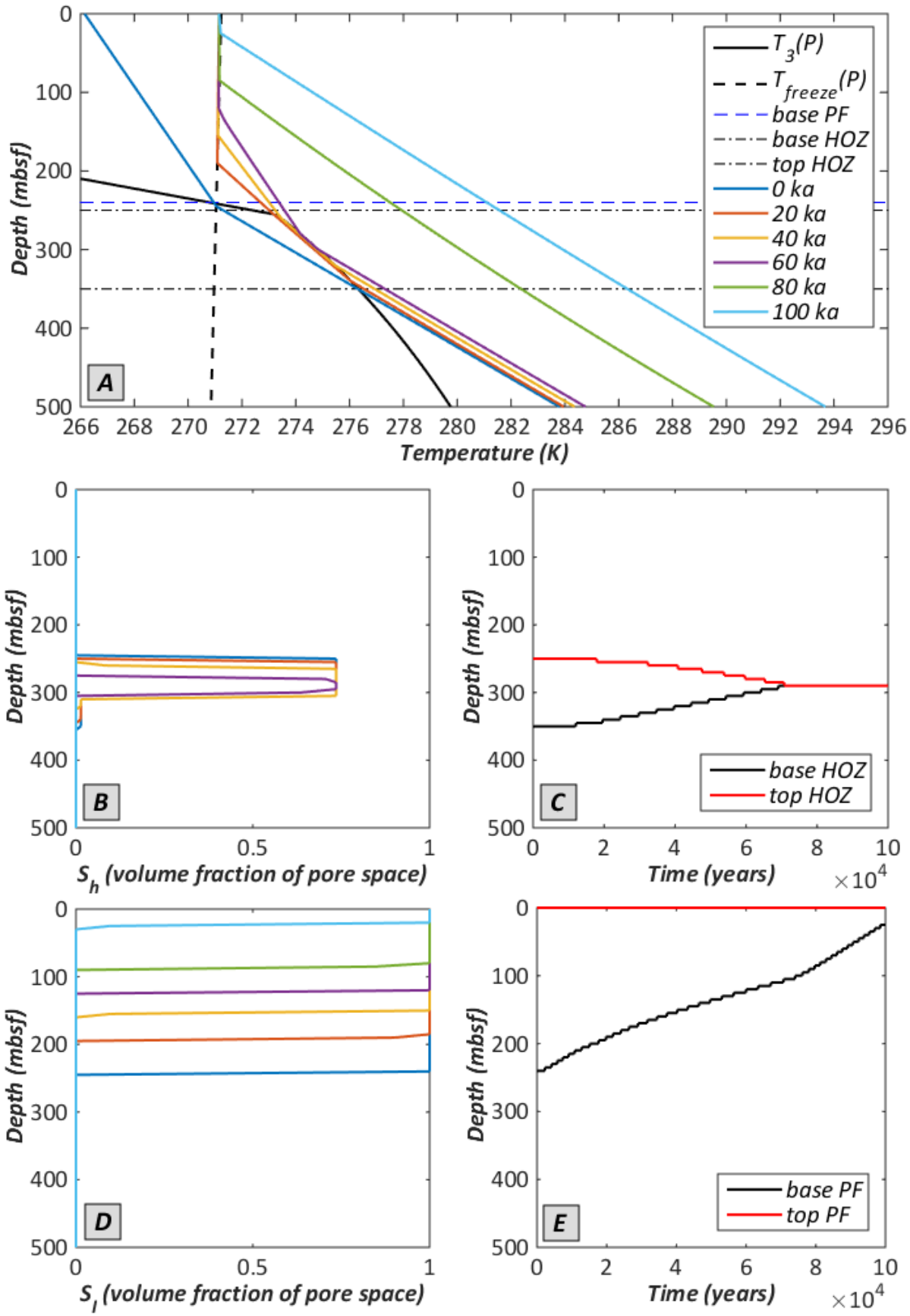

Figure 12. *Evolution of (A) the temperature profile, (B) hydrate saturation profile, (C) base and top of the hydrate occurrence zone (HOZ), (D) ice saturation profile, and (E) base and top of the permafrost (PF), in response to case I environmental changes in a column in the offshore (subsea) permafrost setting. The legend in (A) also applies to (B) and (D).*

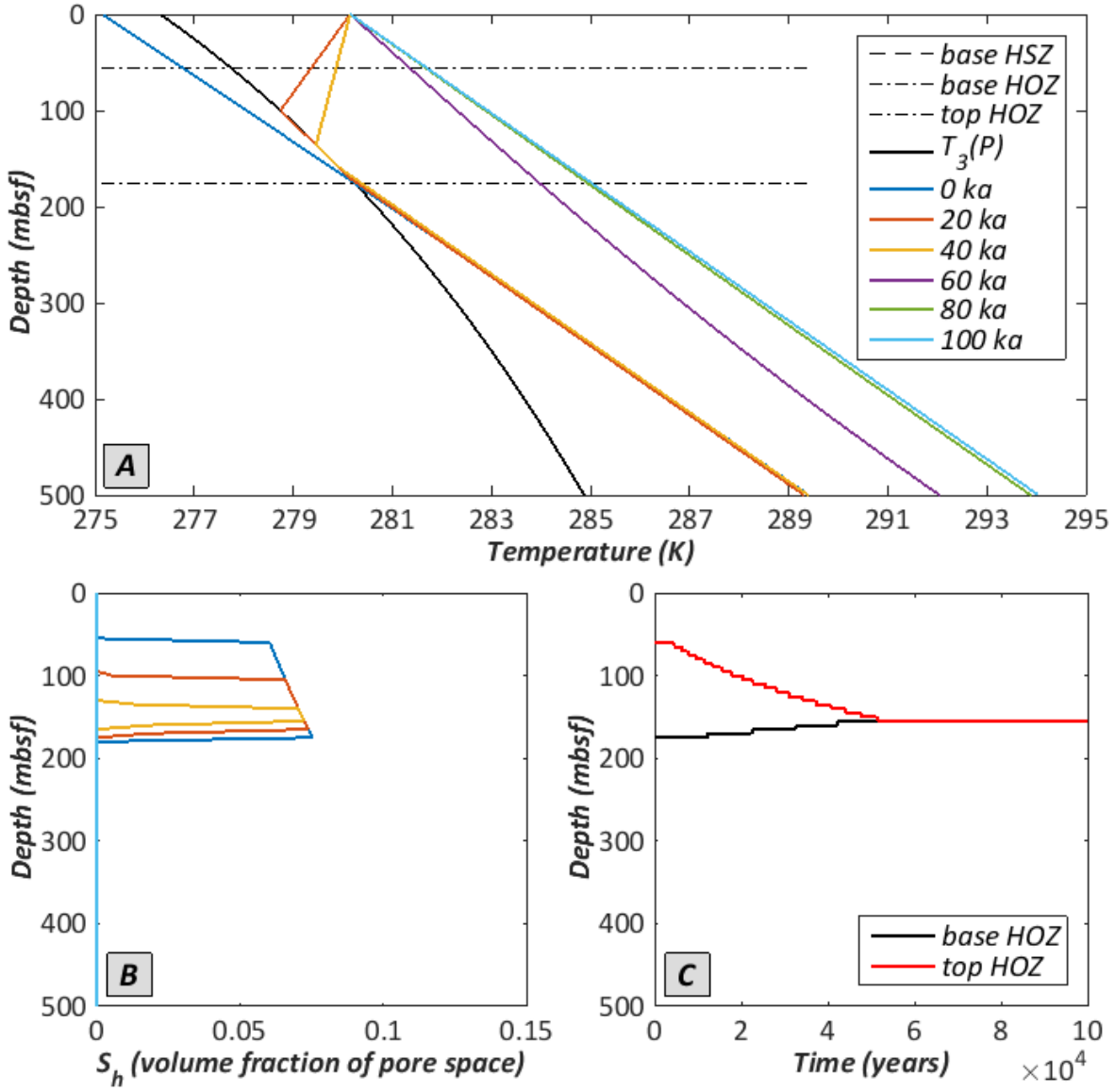

Figure 13. *Evolution of (A) the temperature profile, (B) hydrate saturation profile, and (C) base and top of the hydrate occurrence zone (HOZ), in response to case I environmental changes in a sediment column on the upper continental slope (350 m water depth). The initial position of the base of the HOZ (coinciding with the base of the HSZ) and top of the HOZ are indicated in (A). The legend in (A) also applies to (B).*

The model predicts a 545 m thick HSZ for the sediment column at 1000 m water depth. However, this column is actually occupied by methane hydrate only over the interval between 55 and 355 m depth below seafloor (figure 14A). Hydrates start to dissociate approximately 30 kyr after the onset of the temperature rise at the base of the hydrate occurrence zone. After 100 kyr the hydrate occurrence zone has only shrunk by 5 m (figure 14C). The temperature profile after 100 kyr, which is near equilibrium with the newly imposed bottom water temperature, intersects $T_3(P)$ at a 345 m depth below seafloor (figure 14A), indicating that further dissociation will only affect an additional section of methane hydrate of less than 2 % of the initial hydrate occurrence zone.

Figure 15 provides a schematic overview of the subsurface distribution of methane hydrate and ice at the start and at the end of the case I simulation, in order to summarize how the modelled environmental changes have affected hydrate and permafrost stability across the continental margin.

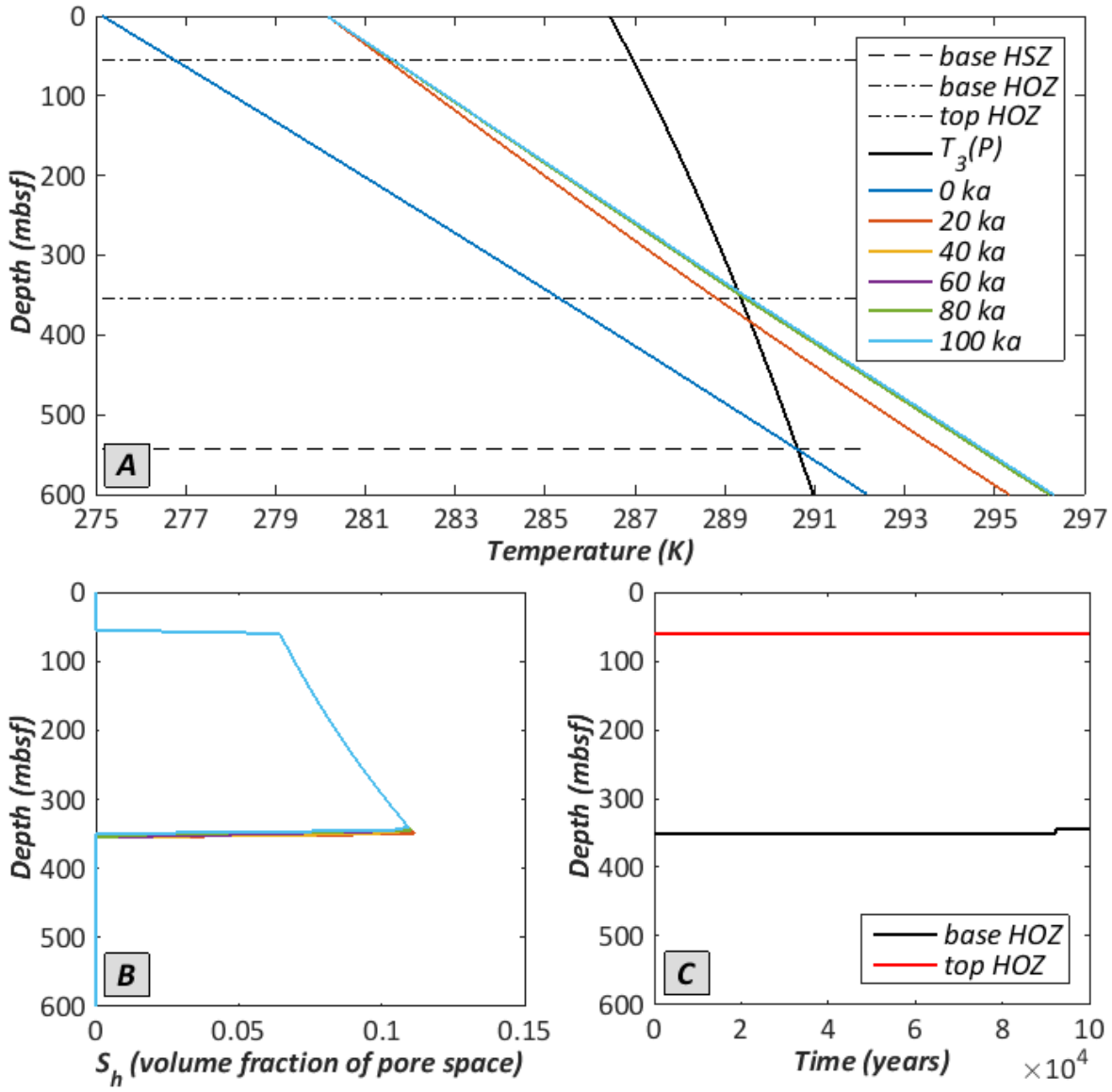

Figure 14. *Evolution of (A) the temperature profile, (B) hydrate saturation profile, and (C) base and top of the hydrate occurrence zone (HOZ), in response to case I environmental changes in a sediment column on the lower continental slope or continental rise (1000 m water depth). The initial position of the base of the HOZ, the base of the HSZ and top of the HOZ are indicated in (A). The legend in (A) also applies to (B).*

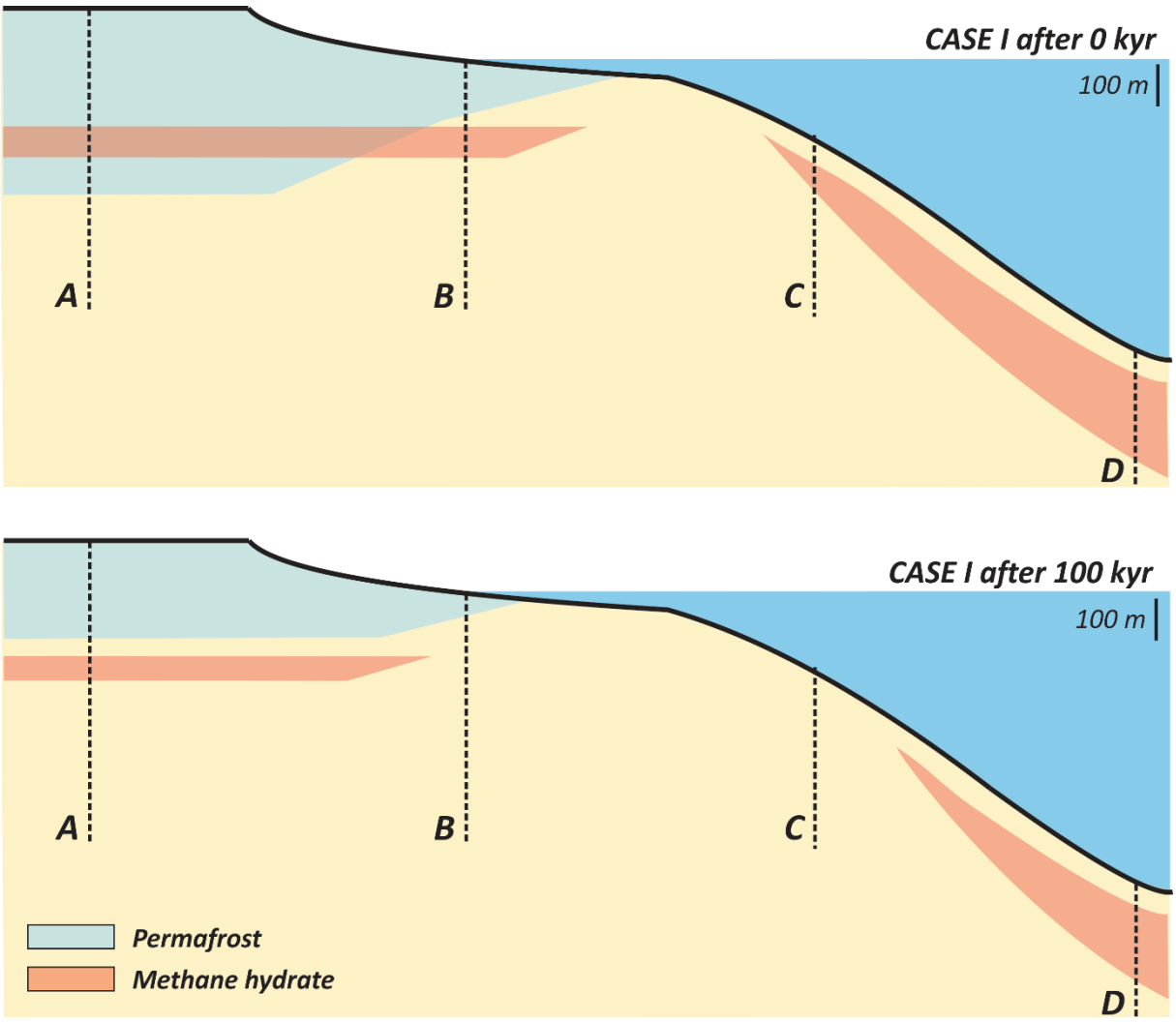

Figure 15. *Schematic overview of the subsurface distribution of methane hydrate and ice at the start (top) and at the end (bottom) of the case I simulation, which summarizes how the modelled environmental changes have affected hydrate and permafrost stability across the continental margin.*

6.2. Case II: uniform gradual temperature increase of 5 °C and simultaneous gradual sea level rise of 100 m over a period of 5 kyr

A temperature increase over the same converted free gas accumulation as in case I is simulated, but now with a simultaneous sea level rise of 100 m, so a subsea-permafrost situation is created on the shelf. The simulation for the onshore permafrost setting, which is not affected by sea level fluctuations, is identical as presented for case I (figure 11). Hydrates in the sediment column on the shelf again occur below the permafrost. They start melting after 28 kyr, but in contrast to case I only from the base. The hydrate occurrence zone is reduced by 95 % after running the model for 100 kyr (figure 16C). The ice-bearing interval degrades from the base, at a rate which shows a decreasing trend. The model predicts that 100 kyr after the start of the temperature rise, no ice will occur anymore in the pore space of the sediment column (figure 16E). The temperature profile is still in a transient state after 100 kyr, as temperature is confined to the dissociation temperature over the depth interval influenced by melting hydrates (figure 16A).

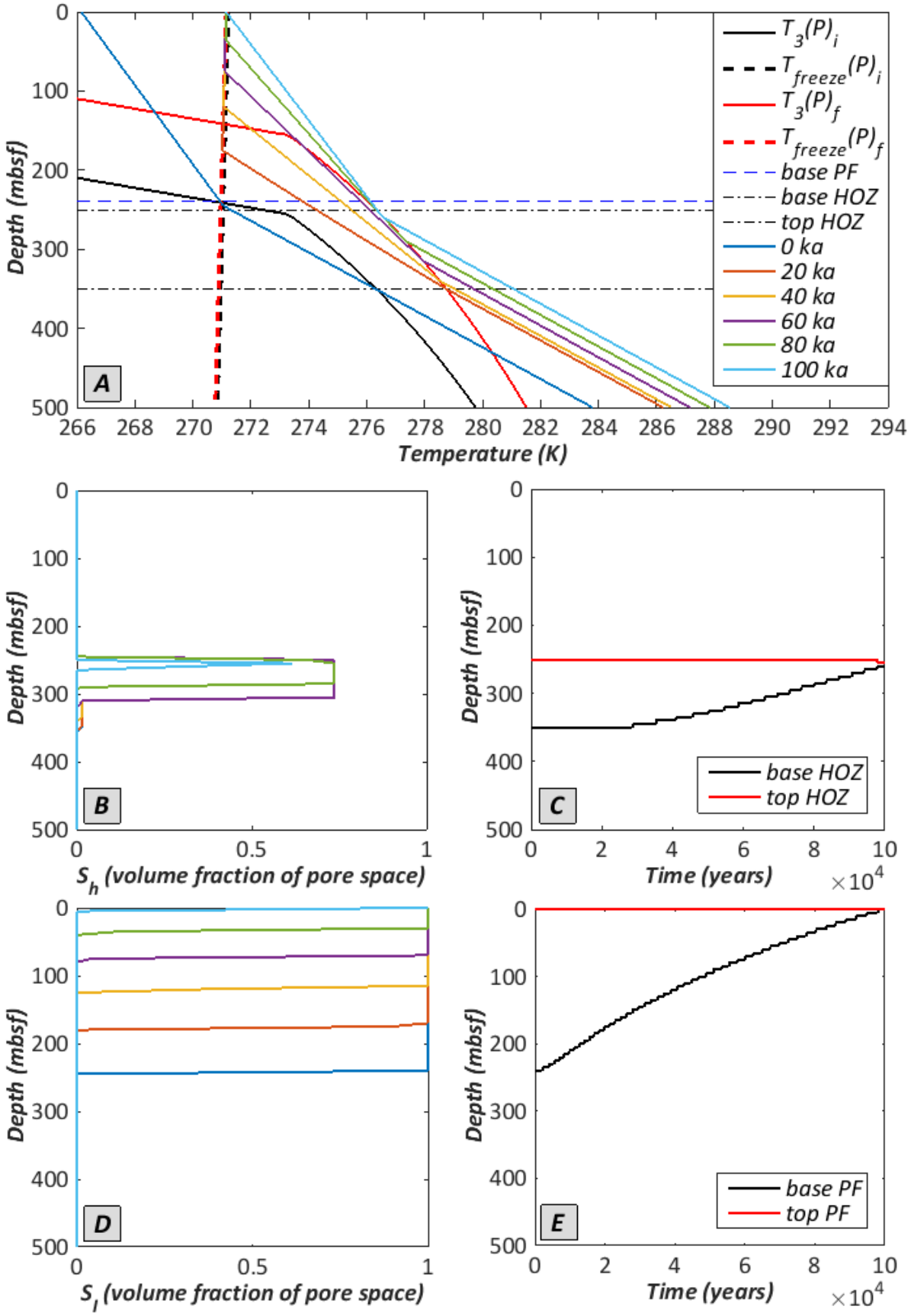

Figure 16. *Evolution of (A) the temperature profile, (B) hydrate saturation profile, (C) base and top of the hydrate occurrence zone (HOZ), (D) ice saturation profile, and (E) base and top of the permafrost (PF), in response to case II environmental changes in a column in the offshore (subsea) permafrost setting. The legend in (A) also applies to (B) and (D).*

The initial methane hydrate saturation profiles for both marine settings are evidently identical to those presented for case I (figure 13B and 14B). Figure 17C shows that it takes 85 kyr to melt all hydrates in the column on the upper continental slope, which is 30 kyr longer than in case I where no simultaneous sea level rise is considered (cfr. figure 13C). Dissociation again progresses both from the top and the base of the hydrate occurrence zone, although the last hydrates to melt occur at a shallower level compared to case I (125 m vs. 150 m below seafloor). The temperature profile after 100 kyr is in equilibrium with the newly imposed bottom water temperature (figure 17A).

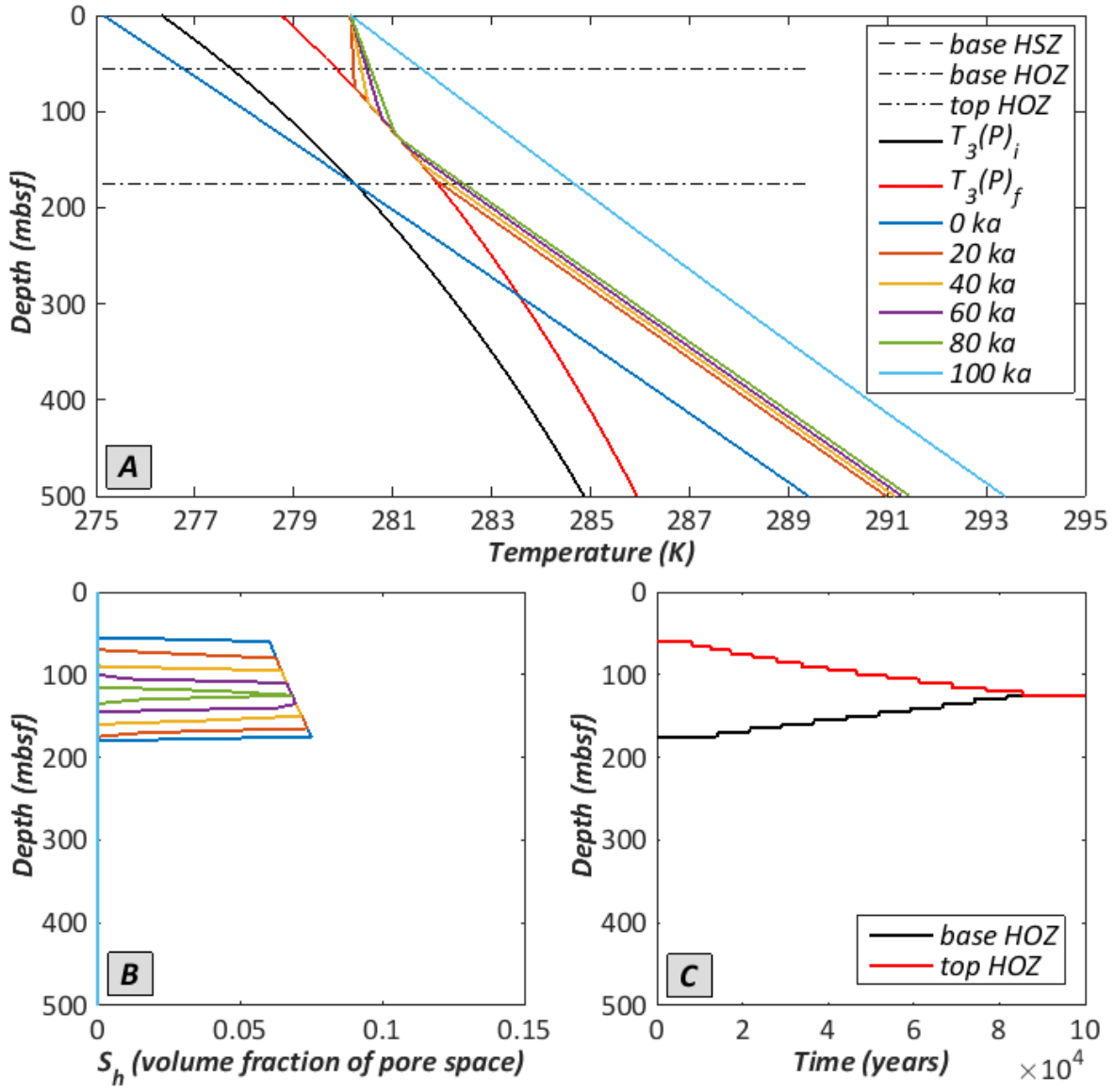

Figure 17. *Evolution of (A) the temperature profile, (B) hydrate saturation profile, and (C) base and top of the hydrate occurrence zone (HOZ), in response to case II environmental changes in a sediment column on the upper continental slope (350 m initial water depth). The initial position of the base of the HOZ (coinciding with the base of the HSZ) and top of the HOZ are indicated in (A). The legend in (A) also applies to (B).*

The methane hydrates in the column at 1000 m water depth remain unaltered during the simulation. The new equilibrium temperature profile, established after approximately 50 kyr, intersects the final $T_3(P)$ profile after the sea level rise below the base of the hydrate occurrence zone (figure 18A). Hence the temperature rise in this case does not affect hydrate stability in the deep water sediment column.

Finally, figure 19 provides a schematic overview of the subsurface distribution of methane hydrate and ice at the start and at the end of the case II simulation, in order to summarize how the modelled environmental changes have affected hydrate and permafrost stability across the continental margin.

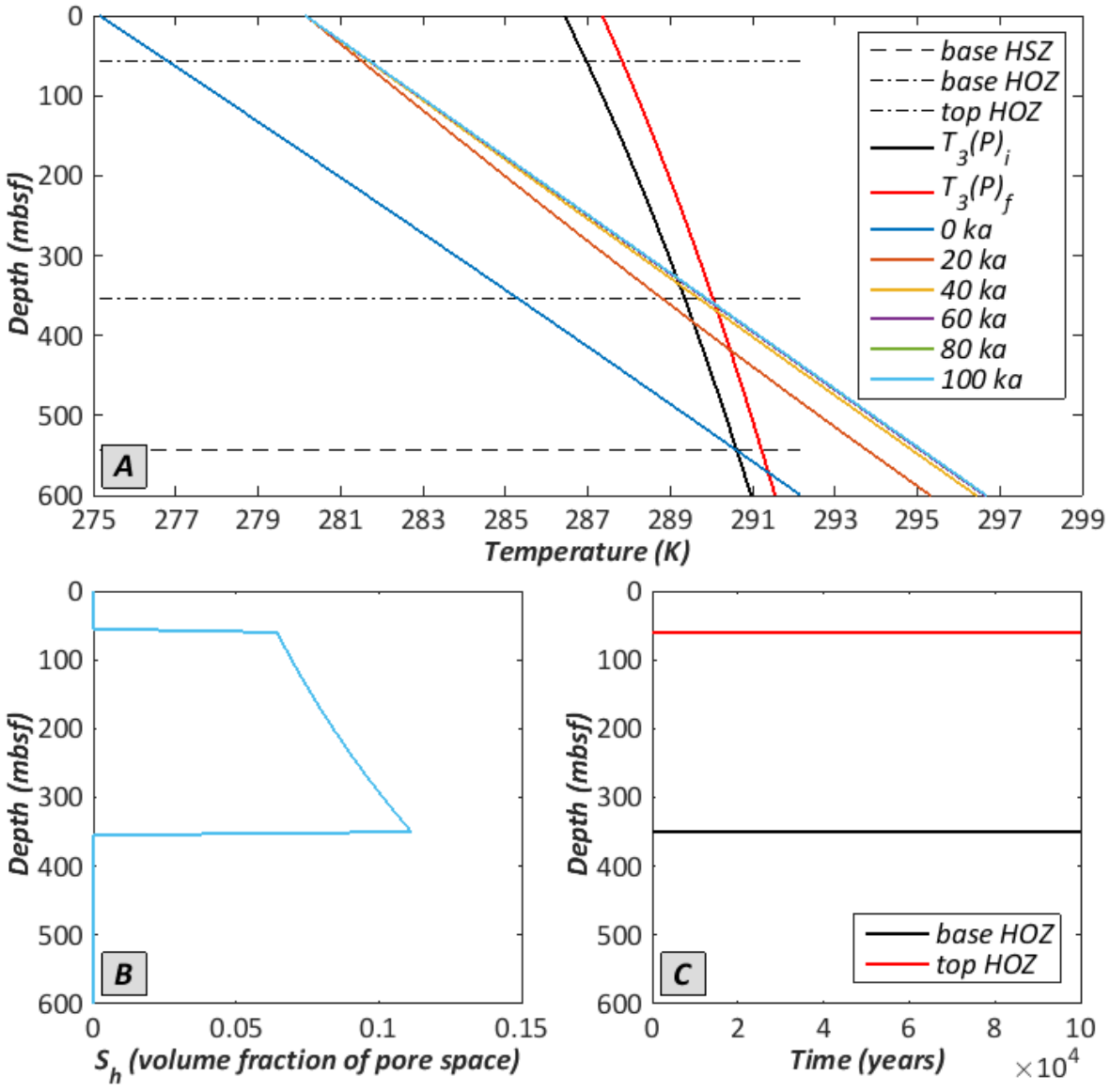

Figure 18. *Evolution of (A) the temperature profile, (B) hydrate saturation profile, and (C) base and top of the hydrate occurrence zone (HOZ), in response to case II environmental changes in a sediment column on the lower continental slope or continental rise (1000 m initial water depth). The initial position of the base of the HOZ, the base of the HSZ and top of the HOZ are indicated in (A). The legend in (A) also applies to (B).*

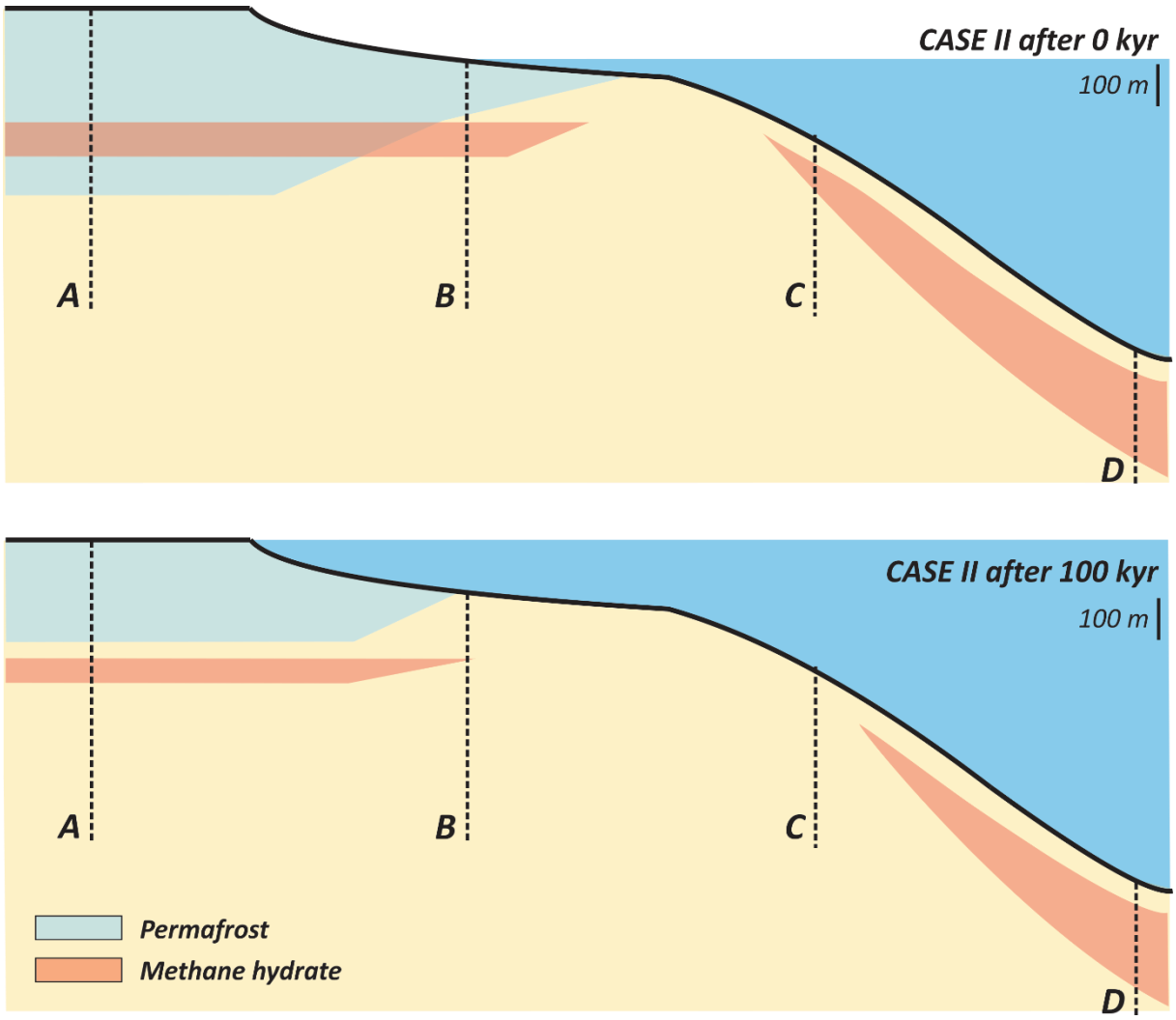

Figure 19. *Schematic overview of the subsurface distribution of methane hydrate and ice at the start (top) and at the end (bottom) of the case II simulation, which summarizes how the modelled environmental changes have affected hydrate and permafrost stability across the continental margin.*

6.3. Case III: gradual sea level fall of 100 m over a period of 5 kyr

The initial free gas accumulation considered in case III spans the interval between 200 m and 350 m depth. After conversion to a methane hydrate accumulation and a sea level fall of 100 m, the subsea permafrost (now aerially exposed) and associated hydrates start to dissociate. Hydrates initially melt from the top at depths where the temperature exceeds the $T_3(P)$ profile for the lowered sea level (figures 20A and 20C). Over this interval the temperature decreases, which disrupts the entire temperature profile. After approximately 35 kyr, the base of the hydrate occurrence also start to shift to a shallower level, as the temperature profile in the column start to rise above the initial temperature profile again. This causes ice to melt at the base of the permafrost bearing zone after 24 kyr, which is preceded by an initial small upward shift of the base of the ice-bearing zone after 2.3 kyr. After running the model for 100 kyr the thickness of the hydrate occurrence zone has decreased by 77 %, while the interval over which ice occurs has degraded by 25 %. Evidently, the continental permafrost column is not affected by the sea level fall, and is therefore not considered in case III.

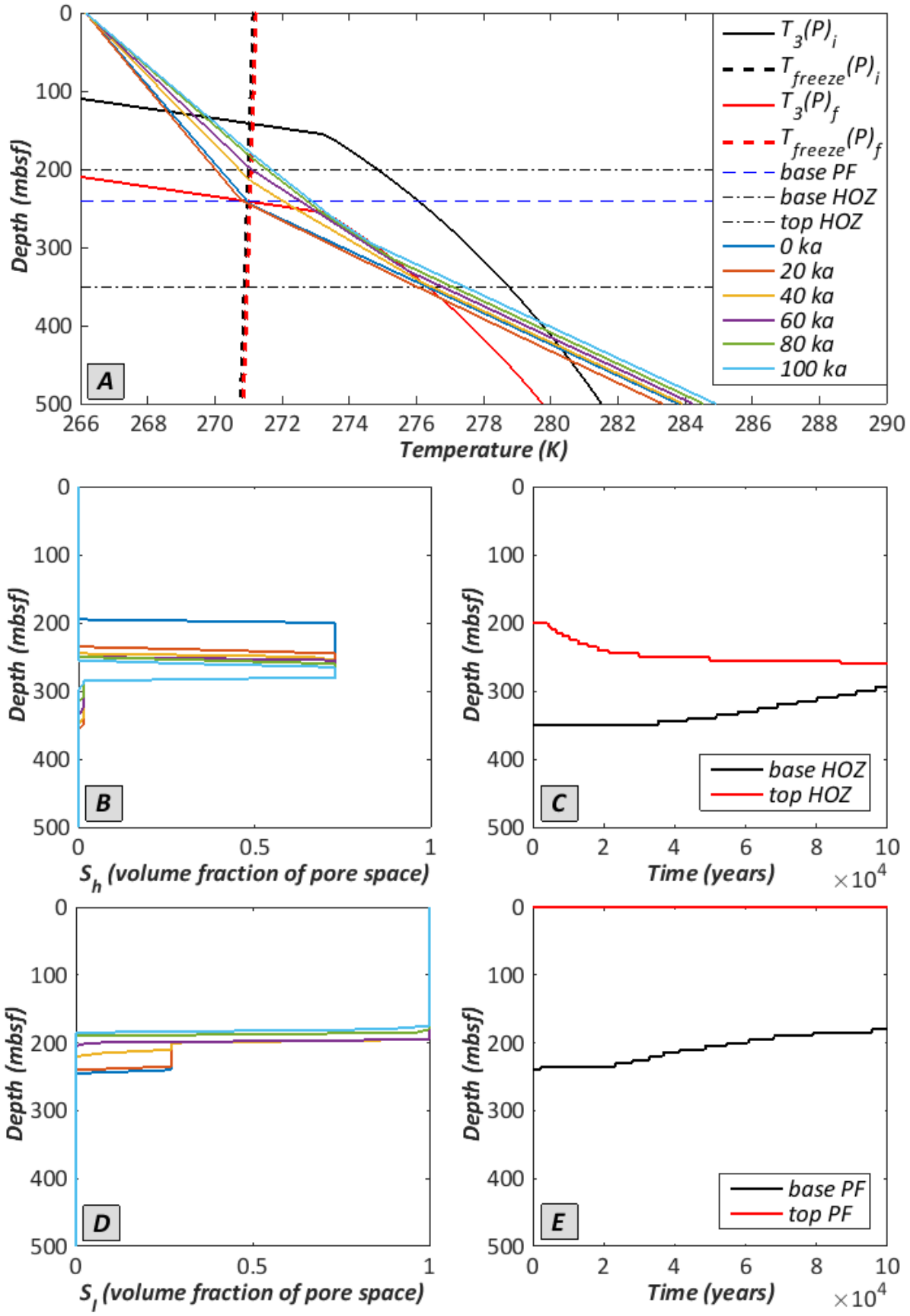

Figure 20. *Evolution of (A) the temperature profile, (B) hydrate saturation profile, (C) base and top of the hydrate occurrence zone (HOZ), (D) ice saturation profile, and (E) base and top of the permafrost (PF), in response to case III environmental changes in a column in the offshore (subsea) permafrost setting. The legend in (A) also applies to (B) and (D).*

Hydrates initially occur over the depth interval from 56 m to 292 m below the sea floor, in equilibrium with the initial conditions prevailing in the upper continental slope column outlined in figure 10. 10 kyr after the sea level stops to fall, the bottom 5 m of hydrates are entirely dissociated. Further melting of hydrates from the base at a slow rate cause the thickness of the hydrate occurrence zone to decrease by 8 % after 100 kyr (figure 21C). As hydrates dissociate, the temperature profile shifts to lower values, and then gradually starts to increase again towards the initial profile. However, after 100 kyr the temperature still is ca. 1 °C lower than the initial temperature in the lower part of the column. This temperature offset decreases towards the top (figure 21A).

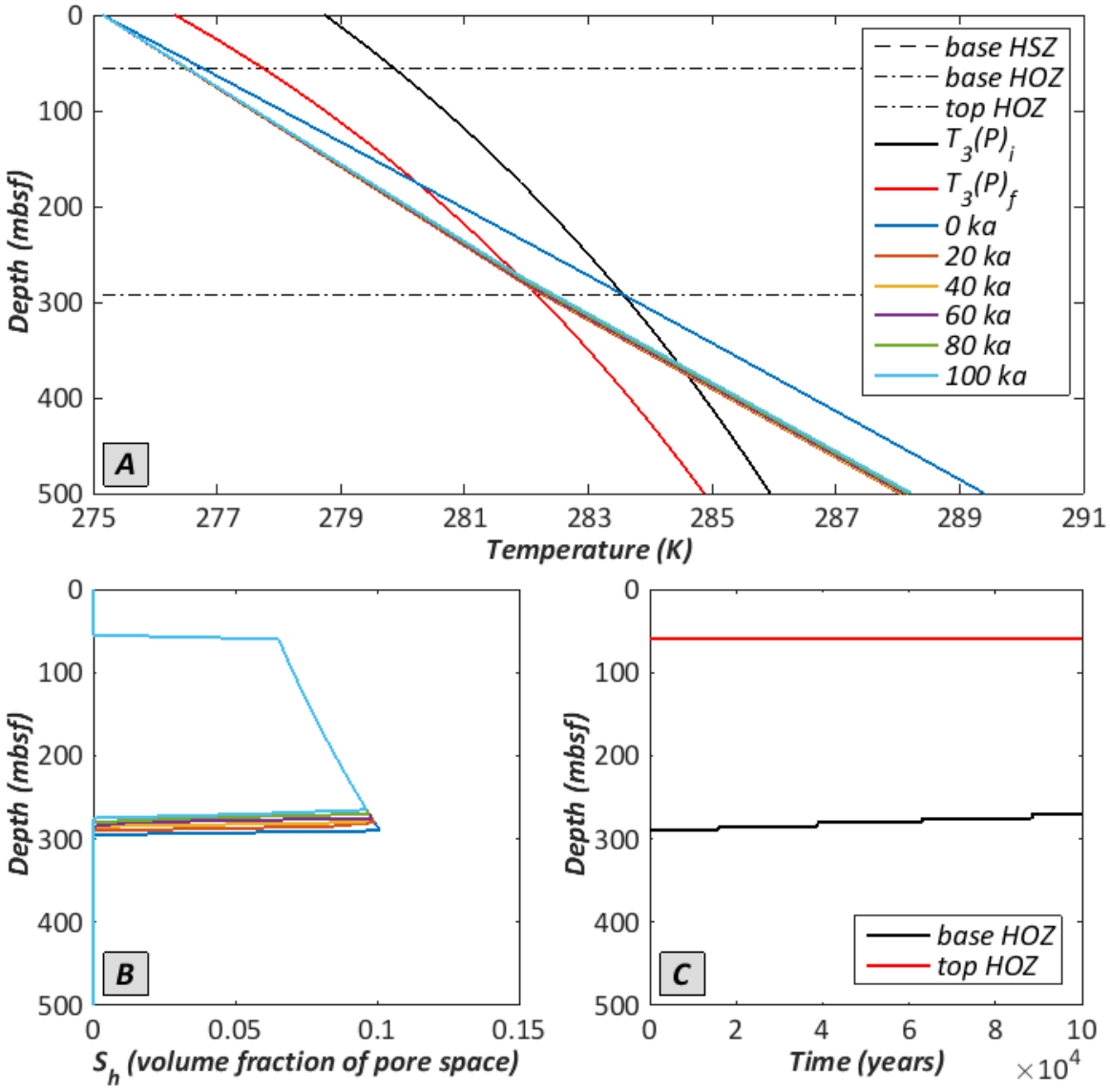

Figure 21. *Evolution of (A) the temperature profile, (B) hydrate saturation profile, and (C) base and top of the hydrate occurrence zone (HOZ), in response to case III environmental changes in a sediment column on the upper continental slope (450 m initial water depth). The initial position of the base of the HOZ (coinciding with the base of the HSZ) and top of the HOZ are indicated in (A). The legend in (A) also applies to (B).*

The HSZ in the sediment column at 1100 m water depth is simulated to be 570 m thick, with the hydrate occurrence zone extending from 56 m to 360 m depth (figure 22A). The temperature profile intersects the $T_3(P)$ profile after the sea level fall below the base of the zone of actual hydrate occurrence. Hence the hydrate reservoir in this column remains stable in the case of a 100 m sea level fall (figure 22C). The temperature is slightly disturbed and shifts to lower values (± 0.5 °C at the base of the column), although no hydrates dissociate.

To summarize, figure 23 provides a schematic overview of the subsurface distribution of methane hydrate and ice at the start and at the end of the case I simulation, which shows how the modelled environmental changes have affected hydrate and permafrost stability across the continental margin.

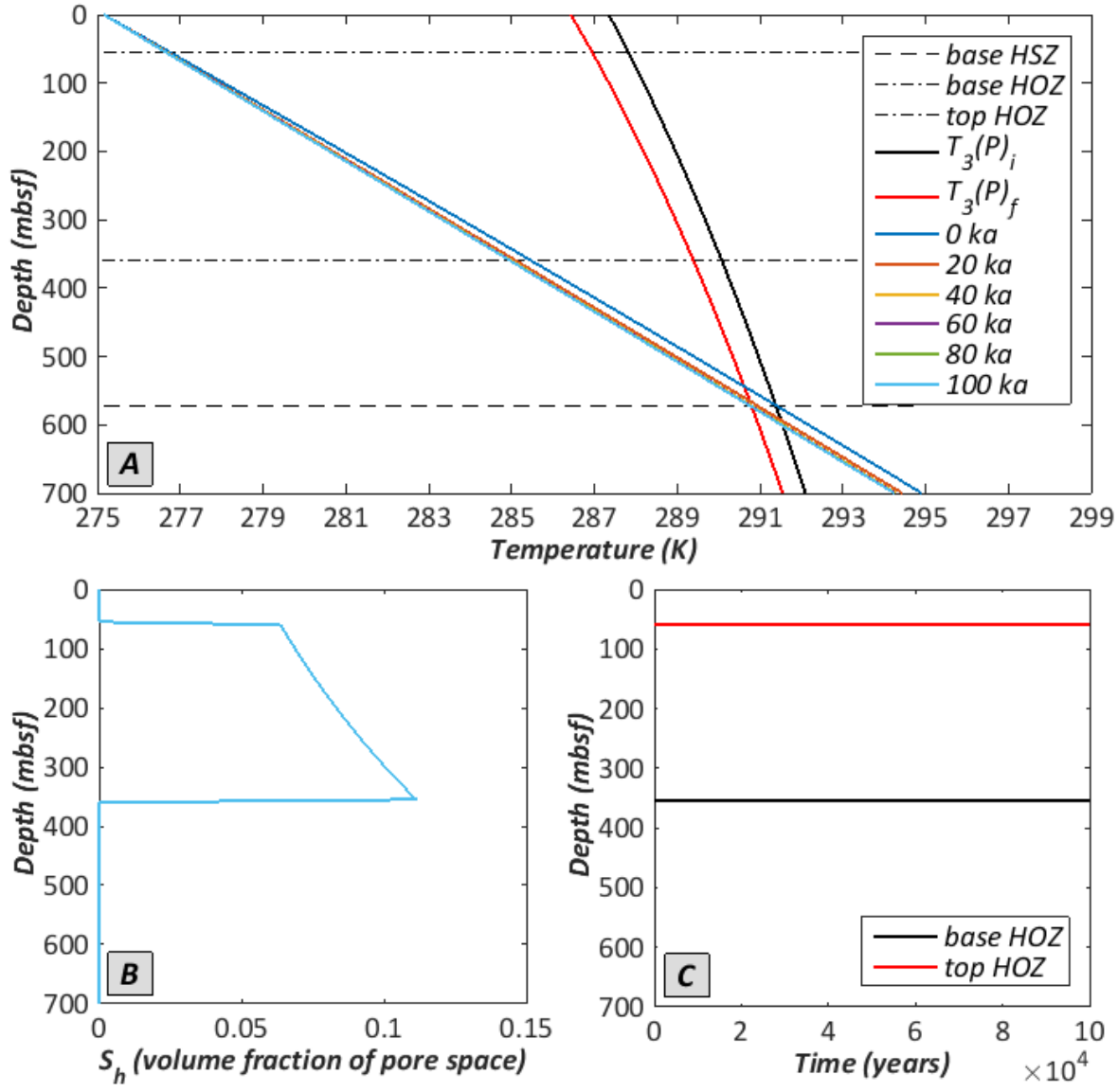

Figure 22. *Evolution of (A) the temperature profile, (B) hydrate saturation profile, and (C) base and top of the hydrate occurrence zone (HOZ), in response to case III environmental changes in a sediment column on the lower continental slope or continental rise (1100 m initial water depth). The initial position of the base of the HOZ, the base of the HSZ and top of the HOZ are indicated in (A). The legend in (A) also applies to (B).*

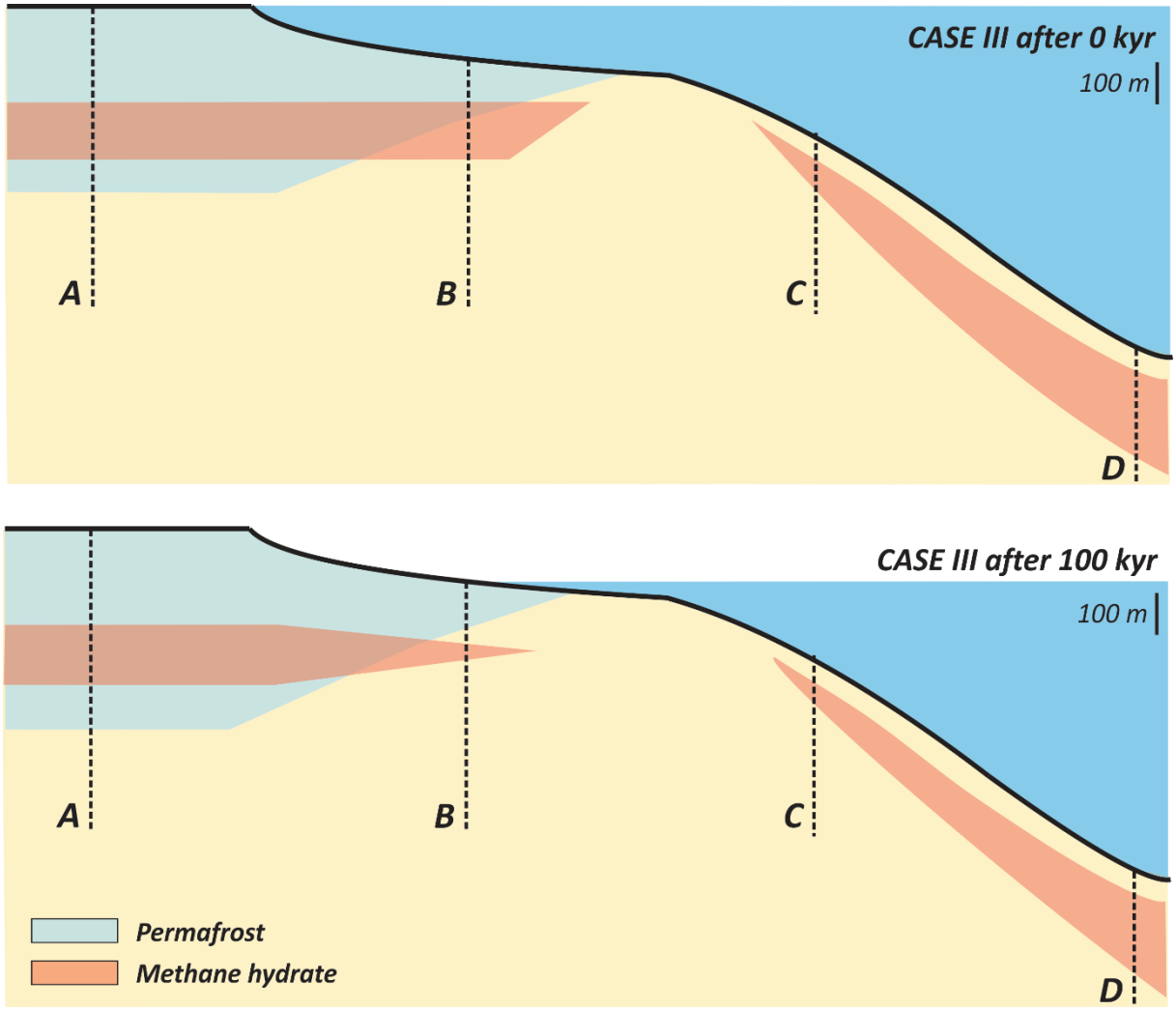

Figure 23. *Schematic overview of the subsurface distribution of methane hydrate and ice at the start (top) and at the end (bottom) of the case III simulation, which summarizes how the modelled environmental changes have affected hydrate and permafrost stability across the continental margin.*

6.4. Case IV: deglaciation following the Last Glacial Maximum

If conditions representative for the deglaciation after the LGM are applied to the thick onshore permafrost setting, the model predicts that methane hydrates, occurring between 250 m and 350 m depth, will remain stable during a 100 kyr simulation (figure 24C). The base of the permafrost rises from 630 m to 285 m at a fairly constant rate. Once the temperature at the surface exceeds the melting temperature of ice (after 2.5 kyr), the permafrost also starts to decay from the top, so that the shallowest occurrence of ice after 100 kyr locates at 235 m depth (figure 24E). The consumption of heat upon melting of ice has a significant impact on the evolution of the subsurface temperature profile, which is far from equilibrium state after 100 kyr (figure 24A).

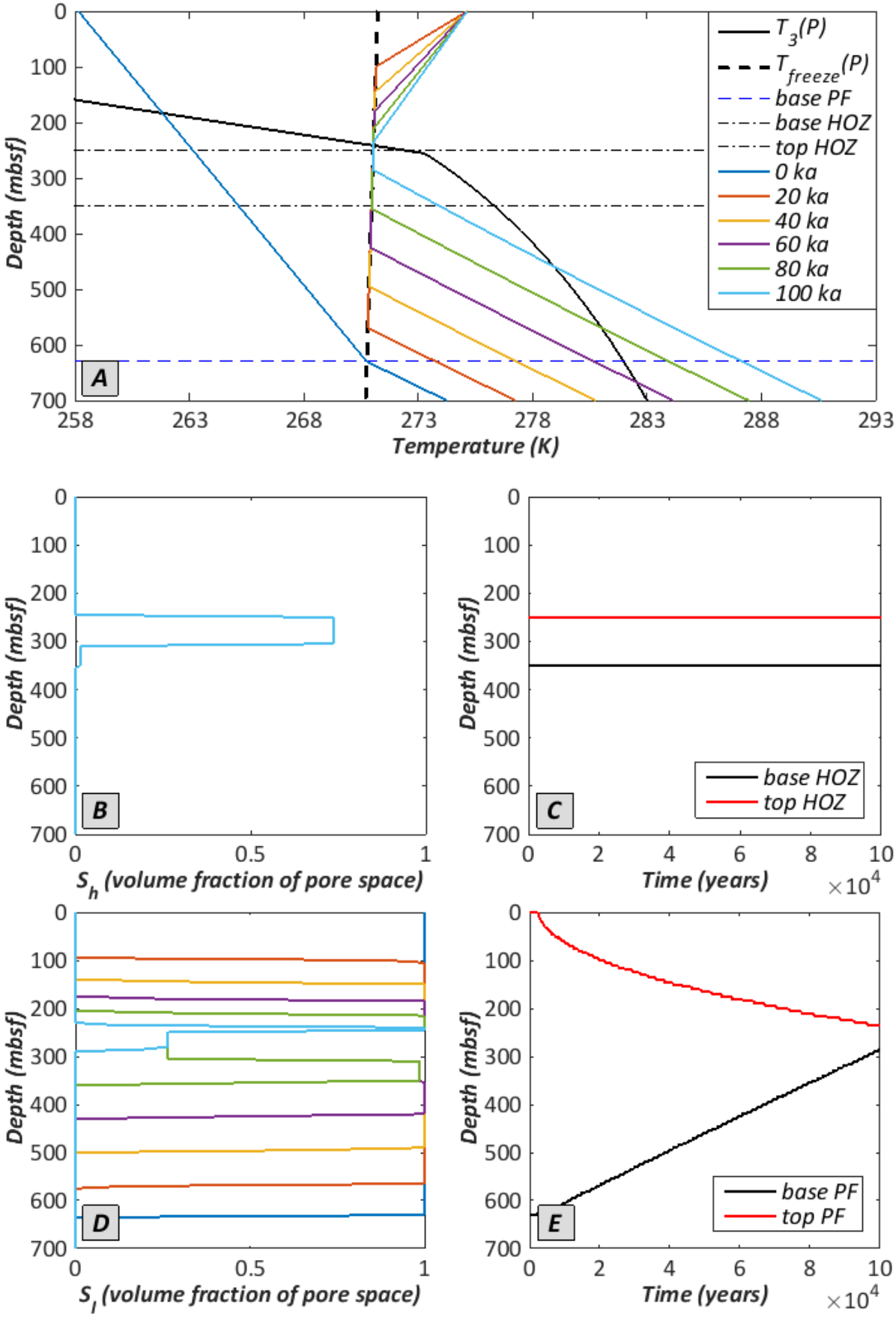

Figure 24. *Evolution of (A) the temperature profile, (B) hydrate saturation profile, (C) base and top of the hydrate occurrence zone (HOZ), (D) ice saturation profile, and (E) base and top of the permafrost (PF), in response to case IV environmental changes in a sediment column in the onshore permafrost setting. The legend in (A) also applies to (B) and (D).*

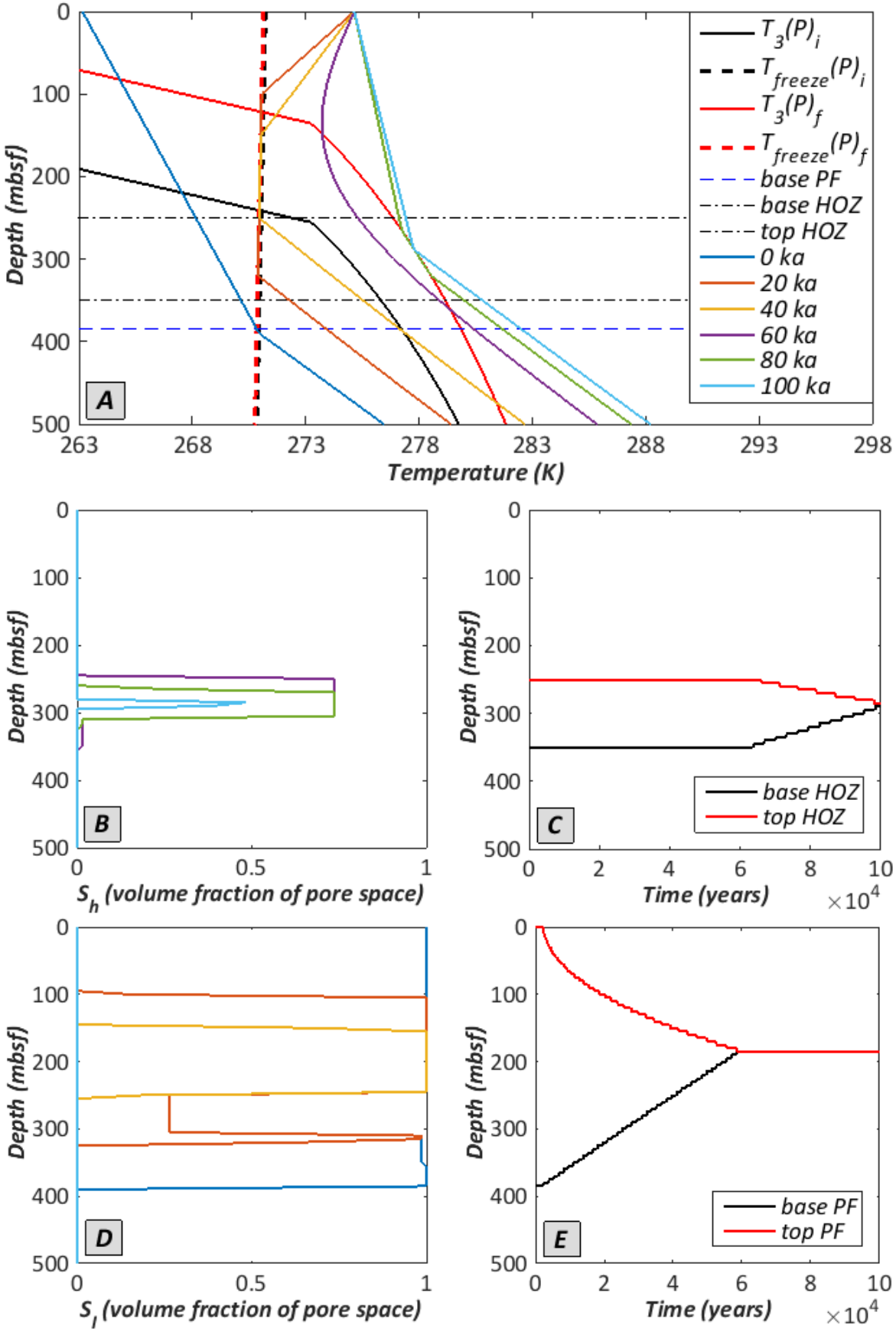

Figure 25. *Evolution of (A) the temperature profile, (B) hydrate saturation profile, (C) base and top of the hydrate occurrence zone (HOZ), (D) ice saturation profile, and (E) base and top of the permafrost (PF), in response to case IV environmental changes in a sediment column in the offshore (subsea) permafrost setting. The legend in (A) also applies to (B) and (D).*

The model anticipates a higher methane hydrate sensitivity to the simulated post-LGM environmental changes in the offshore permafrost setting. Permafrost, initially prevailing to a depth of 385 m, immediately starts degrading from the base at a nearly constant rate, and after 2.3 kyr, once the bottom water has warmed enough to exceed the melting temperature of ice, also from the top at a decreasing rate. All ice degenerates within 59 kyr (figure 25E). Hereafter the hydrate bearing interval starts vanishing from the top after 66 kyr, and at a slightly higher rate from the base after 63 kyr. After 100 kyr methane hydrates only persist in the pore space of sediments over a 5 m thick interval between 285 m and 290 m depth (figure 25C). The evolution of the hydrate and ice saturation profiles are shown in figure 25B and 25D. The evolution of the temperature profile is dictated by the fluctuating intervals where ice and hydrates are melting, as is the case between 285 and 290 m after 100 kyr. Hence a new equilibrium temperature profile has not established within the modelling time frame of 100 kyr (figure 25A).

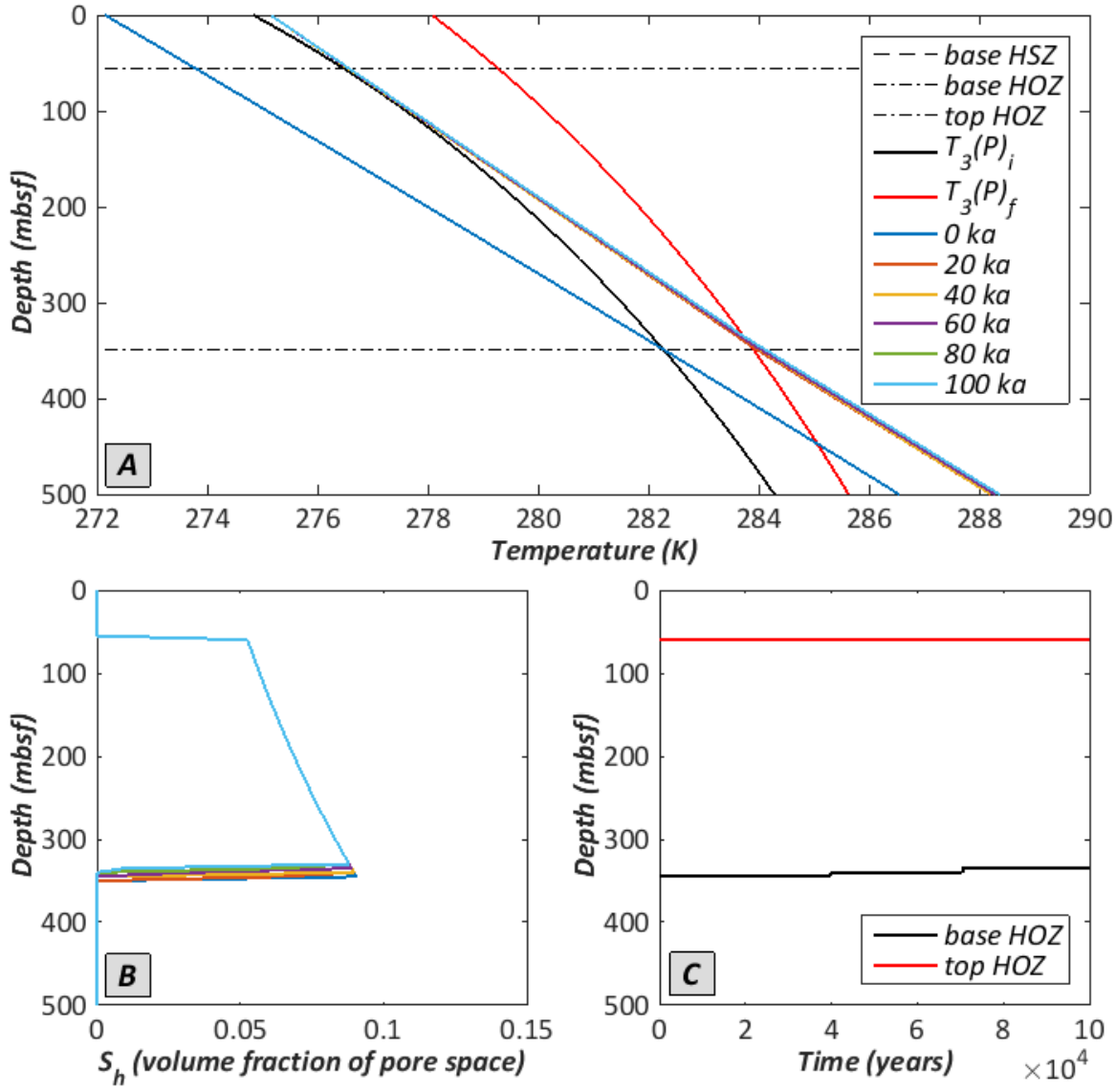

Figure 26. *Evolution of (A) the temperature profile, (B) hydrate saturation profile, and (C) base and top of the hydrate occurrence zone (HOZ), in response to case IV environmental changes in a sediment column on the upper continental slope (300 m initial water depth). The initial position of the base of the HOZ (coinciding with the base of the HSZ) and top of the HOZ are indicated in (A). The legend in (A) also applies to (B).*

The modelled scenario for the upper continental slope setting results in the dissociation of hydrates at the base of the column. However, with only 10 m of melted hydrates within 100 kyr (figure 26C), this effect is rather small. The sea level rise accompanying the temperature increase imposes a significant limit to the extent of hydrate destabilization caused by this temperature increase. If sea level would have remained stable, the entire clathrate reservoir could eventually destabilize, while with sea level rise, only the stability of the lower tens of meters of the hydrate occurrence zone becomes endangered (figure 26A).

The thick methane hydrate bearing zone in the deep water column is not affected by the modelled change in bottom water temperature and sea level rise (figure 27C). Figure 27A indicates that the new equilibrium temperature profile, established after app. 50 kyr, intersects $T_3(P)$ after the sea level rise at a depth where no hydrates occur.

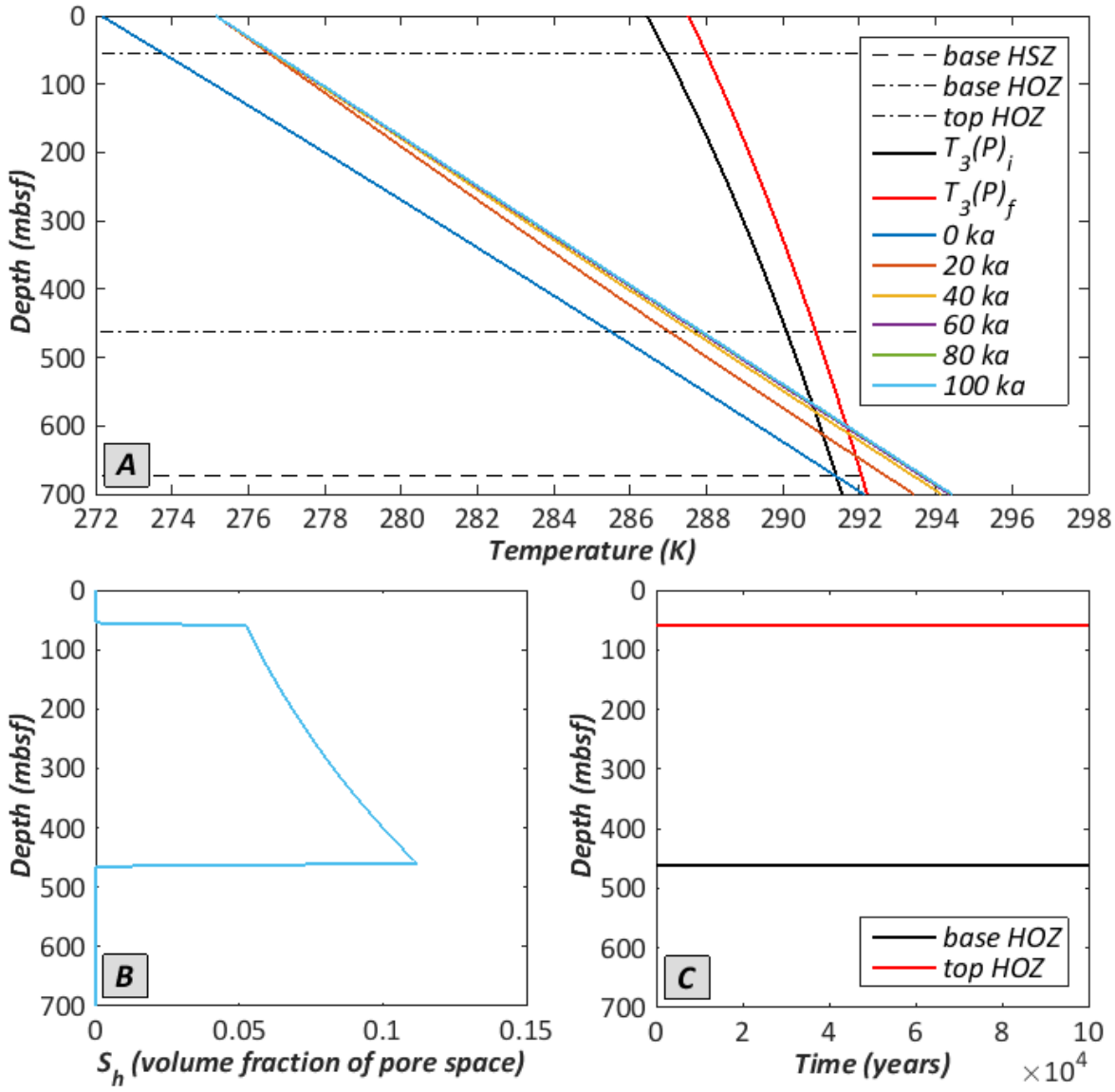

Figure 27. *Evolution of (A) the temperature profile, (B) hydrate saturation profile, and (C) base and top of the hydrate occurrence zone (HOZ), in response to case IV environmental changes in a sediment column on the lower continental slope or continental rise (1000 m initial water depth). The initial position of the base of the HOZ, the base of the HSZ and top of the HOZ are indicated in (A). The legend in (A) also applies to (B).*

6.5. Case V: simulation of contemporary and future climate change

This case is only simulated for the marine settings, as initial temperatures are too high for gas hydrates to occur in a stable initial state in the permafrost environments. Gas hydrates are inferred to initially occur on the upper continental slope between 56 m and 312 m depth below the seafloor. This section of methane hydrate starts to melt upon heating, both from the top and the base. The base of the hydrate occurrence zone starts to shallow after 8.7 kyr, at a faster rate than the deepening of the top, which only initiates after 32 kyr. After 100 kyr, the size of the hydrate occurrence zone has decreased by 28 % (figure 28C). The temperature profile is far from equilibrium after 100 kyr (figure 28A). The 1 m sea level rise does not notably alter the $T_3(P)$ profile and hence does not constitute a significant stabilizing factor.

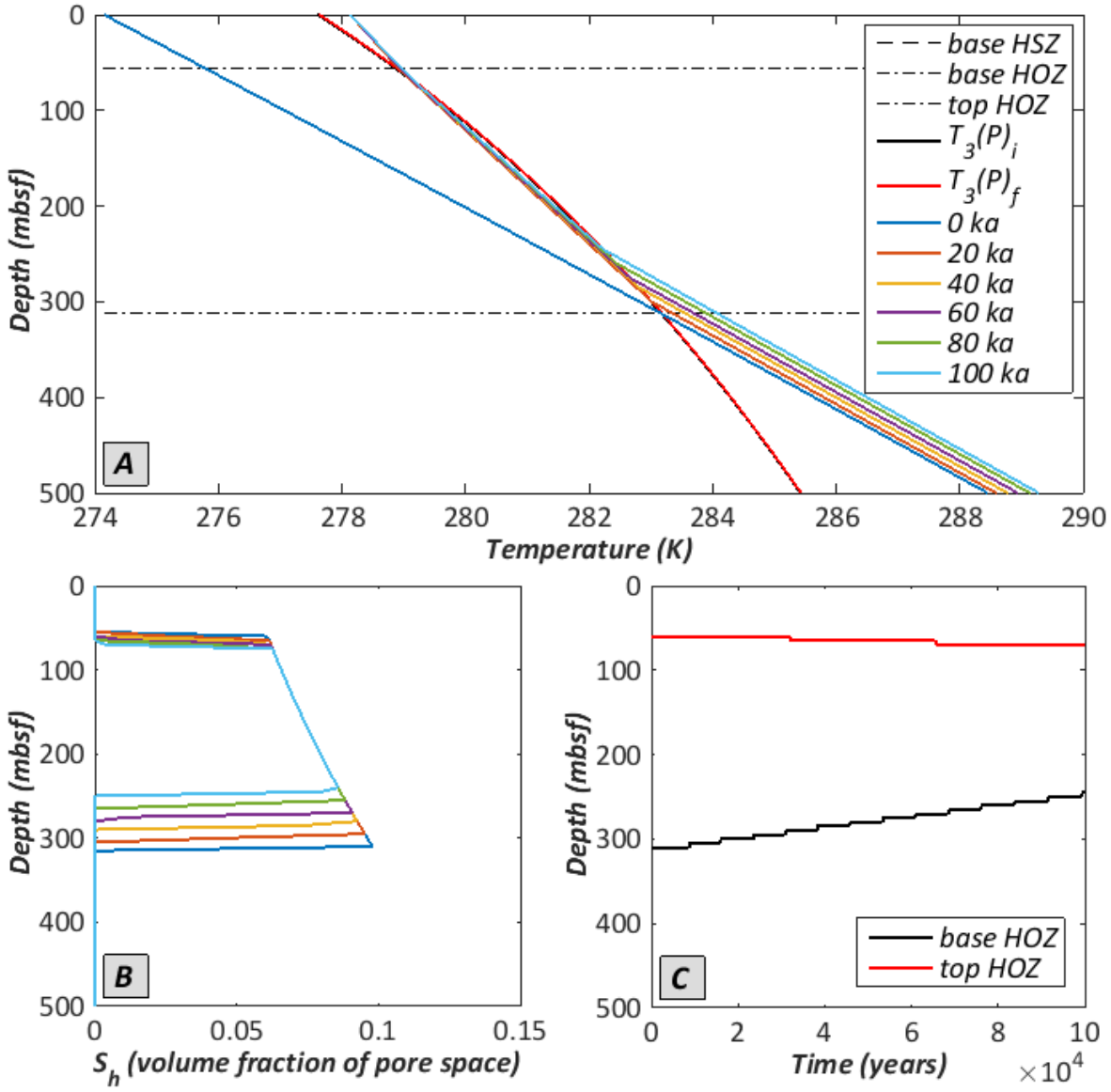

Figure 28. *Evolution of (A) the temperature profile, (B) hydrate saturation profile, and (C) base and top of the hydrate occurrence zone (HOZ), in response to case V environmental changes in a sediment column on the upper continental slope (400 m initial water depth). The initial position of the base of the HOZ (coinciding with the base of the HSZ) and top of the HOZ are indicated in (A). The legend in (A) also applies to (B).*

The model predicts a thick hydrate stability zone in the sediment column at 1000 m water depth, with methane hydrate actually occurring between 56 and 426 m depth in the column. This configuration remains stable during modelling of case V (figure 29C). A new equilibrium temperature profile is achieved after approximately 50 kyr. This new temperature profile intersects $T_3(P)$, which does not significantly change upon a 1m sea level rise, below the base of the hydrate occurrence zone (figure 29A).

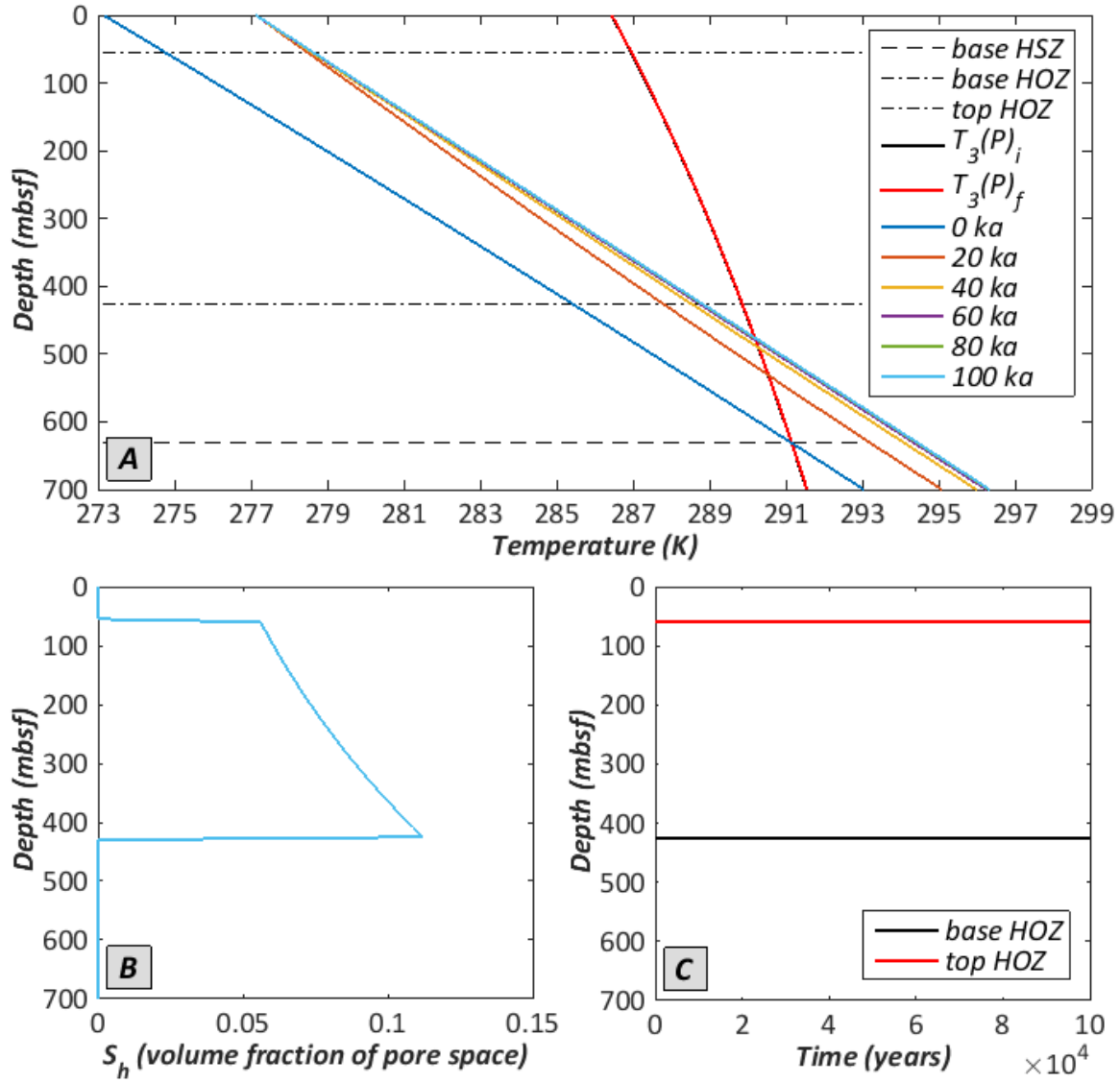

Figure 29. *Evolution of (A) the temperature profile, (B) hydrate saturation profile, and (C) base and top of the hydrate occurrence zone (HOZ), in response to case V environmental changes in a sediment column on the lower continental slope or continental rise (1000 m initial water depth). The initial position of the base of the HOZ, the base of the HSZ and top of the HOZ are indicated in (A). The legend in (A) also applies to (B).*

6.6. Case VI: Palaeocene-Eocene Thermal Maximum

Figure 30A shows that for the high bottom water temperature adopted in case VI, the model predicts a thin hydrate occurrence zone, even in a sediment column at the considered water depth of 1000 m. This configuration is obtained by assuming $q_m = 8 \times 10^{-11}\ kg/(m \cdot s)$, in contrast to $6 \times 10^{-11}\ kg/(m \cdot s)$ in the previous cases, since with the latter value the model anticipates the hydrate occurrence zone to be of zero thickness. The hydrate-bearing interval, initially between 56 m and 119 m beneath the sea floor, degrades from the base after 7 kyr, and from the top at a slightly faster rate after 9 kyr. Clathrates persist longest between 85 m and 90 m depth in the column, until all hydrates are dissociated after 27 kyr (figure 30C). The temperature profile is at equilibrium after the modelling time frame of 100 kyr (figure 30A).

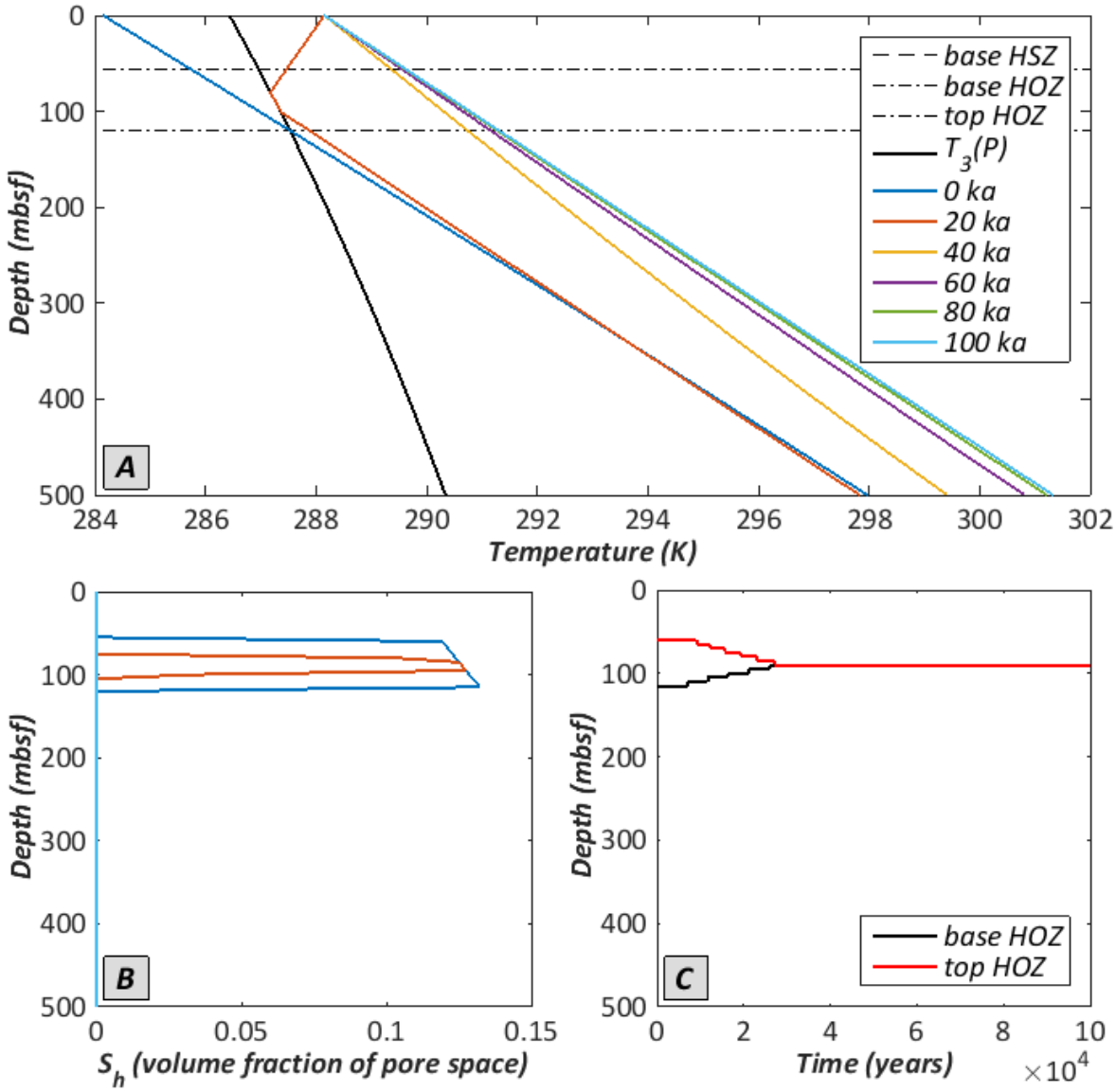

Figure 30. *Evolution of (A) the temperature profile, (B) hydrate saturation profile, and (C) base and top of the hydrate occurrence zone (HOZ), in response to case VI environmental changes in a sediment column on the lower continental slope or continental rise (1000 m water depth). The initial position of the base of the HOZ (coinciding with the base of the HSZ) and top of the HOZ are indicated in (A). The legend in (A) also applies to (B).*

CHAPTER VII. DISCUSSION

7.1. Differential sensitivity of gas hydrates in settings across a high-latitude continental margin – comparison & interpretation of case I-III

The results of this study allow to evaluate and compare the sensitivity of gas hydrate reservoirs to changing environmental conditions in the four distinct geographic settings across high-latitude continental margins. This is essential knowledge when assessing the role of melting gas hydrates in past, contemporary and future climate change.

The results of the case I simulation show that the upper continental slope setting is most sensitive to a gradual 5 °C temperature increase. Figure 13 illustrates that the hydrate-bearing interval starts to decrease in size after 4.6 kyr, and vanishes completely within 50 kyr. The hydrate reservoir in the offshore permafrost setting dissociates completely during the 100 kyr modelling time frame as well, but this requires more time than on the upper continental slope (figure 12), since the subsurface propagation of the temperature pulse is considerably delayed by the consumption of latent heat by melting of ice in the permafrost overlying the hydrate occurrence zone (figure 12A). This effect is even more pronounced in the onshore sediment column, as the permafrost interval is thicker and including the hydrate-bearing zone. Hence hydrate stability in association with thick onshore permafrost proves to be less sensitive to increasing temperatures (figure 11A). Another factor is the presumed larger subsurface depth of gas hydrates in both permafrost-related settings, which delays their response to temperature changes at the surface, as it takes more time for the temperature pulse to propagate towards the hydrate occurrence zone. The model predicts that the deep marine realm is the most stable environment for clathrates under the influence of bottom water warming. Figure 14 demonstrates that only a minor amount of hydrates in this environment dissociates, despite the fact that the HSZ considerably reduces in size. This is explained by the large offset between the base of the HSZ and the HOZ, and indicates that it is important to differentiate between those two zones, in order not to overestimate the amount of dissociated hydrates. The here reported relative order of the settings' susceptibilities to increasing temperatures (upper continental slope and subsea permafrost > onshore permafrost and lower continental slope) is in agreement with previous modelling studies. Reagan and Moridis (2008) for example have modelled the influence of warming bottom waters on shallow-water (± 500 m water depth) and deep-water (> 1000 m water depth) gas hydrates, and also denote the difference between the stable deep marine hydrates and the more volatile shallow marine gas hydrate deposits. Few studies have made a side-by-side comparison of both permafrost-related and oceanic gas hydrates. Ruppel (2011a) highlights the contrast between the stable deep marine and thick onshore permafrost settings on the one hand, and the unstable upper continental slope and subsea permafrost environments on the other. This aligns with the observations in this study.

The above outlined ranking of the settings' sensitivity to changing conditions does not alter when an additional increase in pressure, resulting from rising sea level, is taken into consideration (case II). The pressure increase however has, as could be expected, a stabilizing effect and delays hydrate dissociation. In the upper continental slope column the dissociation rate is slower, especially at the top, and the last hydrates dissociate 30 kyr later than if no 100 m sea level rise would be considered. This also applies to the subsea permafrost setting, although here the dissociation pattern

is altered more drastically as hydrates only start dissociating from the top of the hydrate occurrence zone after 95 kyr. Surprisingly, the pressure increase also causes the ice in the permafrost to disappear at a slightly faster rate (cfr. figure 12E and 15E). This can possibly be explained by the increase in the dissociation temperature of hydrates, i.e. $T_3(P)$, that occur below the base of the permafrost, as a result of the rise in sea level. The pressure increase causes the gas hydrate column in the deep marine setting to remain stable during the simulation.

An important finding is that hydrates in permafrost, but also in shallow marine environments, can dissociate from the top of the hydrate occurrence zone when the newly imposed temperature exceeds $T_{diss}(P)$ at the surface or seafloor (e.g. figure 11, 12 and 13). Methane evolving from this part of the clathrate reservoir is particularly of interest, since it has an enhanced chance to reach the atmosphere for two reasons. First, methane bubbles are more likely to survive their trip through the sediment column, since they do not have to pass the hydrate occurrence zone, which constitutes a physical cap. Second, methane released at the seafloor is more likely to eventually reach the atmosphere as free methane bubbles, since the overlying ocean is shallow. So, if abovementioned temperature conditions are met, a stratigraphic type hydrate deposit in a continental margin section that is under the influence of a single and uniformly warming water mass, can display hydrate dissociation from the top above a particular water depth, while it will only melt from the base below this water depth. This 'critical' water depth is essential knowledge, and can be calculated by replacing P (in kPa) by $(\rho \cdot g \cdot d_{crit})/1000$ (hydrostatic pressure regime) in equation [5] in section 5.2.1:

$$\begin{cases} d_{crit} = \dfrac{1000}{\rho \cdot g} \times exp\left(\dfrac{T_{SF} - 197.65}{9.6349}\right) & T_{SF} \geq 273.15\ K \\ d_{crit} = 1000 \times \dfrac{T_{SF} - 232.7}{0.0158 \cdot \rho \cdot g} & T_{SF} < 273.15\ K \end{cases} \quad [24]$$

where T_{SF} is the newly imposed temperature at the seafloor after warming, given in K. For example, for the case I simulation in this study where the temperature T_{SF} on the continental slope after warming is equal to 280.15 K, d_{crit} is calculated to be 521 m. This means that hydrates in sediment columns that have their top shallower than 521 m water depth can dissociate from the top of the hydrate occurrence zone, while hydrate deposits below deeper water can exclusively melt from their base.

The pressure drop investigated in case III has the largest effect on gas hydrates associated with subsea permafrost (figure 20). $T_3(P)$ decreases because of the sea level fall, and the upper 40 meters of hydrates fall outside the stability field and dissociate. This is delineated by the rapid deepening of the top of the hydrate occurrence zone between 5 kyr and 20 kyr in figure 20C. The reduction in the thickness of the hydrate occurrence zone is accompanied by a small decrease in temperature as heat is consumed by dissociating hydrates. Nevertheless, the model thereafter anticipates the temperature profile to shift to values exceeding the initial temperature profile, although a constant temperature at the seafloor is assumed (figure 20A). This is a result of the tendency of the model to verge towards a linearly increasing temperature with depth, i.e. a constant geothermal gradient, which arises from the assumption that the thermal conductivity is uniform throughout the column and remains constant during the simulation. The initial lower geothermal gradient in the permafrost compared to the ice-free sediments will eventually be cancelled out, and the resulting temperature increase causes further dissociation of hydrates, predominantly from the base, and melting of ice. It is noted that the first upward shift of the base of the ice-bearing zone after 2.3 kyr results from the

small change in the melting temperature of ice with pressure. The pressure decrease also affects hydrates on the upper continental slope, but to a lesser extent and at a slow rate, as indicated by figure 21C. Figure 22A shows that the temperature profile is slightly altered in the lower continental slope column, although no hydrates destabilize. This unexpected result can again be explained by the model behavior, which strives to straighten the initial non-linear temperature profile (cfr. equation [4] in section 5.2.1 for $q_f \neq 0$).

The findings from both case II and III demonstrate that the impact of sea level variations on hydrate stability becomes more important as the initial water depth at the top of the sediment column decreases. This can be explained by the increasing offset between the T_3(P) profiles before and after the sea level change with decreasing water depth. The larger this offset is, the more important the influence of sea level variations on hydrate stability becomes. This shows that it is particularly important to account for large sea level variations when modelling hydrate stability in the subshelf permafrost and upper continental slope settings. The stability of deep-water hydrate reservoirs is clearly less pressure-sensitive.

7.2. Degradation of permafrost

In addition to providing information on the stability of methane hydrates, the model also predicts the rate and mode of degradation of permafrost in response to climate change. The simulations in case I, II and IV demonstrate that the depth interval in which permafrost occurs generally reduces on a timescale of tens of thousands of years or more, and that thick onshore permafrost is more persistent than the subsea permafrost below the shelf. Figure 25E can be used to evaluate the evolution of subsea permafrost after the inundation of the shelf during the last deglaciation. This figure indicates that at present (corresponding to approximately 12 kyr), permafrost is decaying from the top and from the base, but still is present in a large depth interval (> 200 m thickness) in a sediment column at 120 m water depth. The latter is, however, not corroborated by borehole data from the Alaska North Slope, which recorded no permafrost below water depths larger than 50 m (Collett et al., 2011). Previous modelling studies of subsea permafrost below the Russian Arctic shelf (West Yamal) have also predicted faster degradation and a present-day permafrost-free subsurface below 120 m water depth (Portnov et al., 2014). The slow permafrost degradation rate modelled in this study might be a result of the assumption that the pore space is initially entirely occupied by ice (i.e. ice-bonded permafrost), while in nature ice may occupy only a small fraction (ice-bearing permafrost) or even may be completely absent from the pore space of permafrost (ice-free permafrost) (Rachold et al., 2007). In the latter case, a temperature pulse can propagate faster through a permafrost-bearing sediment column, since no latent heat is consumed for the conversion of ice to water. This is also important for the migration of gas released from dissociated hydrates, since without a physical ice-bonded permafrost cap, the gas is more likely to eventually reach the atmosphere (Rachold et al., 2007). Subsea permafrost behavior however remains hard to constrain, since little is known about the subsurface distribution of permafrost and gas hydrates due to the scarcity of direct observations (Rachold et al., 2007), and the inability to distinguish gas hydrates from ice with presently available geophysical methods and borehole tools (Collett et al., 2011).

7.3. Gas hydrates and climate change – discussion case IV-VI

7.3.1. The role of gas hydrates in Late Quaternary climatic oscillations

A variety of studies have presumed that gas hydrates may have played a role in Late Quaternary climatic oscillations (Kennett et al., 2003; Loehle, 1993; Nisbet, 1990; Paull et al., 1991). The case of the last deglaciation following the LGM was simulated in this study (case IV), in order to test a number of hypotheses that have been formulated within the framework of this debate. The results presented in section 6.4 suggest that the rapid warming after the LGM has no effect on the size of the hydrate inventory in the deep marine and onshore permafrost settings, and causes minor destabilization of hydrates in the upper continental slope column, but on timescales as long as 100 kyr. Clathrates in association with subsea permafrost display the highest susceptibility to the changes applied in the simulation. However, the size of the hydrate reservoir in this setting only starts to decrease after app. 60 kyr. Hence the modelling results presented here do not support the hypotheses promoted by Nisbet (1990) and Loehle (1993), which state that rising atmospheric CH_4 and CO_2 levels at the end of the last and penultimate glacial period resulted from methane release from melting hydrates as an immediate response to post-glacial warming. However, here it is shown that the affected hydrate volumes are probably too small and especially that the response is too slow. It is acknowledged that the model presented in this study only accounts for steady-state escape of methane and does not consider a more catastrophic fashion through sliding or slumping, which could rapidly release large volumes of methane. Nevertheless, previous studies have indicated that, for the permeable sediments considered in this study, the build-up of excess pore pressure by the dissociation of hydrates is by itself not sufficient to generate slope failure (Roose et al., 2006; Xu and Germanovich, 2006). Furthermore, the simulation in this study suggests that it takes several tens of thousands of years for the temperature pulse to propagate in the subsurface, so that any pore pressure effect of the conversion of gas hydrates to free gas and water would considerably lag the onset of the deglaciation. This large time lag is somewhat in conflict with the faster response times in the modelling study of Sultan et al. (2004), who attribute the Storegga Slide on the Norwegian continental margin, around 8150 yr BP, to the melting of hydrates since the last deglaciation following the LGM, which started 2000-3000 yr earlier. Importantly, they assume that excess pore pressure can be generated at the top of the hydrate occurrence zone by dissolution (as opposed to dissociation) of hydrates, an idea that is controversial and contested by other researchers (Xu and Germanovich, 2006). The model and assumptions adopted here are different, and can therefore not be compared to the results of Sultan et al. (2004).

Alternatively, hydrate dissociation in response to a sea level fall caused by global cooling has been suggested as a limiting factor to the extent of glaciation (Paull et al., 1991). This situation is actually reverse to the ideas proposed in the above paragraph, as hydrate dissociation is now assumed to have taken place during periods of peak glaciation instead of during deglaciation. The findings from section 6.3 (case III) can be used to assess this hypothesis. As already mentioned above, the model anticipates the pressure drop to have the largest impact on hydrate stability where the water depth is shallowest, i.e. in the subshelf permafrost setting. In this environment, the size of the hydrate reservoir adapts within 20 kyr to the sea level fall, which is sufficiently fast to meet the temporal constraints of the pressure drop hypothesis. Furthermore, the shallow water depth of this environment, in addition to the observation that hydrates melt from the top of the column (figure 20C), enhance the chance that methane gas will eventually reach the atmosphere. However, hydrates in the subsea permafrost setting constitute only a very small fraction (< 0.5 %) of the global

clathrate inventory, and hence potential methane volumes released because of the pressure drop are thought to be small (Ruppel, 2011a). In addition, the cooling that is normally associated with the falling sea level will promote hydrate formation, but is not accounted for in this model. Hence the decrease in size of the Arctic subshelf clathrate inventory in response to a pressure decrease will even be smaller than simulated in this study. Since the pressure drop does not significantly affect the more extensive hydrate reservoirs on the upper and lower continental slope, as suggested by this study, not much methane is expected to be released into the atmosphere by this process and the impact on global climate was thus likely insignificant.

Above theories concern the role of dynamic gas hydrate systems in Quaternary glacial-interglacial alternations, which show an approximate 100 kyr cyclicity (Lowe and Walker, 1997). The *clathrate gun hypothesis* (Kennett et al., 2003) states that melting gas hydrates additionally impinge on higher frequency (millennial-scale) stadial-interstadial climatic oscillations. However, the modelling results and arguments cited for the post-LGM deglaciation simulation (case IV) indicate that hydrate reservoirs are not likely to respond at such (geologically) fast timescales under realistic climate-change scenarios. Further argumentation against the c*lathrate gun hypothesis* was formulated by Archer (2007), who reasons that a sustained increase in steady-state methane release from melting hydrates is required to record a sustained increase in atmospheric methane concentration in ice core records during episodes of warming climate. Single catastrophic spikes of methane release through slumping, as suggested by Kennett et al. (2003), are not likely to be marked in ice core records because of the transient nature of methane in the atmosphere. The most compelling evidence against the hypothesis comes from isotopic measurements on ice core methane by Sowers (2006), who finds that the measured deuterium/hydrogen (D/H) isotope ratios do not support the presumed methane outgassing from a marine methane hydrate source. From balancing global deglacial carbon budgets Maslin and Thomas (2003b) wittily conclude that 'the clathrate gun is firing blanks'. Their alternative explanation is discussed below.

7.3.2. Evaluation of the gas hydrate response to contemporary anthropogenic climate forcing

Contemporary rising atmospheric CO_2 levels as a result of anthropogenic carbon release and subsequent global warming are perceived to be capable of inducing gas hydrate dissociation in the future. How fast this response will manifest is of major importance, since the liberation of CH_4 and its oxidation product CO_2, which are both greenhouse gases, from the gas hydrate reservoir to the atmosphere would provide a positive feedback mechanism with warming climate (Ruppel, 2011a). Some researchers argue that this is already happening today, at methane seep sites on the upper continental slope off Svalbard (Westbrook et al., 2009). Several modelling studies have attempted to outline methane release from hydrates under prospective climate change scenarios. Interpretation of the results of the case V simulation in this study can also make a contribution to this debate.

The model anticipates that on high-latitude upper continental slopes, hydrate dissociation as a response to contemporary climate forcing will not occur within the upcoming millennium (figure 28), and that this will not occur at all in the deep marine realm (figure 29). Remarkably, a range of other modelling studies do report significant hydrate dissociation in shallow and mid-depth environments in the Arctic on century (or even faster) timescales (Biastoch et al., 2011; Hunter et al., 2013; Marín-Moreno et al., 2013; Reagan and Moridis, 2008; Reagan et al., 2011). Besides small variations in the choice of parameter values and imposed climate change scenarios, some major differences between

the modelling approach of these studies and the model deployed in this study should be regarded, in order to understand this discrepancy. First, in numerated models hydrates are assumed to be present over the entire extent of the HSZ, except for the sediments immediately below the seafloor where a sulphate reduction zone with a maximal thickness of 10 m is assumed to impede hydrate formation. Hence hydrates exist at much shallower depths than proposed in this study, where the top of the hydrate occurrence zone is modelled to be present at more than 50 m below the seafloor, because of the diffusive loss of methane towards the seafloor. It is exactly this section of hydrates in the upper tens of meters below the seafloor that is most susceptible to bottom water warming. This can be inferred from the temperature profiles presented in this study, which indicate that the rate of warming, especially in the first hundreds to thousands of years after the onset of the temperature rise at the seafloor, is largest at the top of the sediment columns and decreases with depth. Subsequently, hydrates at very shallow depths will degrade rapidly from the top, given that the newly imposed bottom water temperature exceeds T_3 at the seafloor (see section 7.1). Regarding the bottom end of the column, it can be derived from the simulation results in figure 29 that not differentiating between the base of the HSZ and the base of the hydrate occurrence zone can lead to an over-prediction of the rate and amount of hydrate dissociation from the base. This is especially important in deep water settings, since the offset between the base of the HSZ and HOZ is modelled to be largest here. A second point is that the models of Biastoch et al. (2011) and Hunter et al. (2013) do not account for latent heat consumption during hydrate dissociation, which can also be part of the explanation why the predicted hydrate response times differ at least one order of magnitude between their models and this study.

It appears that knowing the depth of the top of the hydrate occurrence zone is central to the discussion whether methane gas is likely to be released from contemporary warming-induced melting hydrates and bubbling out of the seafloor in the upcoming centuries, or is already doing so on the West Svalbard continental margin as proposed by Westbrook et al. (2009). The model presented in this study, relating on the hydrate formation theory of Xu and Ruppel (1999), suggests that this is not a likely hypothesis, since very climate-sensitive hydrates are predicted to be absent from the shallow sediments in the upper tens of meters below the seabed. This aligns with the hydrate distribution models of Davie and Buffett (2001) and Buffett and Archer (2004), and with the foreseen hydrate melting response timescales of millennia or longer by Archer (2007). Furthermore, results from drilling campaigns, during which hydrate sampling and borehole measurements were used to assess hydrate distribution in the subsurface, generally have not reported the presence of hydrates in the top tens of meters of the seafloor (Davie and Buffett, 2003), except for a small number of spatially confined structural hydrate deposits where very high methane fluxes along faults and channels allow hydrates to prevail near the seafloor, for example in the Gulf of Mexico and at Hydrate Ridge (Archer, 2007). In contrast, the 'believers' of the idea that dissociation of hydrates, induced by recent warming, is the primary cause of the gas seeps on the west Svalbard upper continental slope, do assume that shallow hydrates exist in stratigraphic-type deposits, i.e. over laterally extensive areas. However, a seismic study by Sarkar et al. (2012), on which this assumption is partly based, is not truly compelling regarding the presence of hydrates directly below the methane seeps, as there is no evidence for a BSR in the gas flare region. The latter is argued to not necessarily rule out the presence of hydrates at low saturations (Chabert et al., 2011). Sarkar et al. (2012) further propose that shallow gas pockets, observed below the gas flare region at depths where their modelled hypothetic BSR locates, can be a surrogate for a true BSR, above which

hydrates might prevail in the very shallow subsurface (< 15-25 m below the seafloor). However, such an observation is open to multiple other interpretations that omit the presence of gas hydrates. As long as the existence of gas hydrates over laterally extensive areas at such shallow depths below the gas flares on the west Svalbard upper continental margin is not ground-truthed, the hypothesis of Westbrook et al. (2009) will remain highly speculative, as will the models that foresee century-timescale response to contemporary and future climate change (Biastoch et al., 2011; Hunter et al., 2013; Marín-Moreno et al., 2013). Berndt et al. (2014) corroborate that dissociation of hydrates contributes to the observed gas seeps, but present evidence that this has been going on for at least 3 kyr through the dating of authigenic carbonate crusts that precipitate as a result of anaerobic oxidation of the seeping methane by microbes. At the same time, these authors suggest that seasonal fluctuations in bottom water temperatures of 1-2 °C cause periodic hydrate dissociation and formation at the location of the seeps. Again this is based on modelling of lateral shifts of the HSZ in the top 5 m of surface sediments, and therefore this hypothesis is subject to the same points of criticism already outlined above. An additional argument pleading against seasonal variations in the size of the hydrate reservoir, is that the formation timescale of hydrates is generally believed to be in the order of millions of years (Davie and Buffett, 2001), which greatly exceeds the proposed seasonal scale growth.

To conclude, it appears from this study that gas hydrates will generally be protected from rapid warming and melting, because of their depth in the subsurface. The response time is foreseen to be at least in the order of magnitude of thousands of years. Other carbon pools that have a more direct link to the atmosphere and hence have the ability to create faster feedback mechanisms to contemporary warming, are discussed in section 7.3.

7.3.3. Significance of hydrate dissociation in the PETM carbon isotope excursions

The carbon isotope excursion across the PETM constitutes a third case of how dissociating gas hydrates beneath warming oceans have been invoked to explain past changes in the global carbon cycle. Researchers defending this hypothesis believe that there is a connection between the > 4 °C rise in ocean temperature (inferred from $\delta^{18}O$ values), dissociation of strongly ^{13}C depleted methane hydrates ($\delta^{13}C < -60$ ‰), and the observed worldwide negative shift of carbon isotope values in proxy records. Findings from modelling in this study however reveal issues considering this *gas hydrate dissociation hypothesis* (Dickens et al., 1995), in terms of the size of the Late Palaeocene hydrate inventory and the timescales at which its size can fluctuate.

If the temperature change is applied to size estimates of the present-day gas hydrate inventory, the volumes of released methane from destabilizing hydrates are predicted to be large enough to explain the negative shift of 2-3 ‰ in $\delta^{13}C$ (Dickens et al., 1995). Nevertheless, the model presented here, in accordance with other studies (Buffett and Archer, 2004), indicates that it is not appropriate to use the size of the present-day clathrate inventory as an analog for the Late Palaeocene global hydrate reservoir, for two reasons. First, the hydrate stability zone would have been notably smaller because of the higher bottom water temperatures. The model for example predicts a 545 m thick HSZ in the deep marine column at 1000 m water depth if the sea bottom temperature is 2 °C (figure 14A), as opposed to a barely 110 m thick HSZ at the same water depth for Late Palaeocene conditions (11 °C, see figure 30A). Second, increased bottom water temperatures promote diffusive loss of methane towards the seafloor (Buffett and Archer, 2004), which in addition to the size reduction of the HSZ also reduces the extent of the zone of actual hydrate occurrence. Compensating for this diffusive loss

requires an enhanced supply of methane to the HSZ in order to create a situation where the pore water methane concentration exceeds solubility, so that hydrates can form. The PETM simulation (case VI) in this study, which adopts the hydrate formation model of Xu and Ruppel (1999), reflects the need for higher methane fluxes with rising ocean temperatures, since the hydrate occurrence zone was modelled to have been of zero thickness when an average methane flux of $6 \times 10^{-11}\ kg/(m \cdot s)$, as assumed for the other cases, was used. Similarly, formation models that consider in situ production of methane by microbial conversion of organic matter, also predict that a higher organic carbon input is required for hydrates to form under warmer bottom waters. This stringent requirement will become especially more problematic as the ocean deepens, since carbon rain generally decreases with increasing water depth (Buffett and Archer, 2004). Hence warming ocean temperatures eliminate gas hydrates from sediment columns under shallow water depths because of the shrinkage of the size of the HSZ, but also from deep water columns because of the sharpened demand in terms of methane supply, either through in situ conversion of organic matter or advection from below. This implies that the sediment volume in which gas hydrates can be present must have been considerably smaller in the warm Late Palaeocene oceans than at present. As argued by Dickens (2011), this effect can to some extent be counteracted by a decrease in oceanic O_2 levels, which reversely favors organic carbon supply to seafloor sediments, and by an increase in the biogenic methane production rate in the subsurface with increasing temperature. The model assumptions adopted in this study do not allow to assess the latter parameters.

A second issue to consider when assessing the role of dissociating gas hydrates in the PETM carbon isotope excursion, as well as in five smaller carbon isotope excursions tailing the PETM, is the rate at which the size of the hydrate reservoir can fluctuate. The observed carbon isotope excursions across these hyperthermal events display a rapid release of ^{13}C-depleted carbon (i.e. a rapid negative shift in $\delta^{13}C$) on a time scale of less than 10 kyr, followed by a slow recovery towards the higher initial $\delta^{13}C$ values within a few hundreds of thousands of years (Archer, 2007). Dickens (2011) claims that the observed $\delta^{13}C$ patterns correspond well to the characteristics of the methane hydrate reservoir, which can shrink fast but recharges more slowly, and uses this to validate the *gas hydrate dissociation hypothesis.* The observations from the PETM simulation in this study indicate that a hydrate response time of < 10 kyr after the ocean warming might be a little optimistic, since figure 30 illustrates that the hydrate occurrence zone does not drastically decrease in size within 10 kyr. Nevertheless, with the entire hydrate column disappearing within 27 kyr, the response time scale remains relatively fast. It is furthermore acknowledged that the model presented here does not account for catastrophic release of methane through sediment failure, which could eventually accelerate the response of the hydrate inventory to the imposed warming. A bigger issue could be the formation timescale of gas hydrates, which needs to be sufficiently fast to explain the hyperthermal events that follow the PETM by the *gas hydrate dissociation hypothesis*. Those events follow the PETM with intervening time periods of 100 to 700 kyr (Dickens, 2011). Invoking the dissociation of hydrates to explain these carbon isotope excursions requires that enough hydrates can accumulate within these intervening intervals. However, the formation timescale of clathrates is generally considered to be one order of magnitude larger (Davie and Buffett, 2001). For the assumptions in this study, with an accumulation period τ' equal to 1.88 Ma, the hydrate saturation does not exceed 15 % of the pore space (figure 30B). This suggests that within an accumulation period of only 100 kyr, as was the case between some of the post-PETM hyperthermal events, hydrate saturations can only increase by less than 1 % of the pore space, given that the conditions

are appropriate for the formation of hydrates. This implies that the fluctuations in size of the Late Palaeocene-Early Eocene hydrate inventory, which is already inferred to be smaller than at present (see above), cannot have been very extensive. This effect was also denoted in the study of Archer and Buffett (2005), who point out that the temperature feedback mechanism during melting events becomes more spectacular as climate cools, since the affected hydrate volumes are larger.

To summarize, it appears from this study that the main issue with invoking gas hydrates as the source for ^{13}C-depleted carbon during the PETM revolves around the size of the Late Palaeocene hydrate inventory, which was possibly too small to explain the observed negative shift in $\delta^{13}C$ values. The latter could however not thoroughly be assessed based on the findings from this study, since this would require detailed carbon mass balance equations and the evaluation of a number of parameters (e.g. methanogenesis rates, ocean water O_2 concentrations) that are not considered in the model. The second problem relates to the slow formation rate of hydrates, but does not apply to the PETM event itself, since this was the first event in a series of carbon isotope excursions, leaving ample time for hydrates to accumulate in anticipation of the PETM. The model presented here furthermore suggests that the hydrate dissociation timescale could have been sufficiently fast. Therefore, the *gas hydrate dissociation hypothesis* can be considered to be an acceptable theory for explaining (a part of) the negative carbon excursion and rapid global warming across the PETM. Nevertheless, as long as no truly compelling evidence for or against theory is presented, the source of the ^{13}C-depleted carbon will remain elusive. A number of alternative theories are discussed in the next section.

7.3.4. Gas hydrates and climate change: conclusions and alternatives

Above paragraphs presented an evaluation of a number of theories in which gas hydrates are argued to have a potential link to past, present or future climate change. To conclude this section, the two most decisive aspects in this discussion, i.e. the timescales of the processes and volumes of gas hydrates and free gas involved, are synthesized. Simply stated, two conditions must be fulfilled for the gas hydrate reservoir to be considered as a direct capacitor of climate change: (i) the timescales need to be sufficiently fast, and (ii) the volumes must be sufficiently large (Buffett and Archer, 2004).

7.3.4.1. Timescales

Figure 31 shows how the dissociation timescales modelled in this study relate to the timescales of other processes that govern the size of the clathrate inventory, atmospheric greenhouse gas levels and global climate. A distinction is made between rapid (stadial/interstadial) and slow (glacial/interglacial) climatic cyclicity, and rapid (catastrophic) and slow (steady-state) hydrate dissociation. From this figure it appears that the climatic cycles generally oscillate on a timescale that is faster than the timescale at which the size of the gas hydrate reservoir can fluctuate. This not only applies to the degradation of gas hydrates upon warming, but especially to the restoration of the clathrate reservoir through hydrate formation upon climatic cooling, which is the slowest in the chain of processes apart from the long term cooling trend since peak warmth in the early Cenozoic. The only case for which a direct link is suggestive, is the similarity between the timescales of postglacial warming and catastrophic methane release from the slumping of hydrate-rich sediments. This connection is already discussed above, in the framework of the simulation of the last deglaciation following the LGM. However, even in this case an initial trigger is required to initiate hydrate dissociation and subsequent sediment failure, so that variations in global hydrate volumes would rather follow than lead climate change.

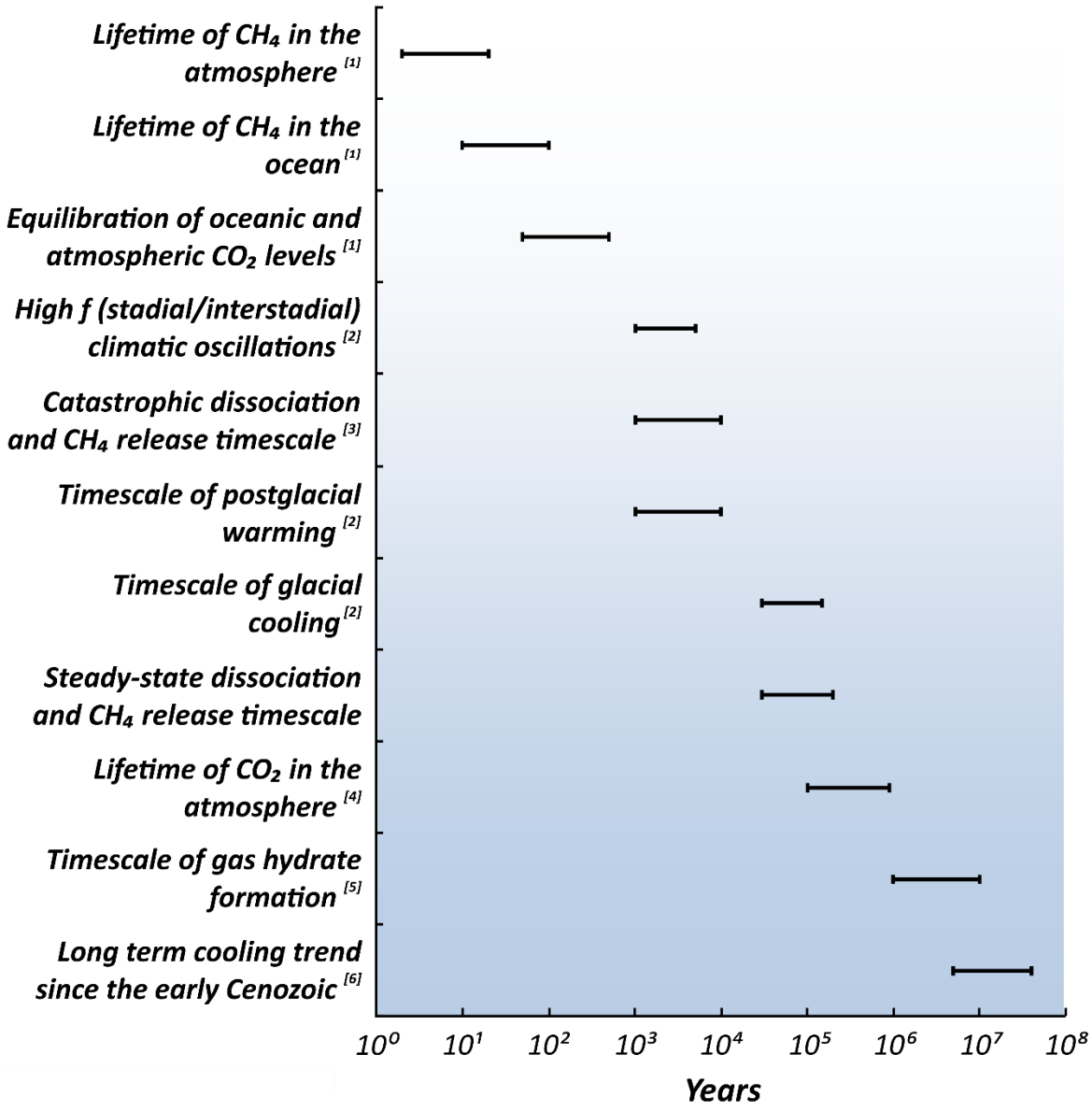

Figure 31. *Compilation of the timescales of processes involved in gas hydrate reservoir size changes, atmospheric greenhouse gas fluctuations, and climatic oscillations. The timescales for chronic release of gas from dissociating hydrates is obtained from this study, other values from: [1] Archer (2007) ; [2] Lowe and Walker (1997) ; [3] Sultan et al. (2004) ; [4] Archer et al. (2009b); [5] Xu and Ruppel (1999) ; [6] Archer and Buffett (2005).*

A primary governing role of hydrates in climate change can thus generally be excluded, and the entire discussion should rather focus on how dynamically gas hydrate dissociation is able to follow climate warming, in order to assess the potential positive feedback of methane release from melting hydrates on climate warming. Modelling results in this study demonstrate that chronic hydrate dissociation and subsequent methane release are likely to occur as a response to climatic forcing, but significantly lag the imposed temperature fluctuations by several tens of thousands of years. This implies that the majority of the methane gas that is stored in the clathrate reservoir, is probably not volatile enough to create a positive feedback mechanism shortly after the initiation of climate warming. Without such a feedback and sufficiently fast response times, it is not straightforward to unravel a close link between fluctuations in the extent of the hydrate reservoir and atmospheric greenhouse gas levels or climatic oscillations. Climate usually changes faster than the rate at which the size of the gas hydrate reservoir can adapt, which means that clathrates are most of the time in a

transient, non-equilibrium state, especially when relatively rapid climatic oscillations, like those recorded during the Late Quaternary, are regarded. This implies that at present, methane hydrate systems are not stable, and neither were they before the onset of contemporary anthropogenic warming. It further appears from the model presented that situations may arise where climate and the size of the hydrate reservoir are even fluctuating in a somewhat 'out of phase' mode, with dissociation of hydrates during climate cooling and formation of hydrates during climate warming. This can, however, not be fully assessed since hydrate formation was not accounted for in the model. Anyhow, it indicates that the interpretation of the role of gas hydrate stability in global climate, although in some cases being suggestive, is not straightforward at all. Furthermore, the ocean water column constitutes an additional buffer between gas hydrates and the atmosphere, which with increasing water depth progressively delays and impedes the release of methane to the atmosphere (Archer, 2007). The timescales in figure 31, however, illustrate that oxidation of methane to CO_2 (both in the water column and in the atmosphere) and equilibration between oceanic and atmospheric CO_2 levels is fast compared to methane release from dissociating hydrates. This implies that it is eventually not a spike of CH_4, but the resulting excess of its oxidation product CO_2 that will persist in the atmosphere, and through its greenhouse potential will contribute to warming climate. It is estimated that subsequent neutralization of the excess atmospheric CO_2 through weathering of silicates takes several hundreds of thousands of years (Archer et al., 2009a).

7.3.4.2. Volumes of potentially volatile methane hydrate

The second matter that is central to the discussion about the significance of gas hydrates in the global climate system is the volume of gas hydrates that is prone to dissociation upon climate warming. This is for example one of the main points of controversy regarding the *gas hydrate dissociation hypothesis* for the PETM, as already discussed in paragraph 7.2.3. Next, it appears from this study that the most volatile part of the global gas hydrate reservoir is primarily restricted to subsea permafrost in high latitude areas and upper continental slope settings. Ruppel (2011a) however estimates that the former setting comprises only less than 1 % , and the latter app. 3.5 % of the global hydrate volume. Moreover, the model predicts that even in these environments, only a small fraction of hydrates occurring at very shallow depths below the seafloor are predicted to melt on a very fast (decadal-centennial) timescale. As already discussed above, hydrates at such shallow depths generally only prevail in structural type deposits, at sites with focused high methane fluxes (e.g. mud volcanos, faults, porous channels, seep sites). Nevertheless, the volume of hydrates held in structural type deposits is small, since most hydrates are presumed to occur in laterally extensive stratigraphic type deposits (Archer et al., 2009a). Hence only a fraction of a small fraction of the global hydrate reservoir is prone to rapid dissociation, for which it should additionally be taken into account that only a small portion of the released methane will eventually reach the atmosphere.

Another mechanism that has been invoked to explain a rapid transfer of large volumes of methane from hydrate reservoirs to the atmosphere is submarine sediment failure and subsequent sliding on continental slopes because of the build-up of excess pore pressure through the dissociation of hydrates. However, the dissociation timescales that appear from this study can be used to raise objections against the significance of this process. The generation of a submarine slide requires build-up of excess pore pressure over relatively large areas of the slope, which can only be achieved through melting of stratigraphic type hydrate deposits. However, the model predicts that it takes thousands to tens of thousands of years before these hydrates start to melt, because of their depth

in the subsurface, and hence a comparatively long time lag should be taken into account between the onset of bottom water warming and eventual sediment failure. To test the *clathrate gun hypothesis*, Maslin et al. (2004) have collected the ages and locations of submarine sediment failures that occurred in the North Atlantic, and tried to correlate them with climate variations over the last 45 kyr. They find that the age of a large fraction of the slides correlates with rising sea level and peaks in atmospheric CH_4 levels during the deglaciation following the LGM, which supports the *clathrate gun hypothesis* for glacial to interglacial transitions. However, a significant number of slides does oppositely correlate with Heinrich events, i.e. intervals characterized by low sea level and, most notably, low atmospheric methane concentrations. This implies that the *clathrate gun hypothesis* does not hold true for millennial-scale stadial/interstadial climatic oscillations, and questions the extent of the methane volumes that are potentially transferred from hydrate reservoirs to the atmosphere through catastrophic submarine sediment failure. Maslin et al. (2004) further use the locations of the slides to infer their cause. The sediment failures that correlate with Heinrich events are primarily located in low-latitude areas, and are probably caused by a reduction in the hydrostatic pore pressure, because of the falling sea level, and associated dissociation of hydrates. In contrast, more recent slides that are associated with the last deglaciation mainly occurred at high-latitudes, where post-glacial isostatic rebound could have triggered earthquakes or reduced the hydrostatic pore pressure. These results indicate that slope failure and climate change are probably primarily linked by pore pressure effects, rather than by warming-induced hydrate dissociation as has been claimed by Kennett et al. (2003) in the *clathrate gun hypothesis*. This is corroborated by this study, as it is indeed shown that changes in pressure can propagate in the subsurface and affect hydrate stability much faster than changes in temperature are able to do.

Since global gas hydrate volumes, as well as their distribution over the different geographic settings and the amount of free gas trapped below them, are still poorly constrained (Piñero et al., 2013; Ruppel, 2011a), it remains challenging to make accurate quantitative estimates of the amounts of gas that can potentially shift from the hydrate reservoir to the atmosphere. After all, even for the largest size estimates, the conclusion is that the parts that by far constitute the largest fraction of the global hydrate reservoir, i.e. stratigraphically constrained hydrates deep in the subsurface of continental margins, are the most stable and commonly respond to warming climate on timescales of tens to hundreds of thousands of years. Without contribution of methane from this part of the reservoir, the volumes of methane that can be rapidly transferred from gas hydrate systems to the atmosphere are probably too limited to interfere with rapid climatic oscillations.

7.3.4.3. Alternative explanations for transfers of methane to the atmosphere

The above discussion reveals that the timescales of warming-induced hydrate dissociation are generally too slow and the involved volumes too small to generate rapid and significantly large transfers of methane from the hydrate reservoir to the atmosphere. This paragraph discusses a number of alternative climate-sensitive carbon pools that have been proposed to explain the close link that has been observed between climate and atmospheric CH_4 and CO_2 levels, or that potentially constitute a positive feedback loop with warming climate.

Plausible alternatives should feature what the hydrate reservoir generally lacks: a fast and direct connection to the atmosphere and large volumes of volatile methane. Most alternative theories regard a terrestrial source of methane, and as such are more likely to fulfill the former demand than the (marine) clathrate reservoir does. For example, escape of methane from natural gas

accumulations that were originally trapped below now degrading permafrost and glaciers is estimated to release 1.5-2 Mton of methane per year in Alaska alone, thus possibly providing a positive feedback mechanism to contemporary warming climate (Walter Anthony et al., 2012). This process can as well have played a role in Late Quaternary climatic oscillations, although evidence in the geologic record is lacking (Etiope, 2012). Additionally, microbial conversion of organic carbon to CH_4 and CO_2 gas within thawing permafrost soils can further reinforce this feedback (Schuur et al., 2015). The latter mechanism has also been invoked to explain the carbon isotope excursions across the PETM and subsequent hyperthermal events (DeConto et al., 2012). This study claims that Arctic and Antarctic terrestrial permafrost (though being controversial) existed at that time, and that the amount of organic matter stored in it was large enough to release several thousands of Gton of carbon to the atmosphere during each of the hyperthermals. Other mechanisms invoked for the PETM comprise rapid oxidation of organic matter deposited in an afterwards subaerially exposed shallow seaway (Higgins and Schrag, 2006), widespread burning of peat (Kurtz et al., 2003), North Atlantic magmatism (Svensen et al., 2004), or more exotically, a comet impact (Kent et al., 2003). Deuterium/hydrogen (D/H) isotope measurements on ice core methane indicate that marine gas hydrates were stable during late Quaternary abrupt warming intervals, and that, amongst others, alterations in methane emissions from wetlands might have affected atmospheric methane levels (Sowers, 2006). On the basis of carbon mass balance equations, Maslin and Thomas (2003a) support this theory and conclude that changes in the extent of wetlands and peat bogs are the primary driver for the observed fluctuations in atmospheric methane concentrations. Furthermore, to have this variations recorded in ice cores, a sustained chronic release of methane is required. The latter is more consistent with a wetland source for methane, rather than a single spike of methane through catastrophic release from dissociating hydrates (Archer, 2007). With a present-day flux of approximately 175 Mton per year (Etiope, 2012) the volumes of methane involved in degassing from wetlands are vast, which further promotes the hypothesis that wetlands can be a significant capacitor in global climate.

7.4. Model evaluation

One should bear in mind that after all, models try to simulate real processes with the aim to approximate nature as close as possible, but that there is no guarantee that they consistently reproduce what is taking place in reality. In general, the best way to evaluate the quality of a model is to test it with field observations in the natural environment. Such a validation is however hard to achieve for the model in this study, because it did not focus on a specific study area but a hypothetic high-latitude continental margin, but also simply because field observations of the dissociation of gas hydrate are not straightforward to recognize or interpret as such, and because the timescales that appear from this study are impossible to test. A proxy for the past evolution of the size of the global gas hydrate reservoir would be an invaluable tool, but unfortunately such a proxy is not known at present. Therefore, the model is evaluated based on the comparison with previous modelling studies, which is already occasionally discussed in the previous paragraph, and literature, to see what the qualities and the weaknesses of the model are.

7.4.1. Qualities of the model

First, the simulations presented in this study allow to assess hydrate stability in four distinct environments, based on a single model that adopts a very similar set of assumptions and modelling approach in both marine and permafrost-related settings. The model therefore excellently lends

itself for comparison between the settings' climate-sensitivities, more than a compilation of results from a variety of setting-specific modelling studies with dissimilar fundamental assumptions would do. Although this research focuses on a high-latitude continental margin, the model is widely applicable to any continental margin and a broad range of pressure-temperature conditions. Despite the fact that the model neglects a number of small-scale and fast operating processes (see below), it is expected that the model's predictions are sufficiently accurate for the scope of this study, i.e. assessing the long-term evolution of hydrate stability on a large scale, as the model accounts for the most fundamental thermodynamic principles and parameters in natural gas hydrate systems.

Second, by implementing robust formation models, realistic initial hydrate saturation profiles are obtained. This appears to be a crucial factor when assessing the role of destabilizing hydrates in moderating global climate. The importance of differentiating between the hydrate stability and occurrence zone for example was illustrated by the case I simulation for the deep marine environment (figure 14), which showed that a significant decrease in the extent of the HSZ not necessarily implies that large hydrate volumes will dissociate. Hence large overestimations of potentially destabilizing hydrates can be expected from studies that presume that the size of the HSZ is representative for the size of the zone where hydrates actually occur. Formation models additionally show that very shallow methane hydrates, which would be most sensitive to changing environmental conditions and in multiple studies inferred to be releasing methane very shortly after the onset of warming (Hunter et al., 2013; Marín-Moreno et al., 2013; Westbrook et al., 2009), are rather the exception than the rule, and that the size of the global clathrate inventory during the Late Palaeocene was probably considerably smaller than at present.

Finally, the model accounts for the latent heat that is consumed during the melting of both gas hydrates and ice. This process, although being neglected in a number of modelling studies published in high impact journals (Biastoch et al., 2011; Hunter et al., 2013), significantly delays the propagation of a temperature pulse in the subsurface. This is demonstrated in this study, for example by the results of the case I simulations. In the deep marine sediment column (figure 14A), in which very few hydrates dissociate, the temperature profile achieves a new equilibrium state in less than 40 kyr. In contrast, this takes approximately 80 kyr in the upper continental slope column where hydrate stability is more strongly affected (figure 13A), and over 100 kyr in the permafrost settings in which both ice and hydrates melt (figure 11A and 12A). This illustrates that the time-lags in modifying the subsurface thermal state resulting from latent heat consumption can be in the order of tens of thousands of years, which cannot be overlooked, especially when the timescales over which is modelled are within the same or a smaller order of magnitude.

7.4.2. Uncertain model parameters and processes not accounted for

Kinetic effects that appear during the formation or melting of gas hydrates are neglected in this model. This is justified by the study of Rempel and Buffett (1997), who find that these effects are negligible in natural environments since they operate at a much faster timescale than the timescales that characterize hydrate formation and dissociation. The model further did not account for capillary effects, which can impede the stability of hydrates at sites where they solely on the basis of temperature, pressure and salinity conditions, should exist. However, for the porous and permeable sediments considered in this study, which are normally characterized by a narrow pore size distribution and a relatively large mean pore size, capillary effects are inferred to be small (Liu and Flemings, 2011).

The model further adopts the hydrate formation model of Xu and Ruppel (1999) for the marine settings, which only applies to homogeneous and porous sediments. Hence the model cannot be used to evaluate hydrate stability in heterogeneous marine sediment columns that for example feature vertical variations in lithology, porosity and permeability. The formation model of Behseresht and Bryant (2012), on which the initial hydrate saturation profiles in the permafrost environments in this study rely, does allow to implement sedimentological variations with depth in the column. This is a point where the model can be extended in the future, in order to simulate hydrate dissociation patterns in permafrost-related converted free gas reservoirs in sediments with vertically varying characteristics. It is also acknowledged that, since the model is one dimensional, gas hydrate distributions and processes like fluid or methane flow can only be modelled in the z direction. This is especially problematic when hydrate saturation patterns are laterally discontinuous, as can be expected in structural type hydrate deposits. However, stratigraphic type deposits which are laterally continuous and after all comprise the largest fraction of global gas hydrate volumes (Archer et al., 2009a), can appropriately be evaluated using the one dimensional modelling approach adopted in this study. Another problem revolves around defining initial temperature profiles, which is a necessary boundary condition to the numerical model. As in most modelling studies, the initial subsurface temperature profiles were assumed to be at equilibrium, although this is not a common situation at all. The results from this study for example indicate that it takes tens of thousands of years before a new equilibrium thermal state is attained after a temperature disturbance at the surface or seafloor.

The thermal conductivity was assumed to be uniform throughout the sediment columns and independent on the relative amounts of the phases (ice, hydrate, gas, liquid) present in the pore space, which actually change as the simulation runs. These changes are expected to be small when hydrate saturations are low, as for example in the upper and lower continental slope settings, because the thermal conductivity then remains fairly constant. This assumption however constitutes a bigger problem in the permafrost settings, since the changes in hydrate or ice saturations were modelled to be potentially large, which implies that the thermal conductivity can significantly change through time. Hence it would be more appropriate to recalculate the thermal conductivity at each time step, based on the phases present at that moment. This is definitely a point where the model can improve in the future. The same accounts for the presumed constant salinity, which fairly holds true for low hydrate saturations in the marine realm (Xu and Germanovich, 2006), whereas significant shifts in salinity can be expected and in fact should be accounted for when calculating hydrate and ice stability in permafrost settings. The pressure regime in permafrost also remains somewhat elusive, which further impedes modelling of hydrate stability in these settings. Hydrostatic pressure was assumed in this model, although it is acknowledged that this could be an underestimation of the true pressure, especially when the permafrost is primarily ice-bonded and conduits (e.g. open taliks) to the surface or ocean are scarce. In the latter case the propagation of pressure changes at seafloor through sea level variations would also be delayed, as opposed to the assumed immediate adaption of pore pressure. Other factors that are hard to assess in permafrost are the self-preservation potential of hydrates through the formation of an ice-crust, and the subsurface distribution of ice-bonded, ice-bearing and ice-free permafrost, which have the ability to notably alter the outcome of the simulations.

Finally, it is recognized that the model does not regard the saturations of free gas evolving from the dissociation of hydrates. This is however information of interest, since the probability that rising gas bubbles eventually reach the ocean floor increases with increasing bubble volume fraction (Archer et al., 2009a). In case of a complete break-down of the hydrate occurrence zone, the volumes of free gas that were originally trapped below can additionally be released to the ocean. The fate and the amounts of gas involved in this process cannot be assessed with the present model.

CHAPTER VIII. CONCLUSIONS

Since the late 1980's gas hydrate systems have been regarded as a potential prominent moderator of global climate. The main concern has been centered around the possible release of methane gas and its oxidation product carbon dioxide from dissociating methane hydrates, triggered by a warming event or sea level fall. As methane and carbon dioxide are potent greenhouse gases, a positive feedback mechanism may be created that amplifies climate warming and accelerates hydrate dissociation. As such, sensitive hydrate reservoirs could play a leading role in (geologically) rapid warming and changes in the global carbon cycle (Archer et al., 2009a). This line of argumentation has been used to support a number of scientific theories on the role of destabilizing gas hydrates in the PETM carbon isotope excursions, Late Quaternary climatic oscillations, and contemporary climate change.

However, these hypotheses are controversial. Central to the discussion is the degree of sensitivity of gas hydrate reservoirs, which determines how much, in what fashion, and on which timescales hydrates melt in response to environmental changes. This study aimed to answer these questions for methane hydrate reservoirs in four distinct geographic settings across a high-latitude continental margin. Clathrates in high-latitude regions are of particular interest, since they are generally expected to be the most volatile because they occur under shallower water depths (Hunter et al., 2013), and because of the more extreme degree of environmental change to which they are subjected (Westbrook et al., 2009). A relatively simple, but robust one-dimensional numerical model was built, that allows assessing and comparing hydrate stability in homogeneous sediment columns in both permafrost (onshore and offshore) and marine (upper and lower continental slope) environments. Existing formation models were implemented to constrain initial gas hydrate saturations and subsurface distributions of stratigraphically constrained hydrate reservoirs, and to be able to differentiate between the HSZ and the zone of actual hydrate occurrence. The consumption of latent heat during the phase transition of methane hydrate to water and free methane gas was accounted for.

A first set of simulations (case I-III) was performed to evaluate how the climate sensitivity of methane hydrates varies between the abovementioned high-latitude geographic settings when they are exposed to a uniform set of environmental changes. Hydrates associated with subsea permafrost and in upper continental slope sediments are found to be most sensitive to warming, with dissociation on timescales of tens of thousands of years. A simultaneous 100 m sea level rise and increase in pore pressure delays hydrate dissociation in these settings with approximately 30 kyr. Importantly, the model shows that hydrates in these shallow-water environments can dissociate from the top of the hydrate occurrence zone, when the seafloor temperature after warming exceeds the dissociation temperature of hydrates at the seafloor. Given that a continental margin section is influenced by a single and uniformly warming bottom water mass, this temperature condition will only be fulfilled for sediment columns that have their top shallower than a certain critical water depth. This critical water depth is essential information, since methane that evolves from dissociating hydrates at the top of the hydrate occurrence zone below shallow water depths has an enhanced chance to eventually reach the atmosphere. An expression has been derived to calculate this depth (see equation [24] in section 7.1). Methane hydrate reservoirs in association with thick onshore permafrost and in the deep marine realm are modelled to be more stable during climate warming, and dissociate only to a

minor extent or remain completely unaffected during the simulation time frame of 100 kyr. The model further indicates that the impact of sea level changes on hydrate stability becomes more important as the ocean depth decreases. A final finding from the case I-III simulations is that the melting of ice in permafrost occurs on similar timescales as the dissociation of clathrates, i.e. tens of thousands of years.

In the second part, the model was used to simulate the response of high-latitude hydrate reservoirs to climate warming during the last deglaciation following the LGM (case IV), during contemporary climate change (case V), and during the PETM (case VI). All simulations indicate that deep, stratigraphically constrained gas hydrate reservoirs, which comprise by far the largest fraction of the global gas hydrate volume, respond to warming surface or seafloor temperatures on timescales of tens to hundreds of thousands of years. This is in conflict with the millennial, or even faster (centennial, decadal) timescales that have been proposed in the *gas hydrate dissociation hypothesis* for the PETM and following carbon isotope excursions (Dickens et al., 1995), in the *clathrate gun hypothesis* for Late Quaternary climatic oscillations (Kennett et al., 2003) and in studies that argue that recent anthropogenic climate forcing will destabilize hydrates within the upcoming centuries (Hunter et al., 2013), or is already doing so off Svalbard (Westbrook et al., 2009). Such rapid dissociation timescales turn out to be solely applicable to hydrates at very shallow depths in the subsurface, which only exist at isolated sites characterized by focused high methane fluxes (e.g. faults, mud volcanoes, seep sites). However, hydrate volumes in the latter type of deposits are inferred to be insignificant to the global carbon budget, and hence are probably not capable to significantly interfere with global climate. It should further be noted that the ocean constitutes an additional buffer that mitigates the direct climate impact of methane released at the seafloor.

The overall conclusion is that of the four hydrate-bearing settings across a high-latitude continental margin, the subsea permafrost and upper continental slope environments are most sensitive to changing environmental conditions, and are consequently most prone to methane release from dissociating hydrates. However, it is illustrated that most of the high-latitude gas hydrate reservoirs, and by extension the entire global clathrate inventory, respond too slowly to create a geologically rapid positive feedback mechanism with warming climate. The model clearly demonstrates that it takes a long time (tens to hundreds of thousands of years) for a temperature pulse to propagate in the subsurface, and induce dissociation of significant volumes of methane hydrate and release of methane bubbles at the seafloor. The formation timescale of hydrates is considered to be even an order of magnitude larger. This study therefore does not support the idea that fluctuations in climate and atmospheric greenhouse gas levels can be primarily dictated by rapid and large variations in the size of the global gas hydrate inventory. Neither is the size of the global gas hydrate reservoir likely to closely follow climatic variations, since climate (especially during the Late Quaternary) oscillates faster than the size of the clathrate inventory can adapt. This implies that gas hydrate reservoirs are most of the time in a transient, non-equilibrium state. Hydrates continuously melt or form, but not as a reflection of a direct and dynamic interrelationship with global climate.

REFERENCE LIST

Archer, D., 2007. Methane hydrate stability and antropogenic climate change. Biogeosciences 4, 521-544.

Archer, D., Buffett, B., 2005. Time-dependent response of the global ocean clathrate reservoir to climatic and anthropogenic forcing. Geochemistry, Geophysics, Geosystems 6.

Archer, D., Buffett, B., Brovkin, V., 2009a. Ocean methane hydrates as a slow tipping point in the global carbon cycle. Proc Natl Acad Sci U S A 106, 20596-20601.

Archer, D., Eby, M., Brovkin, V., Ridgwell, A., Cao, L., Mikolajewicz, U., Caldeira, K., Matsumoto, K., Munhoven, G., Montenegro, A., Tokos, K., 2009b. Atmospheric Lifetime of Fossil Fuel Carbon Dioxide. Annual Review of Earth and Planetary Sciences 37, 117-134.

Bard, E., Hamelin, B., Fairbanks, R.G., 1990. U-Th ages obtained by mass-spectrometry in corals from Barbados - Sea-level during the past 130,000 years. Nature 346, 456-458.

Behseresht, J., Bryant, S.L., 2012. Sedimentological control on saturation distribution in Arctic gas-hydrate-bearing sands. Earth and Planetary Science Letters 341, 114-127.

Berndt, C., Feseker, T., Treude, T., Krastel, S., Liebetrau, V., Niemann, H., Bertics, V.J., Dumke, I., Dunnbier, K., Ferre, B., Graves, C., Gross, F., Hissmann, K., Huhnerbach, V., Krause, S., Lieser, K., Schauer, J., Steinle, L., 2014. Temporal constraints on hydrate-controlled methane seepage off Svalbard. Science 343, 284-287.

Biastoch, A., Treude, T., Rüpke, L.H., Riebesell, U., Roth, C., Burwicz, E.B., Park, W., Latif, M., Böning, C.W., Madec, G., Wallmann, K., 2011. Rising Arctic Ocean temperatures cause gas hydrate destabilization and ocean acidification. Geophysical Research Letters 38, L08602.

Birchwood, R., Dai, J., Shelander, D., Boswell, R., Collett, T.S., Cook, A., Dallimore, S., Fujii, K., Imasato, Y., Fukuhara, M., Kusaka, K., Murray, D., Saeki, T., 2010. Developments in Gas Hydrates. Oilfield Review 22, 18-33.

Boswell, R., Collett, T.S., 2011. Current perspectives on gas hydrate resources. Energy & Environmental Science 4, 1206-1215.

Boswell, R., Rose, K., Collett, T.S., Lee, M., Winters, W., Lewis, K.A., Agena, W., 2011. Geologic controls on gas hydrate occurrence in the Mount Elbert prospect, Alaska North Slope. Marine and Petroleum Geology 28, 589-607.

Buffett, B., Archer, D., 2004. Global inventory of methane clathrate: sensitivity to changes in the deep ocean. Earth and Planetary Science Letters 227, 185-199.

Burwicz, E.B., Rüpke, L.H., Wallmann, K., 2011. Estimation of the global amount of submarine gas hydrates formed via microbial methane formation based on numerical reaction-transport modeling and a novel parameterization of Holocene sedimentation. Geochimica et Cosmochimica Acta 75, 4562-4576.

Caldwell, J., Kwan, Y.Y., 2004. Numerical methods for one-dimensional Stefan problems. Communications in Numerical Methods in Engineering 20, 535-545.

Cha, S.B., Ouar, H., Wildeman, T.R., Sloan, E.D., 1988. A third-surface effect on hydrate formation. Journal of Physical Chemistry 92, 6492-6494.

Chabert, A., Minshull, T.A., Westbrook, G.K., Berndt, C., Thatcher, K.E., Sarkar, S., 2011. Characterization of a stratigraphically constrained gas hydrate system along the western continental margin of Svalbard from ocean bottom seismometer data. Journal of Geophysical Research 116.

Clennell, M.B., Hovland, M., Booth, J.S., Henry, P., Winters, W.J., 1999. Formation of natural gas hydrates in marine sediments: 1. Conceptual model of gas hydrate growth conditioned by host sediment properties. Journal of Geophysical Research 104, 22985-23003.

Collett, T.S., 1993. Natural gas hydrates of the Prudhoe Bay and Kuparuk River area, North Slope, Alaska. AAPG Bulletin 77, 793-812.

Collett, T.S., Johnson, A.H., Knapp, C.C., Boswell, R., 2009. Natural Gas Hydrates: A Review, in: Collett, T.S., Johnson, A.H., Knapp, C.C., Boswell, R. (Eds.), Natural gas hydrates - Energy resource potential and associated geologic hazards: AAPG Memoir 89, pp. 146-219.

Collett, T.S., Lee, M.W., 2011. Downhole well log characterization of gas hydrates in nature - a review, Seventh International Conference on Gas Hydrates, Edinburgh, Scotland, United Kingdom.

Collett, T.S., Lee, M.W., Agena, W.F., Miller, J.J., Lewis, K.A., Zyrianova, M.V., Boswell, R., Inks, T.L., 2011. Permafrost-associated natural gas hydrate occurrences on the Alaska North Slope. Marine and Petroleum Geology 28, 279-294.

Dai, S., Lee, C., Santamarina, C.J., 2011. Formation history and physical properties of sediments from the Mount Elbert Gas Hydrate Stratigraphic Test Well, Alaska North Slope. Marine and Petroleum Geology 28, 427-438.

Davie, M.K., Buffett, B., 2001. A numerical model for the formation of gas hydrate below the seafloor. Journal of Geophysical Research 106, 497-514.

Davie, M.K., Buffett, B., 2003. A steady state model for marine hydrate formation: Constraints on methane supply from pore water sulfate profiles. Journal of Geophysical Research 108, 2495.

Davie, M.K., Zatsepina, O.Y., Buffett, B.A., 2004. Methane solubility in marine hydrate environments. Marine Geology 203, 177-184.

DeConto, R.M., Galeotti, S., Pagani, M., Tracy, D., Schaefer, K., Zhang, T., Pollard, D., Beerling, D.J., 2012. Past extreme warming events linked to massive carbon release from thawing permafrost. Nature 484, 87-91.

Dickens, G.R., 2003. A methane trigger for rapid warming? Science 299, 1017.

Dickens, G.R., 2011. Down the Rabbit Hole: toward appropriate discussion of methane release from gas hydrate systems during the Paleocene-Eocene thermal maximum and other past hyperthermal events. Climate of the Past 7, 831-846.

Dickens, G.R., O'Neil, J.R., Rea, D.K., Owen, R.M., 1995. Dissociation of oceanic methane hydrate as a cause of the carbon isotope excursion at the end of the Paleocene. Paleoceanography 10, 965-971.

Dickens, G.R., Quinby-Hunt, M.S., 1994. Methane hydrate stability in seawater. Geophysical Research Letters 21, 2115-2118.

Etiope, G., 2012. Climate science: Methane uncovered. Nature Geoscience 5, 373-374.

Garg, S.K., Pritchett, J.W., Katoh, A., Baba, K., Fujii, T., 2008. A mathematical model for the formation and dissociation of methane hydrates in the marine environment. Journal of Geophysical Research 113, B01201.

Giancoli, D., 2007. Physics for Scientists and Engineers, volume 1, 4th ed. Pearson Education, Inc, publishing as Prentice Hall.

Greinert, J., Artemov, Y., Egorov, V., De Batist, M., McGinnis, D., 2006. 1300-m-high rising bubbles from mud volcanoes at 2080m in the Black Sea: Hydroacoustic characteristics and temporal variability. Earth and Planetary Science Letters 244, 1-15.

Higgins, J.A., Schrag, D.P., 2006. Beyond methane: Towards a theory for the Paleocene-Eocene Thermal Maximum. Earth and Planetary Science Letters 245, 523-537.

Holtzman, R., Juanes, R., 2011. Thermodynamic and hydrodynamic constraints on overpressure caused by hydrate dissociation: A pore-scale model. Geophysical Research Letters 38, L14308.

Hunter, S.J., Goldobin, D.S., Haywood, A.M., Ridgwell, A., Rees, J.G., 2013. Sensitivity of the global submarine hydrate inventory to scenarios of future climate change. Earth and Planetary Science Letters 367, 105-115.

IPCC, 2013. Climate Change 2013: The Physical Science Basis. Contribution of Working Group I to the Fifth Assessment Report of the Intergovernmental Panel on Climate Change, in: Stocker, T.F., Qin, D., Plattner, G.-K., Tignor, M., Allen, S.K., Boschung, J., Nauels, A., Xia, Y., Bex, V., Midgley, P.M. (Eds.), Cambridge University Press, Cambridge, United Kingdom and New York, NY, USA, p. 1535.

Kennett, J.P., Cannariato, K.G., Hendy, I.L., Behl, R.J., 2003. Methane Hydrates in Quaternary Climate Change: The Clathrate Gun Hypothesis, in: Kennett, J.P., Cannariato, K.G., Hendy, I.L., Behl, R.J. (Eds.), Methane Hydrates in Quaternary Climate Change: The Clathrate Gun Hypothesis, American Geophysical Union, Washington, D.C.

Kent, D.V., Cramer, B.S., Lanci, L., Wang, D., Wright, J.D., Van der Voo, R., 2003. A case for a comet impact trigger for the Paleocene/Eocene thermal maximum and carbon isotope excursion. Earth and Planetary Science Letters 211, 13-26.

Khlystov, O., Batist, M.D., Shoji, H., Hachikubo, A., Nishio, S., Naudts, L., Poort, J., Khabuev, A., Belousov, O., Manakov, A., Kalmychkov, G., 2013. Gas hydrate of Lake Baikal: Discovery and varieties. Journal of Asian Earth Sciences 62, 162-166.

Klauda, B.J., Sandler, S.I., 2005. Global Distribution of Methane Hydrate in Ocean Sediment. Energy & Fuels 19, 459-470.

Knittel, K., Boetius, A., 2009. Anaerobic oxidation of methane: progress with an unknown process. Annual Review of Microbiology 63, 311-334.

Koh, C.A., Sum, A.K., Sloan, E.D., 2012. State of the art: Natural gas hydrates as a natural resource. Journal of Natural Gas Science and Engineering 8, 132-138.

Kurtz, A.C., Kump, L.R., Arthur, M.A., Zachos, J.C., Paytan, A., 2003. Early Cenozoic decoupling of the global carbon and sulfur cycles. Paleoceanography 18, 1090.

Kvenvolden, K.A., 1988. Methane hydrate - a major reservoir of carbon in the shallow geosphere. Chemical Geology 71, 41-51.

Kvenvolden, K.A., 1993. Gas hydrates: Geological perspective and global change. Reviews of Geophysics 31, 173-187.

Kvenvolden, K.A., 2002. Methane hydrate in the global carbon cycle. Terra Nova 14, 302-306.

Landvik, J.Y., Bondevik, S., Elverhøi, A., Fjeldskaar, W., Mangerud, J., Salvigsen, O., Siegert, M.J., Svendsen, J.-I., Vorren, T.O., 1998. The Last Glacial Maximum of Svalbard and the Barents Sea area: ice sheet extent and configuration. Quaternary Science Reviews 17, 43-75.

Liu, X., Flemings, P.B., 2011. Capillary effects on hydrate stability in marine sediments. Journal of Geophysical Research 116, B07102.

Loehle, C., 1993. Geologic methane as a source for post-glacial CO_2 increases: The hydrocarbon pump hypothesis. Geophysical Research Letters 20, 1415-1418.

Lowe, J.J., Walker, M.J.C., 1997. Reconstructing Quaternary Environments, 2nd Edition, 2nd Edition ed. Pearson, Harlow, England.

MacDonald, G.J., 1990. Role of methane clathrates in past and future climates. Climatic Change 16, 247-281.

Marín-Moreno, H., Minshull, T.A., Westbrook, G.K., Sinha, B., Sarkar, S., 2013. The response of methane hydrate beneath the seabed offshore Svalbard to ocean warming during the next three centuries. Geophysical Research Letters 40, 5159-5163.

Maslin, M., Owen, M., Day, S., Long, D., 2004. Linking continental-slope failures and climate change: Testing the clathrate gun hypothesis. Geology 32, 53-56.

Maslin, M., Thomas, E., 2003b. The clathrate gun is firing blanks: Evidence from balancing the deglacial global carbon budget. Geophysical Research Abstracts 5, 12015.

Maslin, M.A., Thomas, E., 2003a. Balancing the deglacial global carbon budget: the hydrate factor. Quaternary Science Reviews 22, 1729-1736.

McGinnis, D.F., Greinert, J., Artemov, Y., Beaubien, S.E., Wüest, A., 2006. Fate of rising methane bubbles in stratified waters: How much methane reaches the atmosphere? Journal of Geophysical Research 111, C09007.

McInerney, F.A., Wing, S.L., 2011. The Paleocene-Eocene Thermal Maximum: A Perturbation of Carbon Cycle, Climate, and Biosphere with Implications for the Future. Annual Review of Earth and Planetary Sciences 39, 489-516.

Mienert, J., 2012. Signs of instability. Nature 490, 491-492.

Milkov, A.V., 2004. Global estimates of hydrate-bound gas in marine sediments: how much is really out there? Earth-Science Reviews 66, 183-197.

Milkov, A.V., 2005. Molecular and stable isotope compositions of natural gas hydrates: A revised global dataset and basic interpretations in the context of geological settings. Organic Geochemistry 36, 681-702.

Miller, G.H., Brigham-Grette, J., Alley, R.B., Anderson, L., Bauch, H.A., Douglas, M.S.V., Edwards, M.E., Elias, S.A., Finney, B.P., Fitzpatrick, J.J., Funder, S.V., Herbert, T.D., Hinzman, L.D., Kaufman, D.S., MacDonald, G.M., Polyak, L., Robock, A., Serreze, M.C., Smol, J.P., Spielhagen, R., White, J.W.C., Wolfe, A.P., Wolff, E.W., 2010. Temperature and precipitation history of the Arctic. Quaternary Science Reviews 29, 1679-1715.

Millero, F.J., Leung, W.H., 1976. The thermodynamics of seawater at one atmosphere. American Journal of Science 276, 1035-1077.

Nisbet, E.G., 1990. The end of the ice age. Canadian Journal of Earth Sciences 27, 148-157.

Park, S.-H., Sposito, G., 2003. Do Montmorillonite Surfaces Promote Methane Hydrate Formation? Monte Carlo and Molecular Dynamics Simulations. Journal of Physical Chemistry B 107, 2281-2290.

Paull, C.K., Matsumoto, R., Wallace, P.J., 1996. Proceedings of the Ocean Drilling Program, Initial Reports 164.

Paull, C.K., Ussler, W., Dillon, W.P., 1991. Is the extent of glaciation limited by marine gas-hydrates? Geophysical Research Letters 18, 432-434.

Phrampus, B.J., Hornbach, M.J., 2012. Recent changes to the Gulf Stream causing widespread gas hydrate destabilization. Nature 490, 527-530.

Piñero, E., Marquardt, M., Hensen, C., Haeckel, M., Wallmann, K., 2013. Estimation of the global inventory of methane hydrates in marine sediments using transfer functions. Biogeosciences 10, 959-975.

Portnov, A., Mienert, J., Serov, P., 2014. Modeling the evolution of climate-sensitive Arctic subsea permafrost in regions of extensive gas expulsion at the West Yamal shelf. Journal of Geophysical Research: Biogeosciences 119, 2082-2094.

Rachold, V., Bolshiyanov, D.Y., Grigoriev, M.N., Hubberten, H.W., Junker, R., Kunitsky, V.V., Merker, F., Overduin, P., Schneider, W., 2007. Nearshore Arctic Subsea Permafrost in Transition. Eos, Transactions of the American Geophysical Union 88, 149-156.

Rajan, A., Mienert, J., Bünz, S., 2012. Acoustic evidence for a gas migration and release system in Arctic glaciated continental margins offshore NW-Svalbard. Marine and Petroleum Geology 32, 36-49.

Reagan, M.T., Moridis, G.J., 2008. Dynamic response of oceanic hydrate deposits to ocean temperature change. Journal of Geophysical Research 113, C12023.

Reagan, M.T., Moridis, G.J., Elliott, S.M., Maltrud, M., 2011. Contribution of oceanic gas hydrate dissociation to the formation of Arctic Ocean methane plumes. Journal of Geophysical Research 116, C09014.

Rempel, A.W., Buffett, B., 1997. Formation and accumulation of gas hydrate in porous media. Journal of Geophysical Research 102, 10151-10164.

Romanovskii, N.N., Hubberten, H.W., Gavrilov, A.V., Eliseeva, A.A., Tipenko, G.S., 2005. Offshore permafrost and gas hydrate stability zone on the shelf of East Siberian Seas. Geo-Marine Letters 25, 167-182.

Roose, F., Poort, J., De Batist, M., 2006. Hydrate dissociation and slope stability on continental margins in response to changes in environmental parameters. Msc. thesis, Ghent University, Faculty of Science, Department WE13.

Ruppel, C.D., 2011a. Methane Hydrates and Contemporary Climate Change. Nature Education Knowledge 2.

Ruppel, C.D., 2011b. Supplementary paper: Methane Hydrates and the Future of Natural Gas. MITEI Natural Gas Report.

Sarkar, S., Berndt, C., Minshull, T.A., Westbrook, G.K., Klaeschen, D., Masson, D.G., Chabert, A., Thatcher, K.E., 2012. Seismic evidence for shallow gas-escape features associated with a retreating gas hydrate zone offshore west Svalbard. Journal of Geophysical Research 117, B09102.

Sassen, R., Joye, S., Sweet, S.T., DeFreitas, D.A., Milkov, A.V., MacDonald, I.R., 1999. Thermogenic gas hydrates and hydrocarbon gases in complex chemosynthetic communities, Gulf of Mexico continental slope. Organic Geochemistry 30, 485-497.

Schuur, E.A., McGuire, A.D., Schadel, C., Grosse, G., Harden, J.W., Hayes, D.J., Hugelius, G., Koven, C.D., Kuhry, P., Lawrence, D.M., Natali, S.M., Olefeldt, D., Romanovsky, V.E., Schaefer, K., Turetsky, M.R., Treat, C.C., Vonk, J.E., 2015. Climate change and the permafrost carbon feedback. Nature 520, 171-179.

Seo, Y., Seol, J., Yeon, S.-H., Koh, D.-Y., Cha, M., Kang, S.-P., Seo, Y.-T., Bahk, J., Lee, J., LEe, H., 2009. Structural, Mineralogical, and Rheological Properties of Methane Hydrates in Smectite Clays. Journal of Chemical & Engineering Data 54, 1284-1291.

Shakhova, N.E., Alekseev, V.A., Semiletov, I.P., 2010. Predicted methane emission on the East Siberian shelf. Doklady Earth Sciences 430, 190-193.

Shipley, T.H., Houston, M.H., Buffler, R.T., Shaub, F.J., McMillen, K.J., Ladd, J.W., Worzel, J.L., 1979. Seismic evidence for widespread possible gas hydrate horizons on continental slopes and rises. AAPG Bulletin 63, 2204-2213.

Sloan, E.D., 1998. Clathrate Hydrate of Natural Gases, 2nd Edition, 2nd Edition ed. Marcel Dekker Inc., New York.

Sloan, E.D., Koh, C.A., 2007. Molecular Structures and Similarities to Ice, Clathrate Hydrates of Natural Gases, Third Edition. CRC Press.

Sowers, T., 2006. Late Quaternary atmospheric CH_4 isotope record suggests marine clathrates are stable. Science 311, 838-840.

Sultan, N., Cochonat, P., Foucher, J.P., Mienert, J., 2004. Effect of gas hydrates melting on seafloor slope instability. Marine Geology 213, 379-401.

Svensen, H., Planke, S., Malthe-Sørenssen, A., Jamtveit, B., Myklebust, R., Eidem, T.F.R., Rey, S.S., 2004. Release of methane from a volcanic basin as a mechanism for initial Eocene global warming. Nature 429, 542-545.

Takeya, S., Uchida, T., Nagao, J., Ohmura, R., Shimada, W., Kamata, Y., Ebinuma, T., Narita, H., 2005. Particle size effect of hydrate for self-preservation. Chemical Engineering Science 60, 1383-1387.

Tishchenko, P., Hensen, C., Wallmann, K., Wong, C.S., 2005. Calculation of the stability and solubility of methane hydrate in seawater. Chemical Geology 219, 37-52.

Waelbroeck, C., Labeyrie, L., Michel, E., Duplessy, J.C., McManus, J.F., Lambeck, K., Balbon, E., Labracherie, M., 2002. Sea-level and deep water temperature changes derived from benthic foraminifera isotopic records. Quaternary Science Reviews 21, 295-305.

Waite, W.F., Stern, L.A., Kirby, S.H., Winters, W.J., Mason, D.H., 2007. Simultaneous determination of thermal conductivity, thermal diffusivity and specific heat in sI methane hydrate. Geophysical Journal International 169, 767-774.

Walter Anthony, K.M., Anthony, P., Grosse, G., Chanton, J., 2012. Geologic methane seeps along boundaries of Arctic permafrost thaw and melting glaciers. Nature Geoscience 5, 419-426.

Westbrook, G.K., Thatcher, K.E., Rohling, E.J., Piotrowski, A.M., Pälike, H., Osborne, A.H., Nisbet, E.G., Minshull, T.A., Lanoisellé, M., James, R.H., Hühnerbach, V., Green, D., Fisher, R.E., Crocker, A.J., Chabert, A., Bolton, C., Beszczynska-Möller, A., Berndt, C., Aquilina, A., 2009. Escape of methane gas from the seabed along the West Spitsbergen continental margin. Geophysical Research Letters 36, L15608.

Xu, W., 2004. Modeling dynamic marine gas hydrate systems. American Mineralogist 89, 1271-1279.

Xu, W., Germanovich, L.N., 2006. Excess pore pressure resulting from methane hydrate dissociation in marine sediments: A theoretical approach. Journal of Geophysical Research 111, B01104.

Xu, W., Ruppel, C., 1999. Predicting the occurrence, distribution, and evolution of methane gas hydrate in porous marine sediments. Journal of Geophysical Research 104, 5081-5095.

Yakushev, V.S., Istomin, V.A., 1992. Gas-hydrate self-preservation effect, in: Maeno, N., Hondoh, T. (Eds.), Physics and Chemistry of Ice. Hokkaido University Press, Sapporo, pp. 136-140.

Zachos, J.C., McCarren, H., Murphy, B., Röhl, U., Westerhold, T., 2010. Tempo and scale of late Paleocene and early Eocene carbon isotope cycles: Implications for the origin of hyperthermals. Earth and Planetary Science Letters 299, 242-249.

Zatsepina, O.Y., Buffett, B., 1998. Thermodynamic conditions for the stability of gas hydrate in the seafloor. Journal of Geophysical Research 103, 24127-24139.

Zillmer, M., Flueh, E.R., Petersen, J., 2005. Seismic investigation of a bottom simulating reflector and quantification of gas hydrate in the Black Sea. Geophysical Journal International 161, 662-678.

APPENDIX. MATLAB CODE

This appendix shows the MATLAB scripts that were written for the model presented in this study. All m-files are available and can be requested via the author (Thomas.Mestdagh@UGent.be).

CODE FOR THE MARINE SETTINGS

```
% SCRIPT NAME: gradualTandPincrease_marine.m
% DESCRIPTION: Simulation of the response of a gas hydrate-bearing sediment column
to a gradual T rise and simultaneous gradual P rise
% Thomas Mestdagh, February - May 2015

% Constants

g = 9.81;                % gravitational acceleration (m/s);
kappa = 3.9e-7;          % thermal diffusivity (in m^2/s), Biastoch et al (2011)
Cph = 2.16e3;            % specific heat capacity of methane hydrate (J/kg.K),
Waite et al. (2007)
L = 4.3e5;               % latent heat of methane hydrate dissociation (J/kg), Xu
and Germanovich (2006)
D_m = 1.3e-9;   % dispersion-diffusion coefficient (kg/(m*s)), Xu and Ruppel (1999)
M_0 = 0;                 % mass fraction of methane in the bottom water (kg/kg)
M_h = 0.134;             % mass fraction of methane in hydrate (kg/kg), Davie &
Buffett (2001)
q_f = 4e-8;              % flux of total mass (kg/(m^2*s)), Xu and Ruppel (1999)
q_e = 0.050;             % flux of total energy (W/m^2), Xu and Ruppel (1999)
q_h = 0;                 % hydrate flux rate (kg/(m^2*s)), Xu and Ruppel (1999)
Q_m = 0;                 % rate of methane production in sediments (kg/(m^3*s))
Q_e = 0;                 % rate of heat production in sediments (W/m^3)
lambda = 1.7;       % bulk thermal conductivity (W/(m*K)), Biastoch et al. (2011)
rho_l = 1024;            % density of the liquid phase(kg/m^3)
rho_h = 930;        % density of methane hydrate (kg/m^3), Rempel & Buffett (1997)
C_l = 4.18e3;       % specific heat capacity of the liquid phase (J/(kg*K)), Xu and
Ruppel (1999)
mu_l = 8.87e-4;     % dynamic viscosity of liquid phase in fluid (kg/(m*s)), Xu and
Ruppel (1999)
S = 35;                          % salinity (in promille)
K_m = D_m * 1000;                % Xu and Ruppel (1999)

% Define setting

accumulation_time = 1.88;        % time period over which hydrates have been
accumulating (in Ma); 1.88 Ma from Collett et al. (2011)
z_0 = 1000;                      % initial water depth (m)
z_f = 700;                       % depth base column (m, below seafloor)
d_step = 5;                      % depth interval (m) --> MIND STABILITY CONDITION
FOR NUMERICAL SOLUTION!

T_0 = -1;                        % T at seafloor (IN DEGREES CELSIUS!)
T_increase = 3;                  % T increase (in K)
periodT_increase = 3000;         % period over which T increases (in years)
rateT_increase = T_increase/periodT_increase;    % rate of T increase (in K/year)

P_0 = z_0*rho_l*g;         % initial pressure (hydrostatic) at the seafloor (in Pa)
SLrise = 120;                    % amount of sea level rise (in m)
period_SLrise = 3000;            % period over which sea level rises (in years)
rateP_increase = (rho_l*g*SLrise)/period_SLrise;      % rate of subsequent P
increase (in  Pa/year)

teta = 0.5;                      % porosity
k = 1e-14;                       % bulk permeability (m^2)

% DEFINITION OF INITIAL CONDITIONS: run XuRuppel.m
XuRuppel;
```

```
% Definition of the sediment column: adopted from XuRuppel.m
Z = abs(z);                     % z (in XuRuppel.m) points upward <--> here Z
points downward (origin at the seafloor, positive values below the seafloor)

% Definition of the time array t
timestep_y = 1;                 % timestep in years
timestep_s = timestep_y * 3.1557e7; % timestep in seconds --> MIND STABILITY
CONDITION FOR NUMERICAL SOLUTION!
Nr_timesteps = 100000;          % number of steps
t = 0:timestep_s:Nr_timesteps*timestep_s;

% Definition of matrices in which T, P, Sh (hydrate saturation), HS
% (hydrate stability: HS = 0: hydrates absent; HS = 1: hydrates present and stable;
% HS = 2: hydrates were stable but are dissociated) and dQ values are stored
T = ones(length(Z),length(t));
P = ones(length(Z),length(t));
Sh = zeros(length(Z),length(t));
HS = zeros(length(Z),1);
dQ = zeros(length(Z),1);

% Set initial T profile
T(:,1) = Ti + 273.15;   % Ti from XuRuppel.m
for x = 2:length(t)
    if t(x) < periodT_increase*3.1557e7
        T(1,x) = T(1,x-1) + rateT_increase*timestep_y;
    else
        T(1,x) = T(1,x-1);
    end
end

% Set P profile (changes through time because of sea level rise)
P(:,1) = Pi;            % Pi from XuRuppel.m
for f = 2:length(t)
    if t(f) < period_SLrise*3.1557e7
        P(:,f) = P(:,f-1) + rateP_increase*timestep_y;
    else
        P(:,f) = P(:,f-1);
    end
end

% Initial gas hydrate saturation profile
for y = 1: length(t)
    Sh(:,y) = S_h.';    % S_h from XuRuppel.m
end

% Definition of initial gas hydrate stability (at t = 0)
for b = 1:length(Z)
    HS(b,1) = (Sh(b,1) ~= 0);
end
if (T(1,1) > (Tdiss(P_0))) && (HS(1,1) == 1) % GH stability at seafloor
    HS(1,1) = 2;
end

% Definition of matrix in which base of HZ at each timestep will be stored,
% value at t = 0 is chosen as initial value
baseHZ = Z(find(HS==1,1,'last')) * ones(1,length(t));
topHZ = Z(find(HS==1,1)) * ones(1,length(t));

% IMPLEMENT NUMERICAL SOLUTION TO THE 1D HEAT EQUATION

for n = 2:length(t)
    % TOP BOUNDARY (seafloor): T defined above

    % SUBSURFACE
    for k = 2:(length(Z)-1)
        T(k,n) = T(k,n-1) + ((kappa*timestep_s)/(d_step)^2)*(T(k-1,n-1)-2*T(k,n-
1)+T(k+1,n-1)); % First calculate T
```

```
        if (HS(k,1) == 1) && (T(k,n) >= (Tdiss(P(k,n)))) % If GH stable/present AND
T >= Teq
            T(k,n) = Tdiss(P(k,n));                % T remains at Teq
            dQ(k,1) = dQ(k,1)+(Cph*kappa*timestep_s/(d_step)^2)*(T(k-1,n-1)-
2*T(k,n-1)+T(k+1,n-1)); % But heat is added
            if dQ(k,1) >= L
                HS(k,1) = 2;
                T(k,n) = T(k,n) + (dQ(k,1)-L)/Cph;
                Sh(k,n:end) = 0;
            else
                Sh(k,n) = Sh(k,1) * (L-dQ(k,1))/L;
            end
        end
    end

    % At lower boundary --> apply bottom boundary condition: constant heat
    % flux (but still account for latent heat if hydrates present
    T(length(Z),n) = T(length(Z)-1,n) + (T(length(Z),1)-T(length(Z)-1,1));
    if (HS(length(Z),1) == 1) && (T(length(Z),n) >= (Tdiss(P(length(Z),n))))
        dQ(length(Z),1) = dQ(length(Z),1)+(T(length(Z),n) -
(Tdiss(P(length(Z),n))))*Cph;
        T(length(Z),n) = Tdiss(P(length(Z),n));
        if dQ(length(Z),1) >= L
            HS(length(Z),1) = 2;
            T(length(Z),n) = T(length(Z),n) + (dQ(length(Z),1)-L)/Cph;
            Sh(length(Z),n:end) = 0;
        else
            Sh(length(Z),n) = Sh(length(Z),1) * (L-dQ(length(Z),1))/L;
        end
    end

    % Determine base and top of the hydrate occurrence zone
    if isempty(find(HS==1,1,'last')) == 0        % if not all hydrates melted away
        baseHZ(1,n)= Z(find(HS==1,1,'last'));
        topHZ(1,n) = Z(find(HS==1,1));
    else
        baseHZ(1,n)= (baseHZ(1,n-1) + topHZ(1,n-1))/2;  % if all hydrates melted:
base/top HZ = average top and base in previous time step (arbitrary chosen value)
        topHZ(1,n)= (baseHZ(1,n-1) + topHZ(1,n-1))/2;
    end

end

% PLOTS
T_3f = ones(1,length(Z));
for o = 1:length(Z)
     T_3f(o) = Tdiss(P(o,period_SLrise));
end

figure;

% Figure 1: Evolution of the temperature profile through time
subplot(2,2,[1,2]);
hold on;
axis ij;
plot(Ti+273.15,abs(z_bHSZ)*ones(1,length(Ti)),'--
k',Ti+273.15,abs(z_lt)*ones(1,length(Ti)),'-
.k',Ti+273.15,abs(z_lb)*ones(1,length(Ti)),'-.k',T_3+273.15,Z,'-k',T_3f,Z,'-r');
for d = 1:length(t)
    if (d == 1) || (t(d)/(3.1557e7*20000) == round(t(d)/(3.1557e7*20000)))
        plot(T(:,d),Z,'LineWidth',1.5);
    end
end
hold off;

% Figure 2: Evolution of gas hydrate saturation through time: plots if t = 0 and
% subsequently every 20000 kyr
subplot(2,2,3);
```

```
hold on;
axis ij;
xlim([0,0.15]);
for e = 1:length(t)
    if (e == 1) || (t(e)/(3.1557e7*20000) == round(t(e)/(3.1557e7*20000)))
        plot(Sh(:,e),Z,'LineWidth',1.5);
    end
end
hold off;

% Figure 3: Evolution of top and base of hydrate occurrence zone through time
subplot(2,2,4);
hold on;
axis ij;
plot(t/(3.1557e7),baseHZ,'-k',t/(3.1557e7),topHZ,'-r','LineWidth',1.5);
ylim([0,z_f]);
hold off;
```

```
% SCRIPT NAME: XuRuppel.m
% DESCRIPTION: This script implements the analytical formation model for gas
hydrates of Xu & Ruppel (1999)

% A. Determine location of methane hydrate STABILITY zone (MHSZ)

%       1) Generate P-T profile according to equation 17, 18 (or alternatively
using equation 19 only)
z = 0:-d_step:-z_f;
Ti = ones(1,length(z));
Pi = ones(1,length(z));
for i = 1:length(z)
    Ti(i) = temperature_eq18(z(i),q_f,q_e,lambda,C_l,T_0);
end
for j = 1:length(z)
    Pi(j) = pressure_eq17(z(j),q_f,P_0,k,mu_l,rho_l,g);
end

%       2) Methane hydrate stability curve
T_3 = ones(1,length(z));
for o = 1:length(z)
     T_3(o) = Tdiss(Pi(o))-273.15;
end

%       3) calculate intersection 1) and 2) --> base MHSZ
if q_f == 0
    P_bHSZ = fzero(@determineMHSZ_qfis0, [P_0,rho_l*g*(z_0+abs(z(end)))]); % in Pa
    T_bHSZ = (P_bHSZ-P_0)*q_e/(rho_l*g*lambda) + T_0 + 273.15;  % in K
else
    P_bHSZ = fzero(@determineMHSZ_qfisnot0, [P_0,rho_l*g*(z_0+abs(z(end)))]);
    T_bHSZ = (q_e-((q_e-q_f*C_l*T_0)/exp((P_bHSZ-
P_0)*q_f*C_l/(lambda*(q_f*mu_l/(k*rho_l)+rho_l*g)))))/(q_f*C_l) + 273.15;
end
z_bHSZ = -(P_bHSZ-P_0)/(q_f*mu_l/(k*rho_l)+rho_l*g); % calculate z @ base HSZ from
eq (17)

% B. Determine position of methane hydrate OCCURRENCE zone (MHZ)

%       1. Calculate c_eq(z)
c_eq = ones(1,length(z));
alpha = 14.5; % Davie et al. (2004) p.182

for m = 1: length(z)
    if z(m) >= z_bHSZ
        c_eq(m) = C_3(T_bHSZ,P_bHSZ/(1e6),(S/58.45))*exp(((Ti(m)+273.15)-
T_bHSZ)/alpha); % T in degrees celsius; T_bHSZ in K; P in Pa; S/molar mass NaCl to
convert salinity from pro mille to mol/kg
    else
        c_eq(m) = C_3(T_bHSZ,P_bHSZ/(1e6),(S/58.45));
    end
```

```
end

%       2. Calculate top and base hydrate OCCURRENCE zone using eq.
%       (20),(21) and (22)
if D_m == 0       % OPM: if D_m = K_m = 0, then z_lt = 0 (see eq. 20)
    z_lt = 0;
else
    z_lt = fzero(@determine_topHZ, [0,z_bHSZ]); % calculates top of HZ by solving
eq (20)
end
z_lb = fzero(@determine_baseHZ, [1000,z(end)]); % calculates base of HZ by solving
eq (22)

%  To retain only realistic values for z_lb and check if clathrates are present:
if z_lb >= z_lt
    z_lb = z_lt;
else
    if z_lb <= z_bHSZ
        z_lb = z_bHSZ;
    end
end

% C. Calculate timescales for gas hydrate accumulation

t_diffusive = (rho_l*(z_lt-z_lb)^2/K_m)/(3.1557e7*1e6);      % equation (23)
t_advective = (rho_l*(z_lt-z_lb)/q_f)/(3.1557e7*1e6);        % equation (24)

% D. Accumulation and distribution

acc_rate = zeros(1,length(z));
S_h = zeros(1,length(z));
for n = 1: length(acc_rate)
    if z(n)<= z_lt && z(n)>=z_lb
        acc_rate(n) = 1/(teta*(rho_h*M_h - rho_l*M_sl(z(n)))) *
(teta*K_m*d2M_sl(z(n)) - q_f*dM_sl(z(n)));
        S_h(n) = acc_rate(n) * accumulation_time * 1e6 * 3.1557e7;
    end
end
```

```
function res = C_3(T,P,S)
    % This function returns solubility at T3(P) in mM, and takes T (in K), P (in
MPa)and S (in mol/kg) as input, after Davie et al. (2004)
    C_3_pure = 156.36 + 6.34*(T-292) + 1.11*(P-20); % C_3 for pure water, equation
(3) & (4)
    res = (1- 0.1*S) * C_3_pure; % to correct for salinity
end
```

```
function res = d2M_sl(z)
% This function calculates the second derivative of M_sl(z)(expressed as mass
fraction)ONLY VALID WITHIN HSZ !! Based on eq (5) from Davie et al. (2004), whith T
written as a function of z based on eq (18) from Xu & Ruppel (1999) (derivatives
calculated in matlab: diff(M_sl,z))

    g = 9.81;                % gravitational acceleration (m/s)
    T_0 = -1;                % T at seafloor (IN DEGREES CELSIUS!)
    z_0 = 1000;              % water depth (m)
    q_f = 4e-8;              % flux of total mass (kg/(m^2*s))
    q_e = 0.050;             % flux of total energy (W/m^2)
    k = 1e-14;               % bulk permeability (m^2)
    lambda = 1.7;            % bulk thermal conductivity (W/(m*K))
    rho_l = 1024;            % density of liquid phase(kg/m^3)
    C_l = 4.18e3;            % specific heat capacity of liquid water (J/(kg*K))
    mu_l = 8.87e-4;        % dynamic viscosity of liquid phase in fluid (kg/(m*s))
    S = 35;                  % salinity (in promille)
    P_0 = z_0 * rho_l * g;   % pressure at the seafloor (in Pa)

    if q_f == 0
        P_bHSZ = fzero(@determineMHSZ_qfis0, [P_0,20e6]); % in Pa
```

```
        T_bHSZ = (P_bHSZ-P_0)*q_e/(rho_l*g*lambda) + T_0 + 273.15;  % in K
    else
        P_bHSZ = fzero(@determineMHSZ_qfisnot0, [P_0,20e6]);
        T_bHSZ = (q_e-((q_e-q_f*C_l*T_0)/exp((P_bHSZ-
P_0)*q_f*C_l/(lambda*(q_f*mu_l/(k*rho_l)+rho_l*g)))))/(q_f*C_l) + 273.15;
    end

    molmass_CH4 = 0.016; % molar mass of methane in kg/mol
    c = C_3(T_bHSZ,P_bHSZ/(1e6),S/58.45)* molmass_CH4/rho_l; % constants in eq
(3),(4)&(5) (Davie et al. 2004) and conversion factors (mM to kg/kg) grouped in one
term c
    alpha = 14.5; % Davie et al.(2004) p.182

    if q_f == 0
        res = (c*q_e^2*exp((T_0 - T_bHSZ - (q_e*z)/lambda +
5463/20)/alpha))/(alpha^2*lambda^2);
    else
        res = (c*exp(((q_e - exp((C_l*q_f*z)/lambda)*(q_e - C_l*T_0*q_f))/(C_l*q_f)
- T_bHSZ + 5463/20)/alpha)*exp((2*C_l*q_f*z)/lambda)*(q_e -
C_l*T_0*q_f)^2)/(alpha^2*lambda^2) - (C_l*c*q_f*exp(((q_e -
exp((C_l*q_f*z)/lambda)*(q_e - C_l*T_0*q_f))/(C_l*q_f) - T_bHSZ +
5463/20)/alpha)*exp((C_l*q_f*z)/lambda)*(q_e - C_l*T_0*q_f))/(alpha*lambda^2);
    end
end
```

```
function res = determine_baseHZ(z)
% This function calculates the base of the hydrate occurrence zone, after
% Xu and Ruppel (1999)
    % Constant parameters
    teta = 0.5;           % porosity
    D_m = 1.3e-9;         % dispersion-diffusion coefficient (kg/(m*s))
    q_f = 4e-8;           % flux of total mass (kg/(m^2*s))
    K_m = D_m * 1000;
    q_m = 6e-11;          % Methane flux (kg/(m*s))

    res = -q_m + q_f*M_sl(z) - teta*K_m*dM_sl(z);
end
```

```
function res = determine_topHZ(z)
% This function calculates the top of the hydrate occurrence zone, after
% Xu and Ruppel (1999)
    % Constant parameters
    teta = 0.5;                     % porosity
    D_m = 1.3e-9;                   % dispersion-diffusion coefficient (kg/(m*s))
    M_0 = 0;                        % mass fraction of methane in the bottom water
    q_f = 4e-8;                     % flux of total mass (kg/(m^2*s))
    K_m = D_m * 1000;

    q_mt = q_f*M_sl(z) - teta*K_m*dM_sl(z);

    if q_f == 0
        res = -z - (teta*K_m/q_mt) * (M_sl(z) - M_0);
    else
        res = -z - (teta*K_m/q_f) * log((q_mt - q_f*M_0)/(q_mt - q_f*M_sl(z)));
    end
end
```

```
function res = determineMHSZ_qfis0(P)
% error function in order to solve the condition for the bottom of the HSZ, in
% case q_f = 0, which takes P (in Pa) as input ; after Xu and Ruppel (1999)

    % Constant parameters
    g = 9.81;                   % gravitational acceleration (m/s)
    T_0 = -1;                   % T at seafloor (IN DEGREES CELSIUS!)
    z_0 = 1000;                 % water depth (m)
    q_e = 0.050;                % flux of total energy (W/m^2)
    lambda = 1.7;               % bulk thermal conductivity (W/(m*K))
    rho_l = 1024;               % density of liquid phase(kg/m^3)
```

```
    P_0 = z_0 * rho_l * g;      % pressure at the seafloor (in Pa)

    res = (P-P_0)*q_e/(rho_l*g*lambda) + T_0 - (9.6349*log(P/(1e3)) + 197.65 -
273.15);
end
```

```
function res = determineMHSZ_qfisnot0(P)
% error function in order to solve the condition for the bottom of the HSZ, in
% case q_f is not zero, which takes P (in Pa) as input ; after Xu and Ruppel (1999)

    % Constant parameters
    g = 9.81;                       % gravitational acceleration (m/s)
    z_0 = 1000;                     % water depth (m)
    T_0 = -1;                       % T at seafloor (IN DEGREES CELSIUS!)
    q_f = 4e-8;                     % flux of total mass (kg/(m^2*s))
    q_e = 0.050;                    % flux of total energy (W/m^2)
    k = 1e-14;                      % bulk permeability (m^2)
    lambda = 1.7;                   % bulk thermal conductivity (W/(m*K))
    rho_l = 1024;                   % density of liquid phase(kg/m^3)
    C_l = 4.18e3;           % specific heat capacity of liquid water (J/(kg*K))
    mu_l = 8.87e-4;         % dynamic viscosity of liquid phase in fluid (kg/(m*s))

    P_0 = z_0 * rho_l * g;          % pressure at the seafloor (in Pa)

    res = (q_e-((q_e-q_f*C_l*T_0)/exp((P-
P_0)*q_f*C_l/(lambda*(q_f*mu_l/(k*rho_l)+rho_l*g)))))/(q_f*C_l) -
(9.6349*log(P/(1e3)) + 197.65 - 273.15);
end
```

```
function res = dM_sl(z)
 % This function calculates the first derivative of M_sl(z)(expressed as mass
fraction); ONLY VALID WITHIN HSZ !! Based on eq (5) from Davie et al. (2004), with
T written as a function of z based on eq (18) from Xu and Ruppel
(1999);(derivatives calculated in matlab: diff(M_sl,z))

    g = 9.81;                       % gravitational acceleration (m/s)
    T_0 = -1;                       % T at seafloor (IN DEGREES CELSIUS!)
    z_0 = 1000;                     % water depth at seafloor (m)
    q_f = 4e-8;                     % flux of total mass (kg/(m^2*s))
    q_e = 0.050;                    % flux of total energy (W/m^2)
    k = 1e-14;                      % bulk permeability (m^2)
    lambda = 1.7;                   % bulk thermal conductivity (W/(m*K))
    rho_l = 1024;                   % density of liquid phase(kg/m^3)
    C_l = 4.18e3;           % specific heat capacity of liquid water (J/(kg*K))
    mu_l = 8.87e-4;         % dynamic viscosity of liquid phase in fluid (kg/(m*s))
    S = 35;                         % salinity (in promille)
    P_0 = z_0 * rho_l * g;          % pressure at the seafloor (in Pa)

    if q_f == 0
        P_bHSZ = fzero(@determineMHSZ_qfis0, [P_0,20e6]); % in Pa
        T_bHSZ = (P_bHSZ-P_0)*q_e/(rho_l*g*lambda) + T_0 + 273.15;  % in K
    else
        P_bHSZ = fzero(@determineMHSZ_qfisnot0, [P_0,20e6]);
        T_bHSZ = (q_e-((q_e-q_f*C_l*T_0)/exp((P_bHSZ-
P_0)*q_f*C_l/(lambda*(q_f*mu_l/(k*rho_l)+rho_l*g)))))/(q_f*C_l) + 273.15;
    end

    molmass_CH4 = 0.016; % molar mass of methane in kg/mol
    c = C_3(T_bHSZ,P_bHSZ/(1e6),S/58.45)* molmass_CH4/rho_l; % constants in eq
(3),(4)&(5) (Davie et al. 2004) and conversion factors (mM to kg/kg) grouped in one
term c
    alpha = 14.5; % Davie et al.(2004) p.182

    if q_f == 0
        res = -(c*q_e*exp((T_0 - T_bHSZ - (q_e*z)/lambda +
5463/20)/alpha))/(alpha*lambda);
    else
```

```
        res = -(c*exp(((q_e - exp((C_l*q_f*z)/lambda)*(q_e -
C_l*T_0*q_f))/(C_l*q_f) - T_bHSZ + 5463/20)/alpha)*exp((C_l*q_f*z)/lambda)*(q_e -
C_l*T_0*q_f))/(alpha*lambda);
    end
end
```

```
function res = M_sl(z)
% This function calculates the solubility of methane in sea water (expressed as
mass fraction), as a function of z ; ONLY VALID WITHIN HSZ !! Based on eq (5) from
Davie et al. (2004), where T is written as a function of z based on eq (18) from Xu
& Ruppel (1999)

    g = 9.81;                       % gravitational acceleration (m/s)
    T_0 = -1;                       % T at seafloor (IN DEGREES CELSIUS!)
    z_0 = 1000;                     % water depth (m)
    q_f = 4e-8;                     % flux of total mass (kg/(m^2*s))
    q_e = 0.050;                    % flux of total energy (W/m^2)
    k = 1e-14;                      % bulk permeability (m^2)
    lambda = 1.7;                   % bulk thermal conductivity (W/(m*K))
    rho_l = 1024;                   % density of liquid phase(kg/m^3)
    C_l = 4.18e3;          % specific heat capacity of liquid water (J/(kg*K))
    mu_l = 8.87e-4;        % dynamic viscosity of liquid phase in fluid (kg/(m*s))
    S = 35;                         % salinity (in promille)
    P_0 = z_0 * rho_l * g;          % pressure at the seafloor (in Pa)

    if q_f == 0
        P_bHSZ = fzero(@determineMHSZ_qfis0, [P_0,20e6]); % in Pa
        T_bHSZ = (P_bHSZ-P_0)*q_e/(rho_l*g*lambda) + T_0 + 273.15;  % in K
    else
        P_bHSZ = fzero(@determineMHSZ_qfisnot0, [P_0,20e6]);
        T_bHSZ = (q_e-((q_e-q_f*C_l*T_0)/exp((P_bHSZ-
P_0)*q_f*C_l/(lambda*(q_f*mu_l/(k*rho_l)+rho_l*g)))))/(q_f*C_l) + 273.15;
    end

    molmass_CH4 = 0.016; % molar mass of methane in kg/mol
    c = C_3(T_bHSZ,P_bHSZ/(1e6),S/58.45)* molmass_CH4/rho_l; % constants in eq
(3),(4)&(5) (Davie et al. 2004) and conversion factors (mM to kg/kg) grouped in one
term c
    alpha = 14.5; % Davie et al. (2004) p.182

    if q_f == 0
        res = c * exp(((T_0 - (q_e*z/lambda)) + 273.15 - T_bHSZ)/alpha);
    else
        res = c * exp(((q_e - ((q_e - q_f*C_l*T_0)/(exp(-
q_f*C_l*z/lambda))))/(q_f*C_l) - T_bHSZ + 273.15)/alpha);
    end
end
```

```
function res = P_ifv_T_equation19(T,q_f,q_e)
    % This function returns the pressure for a given temperature (IN DEGREES
CELSIUS!!), fluid flux q_f and energy flux q_e, according to formula (19) from Xu
and Ruppel (1999)

    % Constant parameters (from Xu & Ruppel, 1999)
    g = 9.81;                       % gravitational acceleration (m/s)
    z_0 = 1000;                     % sea surface (m)
    k = 1e-14;                      % bulk permeability (m^2)
    rho_l = 1024;                   % density of liquid phase(kg/m^3)
    mu_l = 8.87e-4;        % dynamic viscosity of liquid phase in fluid (kg/(m*s))
    lambda = 1.7;                   % bulk thermal conductivity (W/(m*K))
    C_l = 4.18e3;          % specific heat capacity of liquid water (J/(kg*K))
    T_0 = -1;                        % T at seafloor (degr Celsius)

    P_0 = z_0 * rho_l * g;          % pressure at the seafloor (in Pa)

    % Equation 19
    if q_f == 0
        res = P_0 + (rho_l*g*lambda)*(T-T_0)/q_e;
```

```
    else
        res = P_0 + ((q_f*mu_l)/(k*rho_l)+(rho_l*g)) * lambda/(q_f*C_l) * log((q_e-
q_f*C_l*T_0)/(q_e-q_f*C_l*T));
    end
end
```

```
function res = pressure_eq17(z,q_f,P_0,k,mu_l,rho_l,g)
% This function returns the pressure for a given depth z and fluid flux q_f,
according to formula (17) from Xu and Ruppel (1999)

    % Equation (17)
    res = P_0 + (-((q_f*mu_l)/(k*rho_l)+(rho_l*g))*z);
end
```

```
function res = Tdiss(P)
% This function calculates the temperature of dissociation at a given pressure P
% for pure methane hydrate in equilibrium with seawater with salinity of 0.035
weight percent NaCl
% It takes P (in Pa) and returens Tdiss (in K)
% Two equations are obtained (one for pressures below 2576 kPa (linear) and one for
pressures above (logaritmic)) by fitting a trendline to P-Tdiss datapoints
% obtained from the CMSHYD program of Sloan (1998)

    if P <= (2576.74*1e3)
        res = 0.0158*(P/(1e3)) + 232.7;
    else
        res = 9.6349*log(P/(1e3)) + 197.65;
    end
end
```

```
function res = temperature_eq18(z,q_f,q_e,lambda,C_l,T_0)
    % This function returns the temperature for a given depth z, fluid flux
    % q_f and energy flux q_e
    % according to formula (18) from Xu and Ruppel (1999)
    % !! T IS CALCULATED AND RETURNED IN DEGREES CELSIUS !!

    % Equation (18), explicitly written to T(z,q_e,q_f,lambda,C_l,T_0)
    if q_f == 0
        res = T_0 - (q_e*z/lambda);
    else
        aux = (q_e - q_f*C_l*T_0)/(exp(-q_f*C_l*z/lambda));
        res = (q_e - aux)/(q_f*C_l);
    end
end
```

CODE FOR THE PERMAFROST SETTINGS

```
% SCRIPT NAME: gradualTandPincrease_permafrost
% DESCRIPTION: Simulation of a gradual T increase and simultaneous sea
% level rise in a gas hydrate- and permafrost-bearing sediment column
% Thomas Mestdagh, February - May 2015

% Constants
kappa = 3.9e-7;      % thermal diffusivity (in m^2/s); Biastoch et al (2011)
G = 0.05;            % Geothermal gradient (in K/m)
Gpf = 0.02;          % Geothermal gradient in permafrost (in K/m)
Cph = 2.16;          % specific heat capacity of methane hydrate (kJ/kg.K); Waite et
al., 2007
Cpi = 2.03;          % specific heat capacity of ice (kJ/kg.K); Giancoli (2007)
L_GH = 430;          % latent heat of methane hydrate dissociation (kJ/kg); Xu and
Germanovich (2006)
L_PF = 334;          % latent heat of melting ice (kJ/kg); Giancoli (2007)
rho = 1024;          % water density (kg/m^3)
g = 9.81;            % gravitational acceleration (m/s^2)
S = 35;              % salinity of the water (promille)
```

```
% Definition of the sediment column
d_topcolumn = 0;    % Initial depth of seafloor at location of sediment column(in m)
z0 = 0;             % Top of the considered column (mbsf)
zf = 600;           % Base of the considered column (mbsf)
depth_interval = 5;
Z = z0:depth_interval:zf;

% Definition of the time array
timestep_y = 1;      % Timestep in years
timestep_s = timestep_y * 3.1557e7;  % Timestep in seconds
Nr_timesteps = 100000; % Number of timesteps
t = 0:timestep_s:Nr_timesteps*timestep_s;

% Definition of initial T @ surface and T @ surface after T increase (in K),
% and the period over which temperature increases (in years)
initialT_atSurface = 263.15;
finalT_atSurface = 275.15;
period = 3000;

% Definition of amount and rate of sea level rise
SLrise = 120;                   % sea level rise (in m)
period_SLrise = 3000;           % period over which sea level rises (in years)
rateP_increase = (rho*g*SLrise)/period_SLrise;  % rate of subsequent P increase (in
Pa/year)

% Definition of matrix in which T, Sh (hydrate saturation), Spf (ice saturation),
HS (hydrate stability), PF (permafrost flag) and dQ values are stored
% HS = 1 --> hydrates present and stable; HS = 2 --> hydrates initially present but
% dissociated; HS = 0 --> hydrates absent (idem for PF and ice stability)
% dQGH and dQPF matrices to store heat that is being added during phase
% transition
T = ones(length(Z),length(t));
P = ones(length(Z),length(t));
Sh = zeros(length(Z),length(t));
Spf = zeros(length(Z),length(t));
HS = zeros(length(Z),1);
PF = zeros(length(Z),1);
dQGH = zeros(length(Z),1);
dQPF = zeros(length(Z),1);

% Set initial T profile;
% Geothermal gradient depends on presence of permafrost:
T(1,1) = initialT_atSurface;
for a = 2:length(Z)
    if T(a-1,1) < T_freeze(rho*g*(Z(a)+d_topcolumn),S)
        T(a,1) = T(a-1,1) + Gpf*depth_interval;
    else
        T(a,1) = T(a-1,1) + G*depth_interval;
    end
end

% Set P profile (changes through time because of sea level rise)
for m = 1:length(Z)
    P(m,1) = rho*g*(Z(m)+d_topcolumn);
end
for f = 2:length(t)
    if t(f) <= period_SLrise*3.1557e7
        P(:,f) = P(:,f-1) + rateP_increase*timestep_y;
    else
        P(:,f) = P(:,f-1);
    end
end

% Definition of initial gas hydrate stability (at t = 0) according to model
% of BEHSESERESHT & BRYANT (2012)
% Define depth interval (in m) over which initial gas occurs:
```

```
depthinGC = 250:1:350; % interval over which gas occurs, step has to be 1m
(calculations in BehBryant.m are done for a stack of 1m^3 cubes)
BehBryant;
for b = 1:length(Z)
    HS(b,1) = (Z(b) >= depthinGC(1)) && (Z(b) <= depthinGC(end)); % Make sure that
depthinGC is within HSZ
end

% Definition of initial permafrost presence (at t = 0)
for i = 1:length(Z)
    PF(i,1) = (T(i,1) < T_freeze(P(i,1),S));
end

% Definition of matrix in which base of HZ and PF at each timestep will be stored,
% value at t = 0 is chosen as initial value
baseHZ = Z(find(HS==1,1,'last')) * ones(1,length(t));
basePF = Z(find(PF==1,1,'last')) * ones(1,length(t));
topHZ = Z(find(HS==1,1)) * ones(1,length(t));
topPF = Z(find(PF==1,1)) * ones(1,length(t));

% Definition of initial gas hydrate saturation: S_h values obtained
% from running BehBryant.m
for c = 1:length(Z)
    if HS(c,1) == 1
        Sh(c,:) = S_h(find(depthinGC == Z(c),1));
    end
end

% Definition of initial ice saturation in permafrost-bearing zone
% assumption: Spf = 1 - Sh:
for j = 1:length(Z)
    if PF(j,1) == 1
        Spf(j,:) = 1-Sh(j,1);
    end
end

% Implementt solution to the 1D heat equation

for n = 2:length(t)
    % TOP BOUNDARY (seafloor): evolution of T at top boundary through time: gradual
T increase
    if t(n) < period*3.1557e7
        T(1,n) = T(1,n-1) + ((finalT_atSurface - initialT_atSurface)/period)
*timestep_y;
    else
        T(1,n) = T(1,n-1);
    end

    if (T(1,n) > Tdiss(P(1,n))) && (HS(1,1)==1) % GH stability at seafloor
        dQGH(1,1)= dQGH(1,1) + (T(1,n)-Tdiss(P(1,n)))*Cph;
        if dQGH(1,1)>= L_GH
            HS(1,1) = 2;
            Sh(1,n:end) = 0;
        else
            Sh(1,n) = Sh(1,1)*(L_GH-dQGH(1,1))/L_GH;
        end
    end

    if (T(1,n) >= T_freeze(P(1,n),S)) && (PF(1,1)==1) % PF stability at seafloor
        dQPF(1,1) = dQPF(1,1) + (T(1,n)-T_freeze(P(1,n),S))*Cpi;
        if dQPF(1,1)>= L_PF
            PF(1,1) = 2;
            Spf(1,n:end) = 0;
        else
            Spf(1,n) = Spf(1,1)*(L_PF-dQPF(1,1))/L_PF;
        end
    end
```

```
    % SUBSURFACE
    for k = 2:(length(Z)-1)

        % CASE I: if initially no hydrate or permafrost present, or both are
present but stable --> no phase transition --> no need to account for latent
        % heat consumption
        T(k,n) = T(k,n-1) + ((kappa*timestep_s)/(depth_interval)^2)*(T(k-1,n-1)-
2*T(k,n-1)+T(k+1,n-1)); % first calculate T

        % CASE II: hydrates initially present and thermodynamically unstable,
permafrost not
        if (HS(k,1) == 1) && (PF(k,1) ~= 1) && (T(k,n) >= Tdiss(P(k,n))) % If GH
stable/present AND T >= Teq
            T(k,n) = Tdiss(P(k,n));                % T remains at Teq
            dQGH(k,1) = dQGH(k,1)+(Cph*kappa*timestep_s/(depth_interval)^2)*(T(k-
1,n-1)-2*T(k,n-1)+T(k+1,n-1));% while heat is being added
            if dQGH(k,1) >= L_GH
                HS(k,1) = 2;
                T(k,n) = T(k,n) + (dQGH(k,1)-L_GH)/Cph;
                Sh(k,n:end) = 0;
            else
                Sh(k,n) = Sh(k,1) * (L_GH-dQGH(k,1))/L_GH;
            end
        end

        % CASE III: permafrost initially present and thermodynamically unstable,
hydrates not
        if (PF(k,1) == 1) && (HS(k,1) ~= 1) && (T(k,n) >= T_freeze(P(k,n),S))
            T(k,n) = T_freeze(P(k,n),S);
            dQPF(k,1) = dQPF(k,1) + (Cpi*kappa*timestep_s/(depth_interval)^2)*(T(k-
1,n-1)-2*T(k,n-1)+T(k+1,n-1));
            if dQPF(k,1) >= L_PF
                PF(k,1) = 2;
                T(k,n) = T(k,n) + (dQPF(k,1)-L_PF)/Cpi;
                Spf(k,n:end) = 0;
            else
                Spf(k,n) = Spf(k,1) * (L_PF-dQPF(k,1))/L_PF;
            end
        end

        % CASE IV: both permafrost and hydrates are initially present, but only
        % permafrost is thermodynamically unstable
        if (PF(k,1) == 1) && (HS(k,1) == 1) && (T(k,n)>= T_freeze(P(k,n),S)) &&
(T(k,n) < Tdiss(P(k,n)))
            T(k,n) = T_freeze(P(k,n),S);
            dQPF(k,1) = dQPF(k,1) + (Cpi*kappa*timestep_s/(depth_interval)^2)*(T(k-
1,n-1)-2*T(k,n-1)+T(k+1,n-1));
            if dQPF(k,1) >= L_PF
                PF(k,1) = 2;
                T(k,n) = T(k,n) + (dQPF(k,1)-L_PF)/Cpi;
                Spf(k,n:end) = 0;
            else
                Spf(k,n) = Spf(k,1) * (L_PF-dQPF(k,1))/L_PF;
            end
        end

        % CASE V: both permafrost and hydrates are initially present, but only
        % hydrates are thermodynamically unstable
        if (PF(k,1) == 1) && (HS(k,1) == 1) && (T(k,n) < T_freeze(P(k,n),S)) &&
(T(k,n) >= Tdiss(P(k,n)))
            T(k,n) = Tdiss(P(k,n));
            dQGH(k,1) = dQGH(k,1)+(Cph*kappa*timestep_s/(depth_interval)^2)*(T(k-
1,n-1)-2*T(k,n-1)+T(k+1,n-1));
            if dQGH(k,1) >= L_GH
                HS(k,1) = 2;
                T(k,n) = T(k,n) + (dQGH(k,1)-L_GH)/Cph;
                Sh(k,n:end) = 0;
            else
```

```
                Sh(k,n) = Sh(k,1) * (L_GH-dQGH(k,1))/L_GH;
            end
        end

        % CASE VI: both permafrost and hydrates are initially present, and both are
        % thermodynamically unstable
        if(PF(k,1) == 1) && (HS(k,1) == 1) && (T(k,n) >= Tdiss(P(k,n))) &&
(T(k,n)>= T_freeze(P(k,n),S))
            T(k,n) = min(T_freeze(P(k,n),S),Tdiss(P(k,n)));
            dQGH(k,1) = dQGH(k,1)+(Cph*kappa*timestep_s/(depth_interval)^2)*(T(k-
1,n-1)-2*T(k,n-1)+T(k+1,n-1));
            dQPF(k,1) = dQPF(k,1) + (Cpi*kappa*timestep_s/(depth_interval)^2)*(T(k-
1,n-1)-2*T(k,n-1)+T(k+1,n-1));
            if dQPF(k,1) >= L_PF
                PF(k,1) = 2;
                Spf(k,n:end) = 0;
                dQGH(k,1) = dQGH(k,1) + (dQPF(k,1)-L_PF);
            else
                Spf(k,n) = Spf(k,1) * (L_PF-dQPF(k,1))/L_PF;
            end
            if dQGH(k,1) >= L_GH
                HS(k,1) = 2;
                Sh(k,n:end) = 0;
                T(k,n) = T(k,n) + (dQGH(k,1)-L_GH)/Cph;
            else
                Sh(k,n) = Sh(k,1) * (L_GH-dQGH(k,1))/L_GH;
            end
        end

    end

    % LOWER BOUNDARY --> apply bottom boundary condition: constant heat
    % flux (but still account for latent heat if hydrates or PF present
    T(length(Z),n) = T(length(Z)-1,n) + G*depth_interval;

    % CASE I: hydrates initially present and thermodynamically unstable, permafrost
not
    if (HS(length(Z),1) == 1) && (PF(length(Z),1) ~= 1) && (T(length(Z),n) >=
Tdiss(P(length(Z),n))) % If GH stable/present AND T >= Teq
        dQGH(length(Z),1) = dQGH(length(Z),1)+(T(length(Z),n) -
Tdiss(P(length(Z),n)))*Cph;
        T(length(Z),n) = Tdiss(P(length(Z),n));
        if dQGH(length(Z),1) >= L_GH
            HS(length(Z),1) = 2;
            T(length(Z),n) = T(length(Z),n) + (dQGH(length(Z),1)-L_GH)/Cph;
            Sh(length(Z),n:end) = 0;
        else
            Sh(length(Z),n) = Sh(length(Z),1) * (L_GH-dQGH(length(Z),1))/L_GH;
        end
    end

    % CASE II: permafrost initially present and thermodynamically unstable,
hydrates not
    if (PF(length(Z),1) == 1) && (HS(length(Z),1) ~= 1) && T(length(Z),n) >=
T_freeze(P(length(Z),n),S)
        dQPF(length(Z),1) = dQPF(length(Z),1)+(T(length(Z),n) -
T_freeze(P(length(Z),n),S))*Cpi;
        T(length(Z),n) = T_freeze(P(length(Z),n),S);
        if dQPF(length(Z),1) >= L_PF
            PF(length(Z),1) = 2;
            T(length(Z),n) = T(length(Z),n) + (dQPF(length(Z),1)-L_PF)/Cpi;
            Spf(length(Z),n:end) = 0;
        else
            Spf(length(Z),n) = Spf(length(Z),1) * (L_PF-dQPF(length(Z),1))/L_PF;
        end
    end

    % CASE III: both permafrost and hydrates are initially present, but only
```

```
    % permafrost is thermodynamically unstable
    if (PF(length(Z),1) == 1) && (HS(length(Z),1) == 1) && (T(length(Z),n)>=
T_freeze(P(length(Z),n),S)) && (T(length(Z),n) < Tdiss(P(length(Z),n)))
        dQPF(length(Z),1) = dQPF(length(Z),1)+(T(length(Z),n) -
T_freeze(P(length(Z),n),S))*Cpi;
        T(length(Z),n) = T_freeze(P(length(Z),n),S);
        if dQPF(length(Z),1) >= L_PF
            PF(length(Z),1) = 2;
            T(length(Z),n) = T(length(Z),n) + (dQPF(length(Z),1)-L_PF)/Cpi;
            Spf(length(Z),n:end) = 0;
        else
            Spf(length(Z),n) = Spf(length(Z),1) * (L_PF-dQPF(length(Z),1))/L_PF;
        end
    end

    % CASE IV: both permafrost and hydrates are initially present, but only
    % hydrates are thermodynamically unstable
    if (PF(length(Z),1) == 1) && (HS(length(Z),1) == 1) && (T(length(Z),n) <
T_freeze(P(length(Z),n),S)) && (T(length(Z),n) >= Tdiss(P(length(Z),n)))
        dQGH(length(Z),1) = dQGH(length(Z),1)+(T(length(Z),n) -
Tdiss(P(length(Z),n)))*Cph;
        T(length(Z),n) = Tdiss(P(length(Z),n));
        if dQGH(length(Z),1) >= L_GH
            HS(length(Z),1) = 2;
            T(length(Z),n) = T(length(Z),n) + (dQGH(length(Z),1)-L_GH)/Cph;
            Sh(length(Z),n:end) = 0;
        else
            Sh(length(Z),n) = Sh(length(Z),1) * (L_GH-dQGH(length(Z),1))/L_GH;
        end
    end

    % CASE V: both permafrost and hydrates are initially present, and both are
    % thermodynamically unstable
    if (PF(length(Z),1) == 1) && (HS(length(Z),1) == 1) && (T(length(Z),n) >=
Tdiss(P(length(Z),n))) && (T(length(Z),n)>= T_freeze(P(length(Z),n),S))
        dQGH(length(Z),1) = dQGH(length(Z),1)+(T(length(Z),n) -
Tdiss(P(length(Z),n)))*Cph;
        dQPF(length(Z),1) = dQPF(length(Z),1)+(T(length(Z),n) -
T_freeze(P(length(Z),n),S))*Cpi;
        T(length(Z),n) = min(T_freeze(P(length(Z),n),S),Tdiss(P(length(Z),n)));

        if dQPF(length(Z),1) >= L_PF
            PF(length(Z),1) = 2;
            Spf(length(Z),n:end) = 0;
            dQGH(length(Z),1) = dQGH(length(Z),1) + (dQPF(length(Z),1)-L_PF);
        else
            Spf(length(Z),n) = Spf(length(Z),1) * (L_PF-dQPF(length(Z),1))/L_PF;
        end
        if dQGH(length(Z),1) >= L_GH
            HS(length(Z),1) = 2;
            Sh(length(Z),n:end) = 0;
            T(length(Z),n) = T(length(Z),n) + (dQGH(length(Z),1)-L_GH)/Cph;
        else
            Sh(length(Z),n) = Sh(length(Z),1) * (L_GH-dQGH(length(Z),1))/L_GH;
        end
    end

    % Determine base and top of the hydrate occurrence zone
    if isempty(find(HS==1,1,'last')) == 0       % if not all hydrates melted away
        baseHZ(1,n)= Z(find(HS==1,1,'last'));
        topHZ(1,n) = Z(find(HS==1,1));
    else
        baseHZ(1,n)= (baseHZ(1,n-1) + topHZ(1,n-1))/2;  % if all hydrates melted:
base/top HZ = average top and base in previous time step (arbitrary chosen value)
        topHZ(1,n)= (baseHZ(1,n-1) + topHZ(1,n-1))/2;
    end

    % Determine base of the permafrost zone
```

```
    if isempty(find(PF==1,1,'last')) == 0    % if not all permafrost melted away
        basePF(1,n)= Z(find(PF==1,1,'last'));
        topPF(1,n) = Z(find(PF==1,1));
    else
        basePF(1,n)= (basePF(1,n-1) + topPF(1,n-1))/2;   % if all permafrost
melted: base/top PF = average top and base in previous timestep (arbitrary chosen
value)
        topPF(1,n) = (basePF(1,n-1) + topPF(1,n-1))/2;
    end
end

% PLOTS

% Figure 1: Temperature evolution through time: plots if t = 0 and
% subsequently every 20000 kyr
figure;

subplot(2,3,[1,4]);
hold on;
axis ij;

T_diss_i = ones(1,length(Z));
Tfreeze_i = ones(1,length(Z));
T_diss_f = ones(1,length(Z));
Tfreeze_f = ones(1,length(Z));
for f = 1:length(Z)
    T_diss_i(f) = Tdiss(P(f,1));
    Tfreeze_i(f) = T_freeze(P(f,1),S);
    T_diss_f(f) = Tdiss(P(f,period_SLrise));
    Tfreeze_f(f) = T_freeze(P(f,period_SLrise),S);
end
plot(T_diss_i,Z,'-k',Tfreeze_i,Z,'--k',T_diss_f,Z,'-r',Tfreeze_f,Z,'--
r','LineWidth',1.5);
plot(250:1:300,basePF(1,1)*ones(1,51),'--b',250:1:300,baseHZ(1,1)*ones(1,51),'-
.k',250:1:300,topHZ(1,1)*ones(1,51),'-.k');
for d = 1:length(t)
    if t(d) == 1 || t(d)/(3.1557e7*20000) == round(t(d)/(3.1557e7*20000))
        plot(T(:,d),Z,'LineWidth',1.5);
    end
end
xlim([initialT_atSurface-0.15,300]);
ylim([z0,zf]);
hold off;

% Figure 2: Evolution of gas hydrate saturation through time: plots at t = 0 and
% subsequently every 20000 kyr
subplot(2,3,2);
hold on;
axis ij;
xlim([0,1]);
ylim([z0,zf]);
for h = 1:length(t)
    if t(h) == 1 || t(h)/(3.1557e7*20000) == round(t(h)/(3.1557e7*20000))
        plot(Sh(:,h),Z,'LineWidth',1.5);
    end
end
hold off;

% Figure 3: Evolution of ice saturation through time: plots at t = 0 and
% subsequently every 20000 kyr
subplot(2,3,5);
hold on;
axis ij;
xlim([0,1]);
ylim([z0,zf]);
for e = 1:length(t)
    if t(e) == 1 || t(e)/(3.1557e7*20000) == round(t(e)/(3.1557e7*20000))
        plot(Spf(:,e),Z,'LineWidth',1.5);
```

```
    end
end
hold off;


% Figure 4: Evolution of base and top of hydrate occurrence zone through time
subplot(2,3,3);
hold on;
axis ij;
plot(t/(3.1557e7),baseHZ,'-k',t/(3.1557e7),topHZ,'-r','LineWidth',1.5);
ylim([z0,zf]);
hold off;

% Figure 5: Evolution of base and top of permafrost zone through time
subplot(2,3,6);
hold on;
axis ij;
plot(t/(3.1557e7),basePF,'-k',t/(3.1557e7),topPF,'-r','LineWidth',1.5);
ylim([z0,zf]);
hold off;
```

```
% SCRIPT NAME: BehBryant.m
% DESCRIPTION: This script implements the box model for hydrate formation in a
% 'converted free gas' hydrate accumulation (Behseresht & Bryant, 2012).
% Initially a gas accumulation, ISOLATED from the gas source, is present.
% Then hydrate stability conditions are imposed, and the base of the HSZ
% migrates down the gas accumulation, resulting in gas hydrate formation.
% The sediment column is considered as a stack of boxes to which the box model can
be applied
% This way a hydrate saturation is obtained (time scale for formation is
% not addressed)

% Constants and parameters (from Behseresht & Bryant, 2012)
N = 6;                          % hydration number: CH4.N(H2O)
porosity = 0.5;                 % porosity (volume percentage)
initial_Sg = 0.8;               % initial gas saturation (volume percentage)
residual_Sg = 0.03;             % residual gas saturation (volume percentage)

% Calculated parameters; values from Behseresht & Bryant (2012)
MWh = 0.124; rhoh = 914;        % Molecular weight (kg/mol) and density (kg/m^3)
MWg = 0.016; rhog = 55;         % of hydrate, gaseous and aqueous phase
MWw = 0.018; rhow = 1024;
V_h = MWh/rhoh;                 % Molar volume (m^3/mole) of hydrate, gaseous
V_g = MWg/rhog;                 % and aqueous phase
V_w = MWw/rhow;

Ktrans = ((N*V_w + V_g)/V_h)-1; % total phase (gas+aqueous) volume transported
                                % per unit volume of hydrate formed (dimensionless)

GWC = depthinGC(end);           % Initial position (in m below initial top of gas
column) of the gas-water contact
S_gi = initial_Sg*ones(1,length(depthinGC)); % Initial gas saturation throughout
the column
S_h = ones(1,length(depthinGC));

% Calculate hydrate saturation profile after the base of the HSZ has passed
% descended through the gas column
for i = 1:length(depthinGC)
    if depthinGC(i) < GWC               % ABOVE GWC
        Rv = 0.55;                      % Gas phase volume ratio of transported phases
(dimensionless) (Behseresht & Bryant, 2012)
        S_h(i) = V_h*S_gi(i)/(Rv*(V_h-V_g-N*V_w)+V_g);  % Rv < 0.6 --> excess
aqueous phase situation: calculate Sh using eq (19)
        % Calculate new position of GWC
        delta_VGWC = Ktrans*S_h(i)*porosity*Rv;
        GWC = GWC - (delta_VGWC/(porosity*(1-residual_Sg)));
    else                                % BELOW GWC: Rv = 0
        Rv = 0;
```

```
        S_gi(i) = residual_Sg;
        S_h(i) = V_h*S_gi(i)/(Rv*(V_h-V_g-N*V_w)+V_g);
    end
end
```

```
function res = Tdiss(p)
% This function calculates the temperature of dissociation at a given pressure P
% for pure methane hydrate in equilibrium with seawater with salinity of 0.035
weight percent NaCl
% It takes P (in Pa) and returens Tdiss (in K)
% Two equations are obtained (one for pressures below 2576 kPa (linear) and
% one for pressures above 2576 kPa(logaritmic)) by fitting a trendline to P-Tdiss
datapoints obtained from the CMSHYD program of Sloan (1998)
    P_kPa = p/(1e3);
    if P_kPa <= 2576.74
        res = 0.0158*(P_kPa) + 232.7;
    else
        res = 9.6349*log(P_kPa) + 197.65;
    end
end
```

```
function res = T_freeze(P,S)
% This function returns the freezing temperature of seawater (in degrees Kelvin)
% as a function of P (given in Pa) and salinity (in PSS-78: practical salinity:
idem to promille), according to the formula of Millero & Leung (1976); valid for
pressures up to 500 dbar (5 MPa);
    res = -0.0575*S + 1.710523e-3*(S^(3/2)) - 2.154996e-4*(S^2) - 7.53e-4*(P/(1e4))
+ 273.15;
end
```